Electrical properties of graphene/multiphase polymer nanocomposites: A review

Thibaut Lalire, Claire Longuet, A. Taguet

▶ **To cite this version:**

Thibaut Lalire, Claire Longuet, A. Taguet. Electrical properties of graphene/multiphase polymer nanocomposites: A review. Carbon, 2024, 225, pp.119055. 10.1016/j.carbon.2024.119055 . hal-04549270

HAL Id: hal-04549270

https://imt-mines-ales.hal.science/hal-04549270

Submitted on 17 Apr 2024

HAL is a multi-disciplinary open access archive for the deposit and dissemination of scientific research documents, whether they are published or not. The documents may come from teaching and research institutions in France or abroad, or from public or private research centers.

L'archive ouverte pluridisciplinaire **HAL**, est destinée au dépôt et à la diffusion de documents scientifiques de niveau recherche, publiés ou non, émanant des établissements d'enseignement et de recherche français ou étrangers, des laboratoires publics ou privés.

Distributed under a Creative Commons Attribution - NonCommercial 4.0 International License

Carbon 225 (2024) 119055

Contents lists available at ScienceDirect

Carbon

journal homepage: www.elsevier.com/locate/carbon

Electrical properties of graphene/multiphase polymer nanocomposites: A review

Thibaut Lalire, Claire Longuet, Aurélie Taguet *

Polymers Composites and Hybrids (PCH), IMT Mines Ales, Ales, France

ARTICLE INFO

Keywords:
Polymer blend nanocomposites
Graphene
Electrical conductivity
Localization
Applications

ABSTRACT

Graphene and their derivatives exhibit interesting properties (mechanical properties, electrical and thermal conductivities). When incorporated into polymer matrices, many applications are possible in fields like electronics, medicine, transportation. The goal of the present review is to highlight how graphene can influence the electrical properties of polymer nanocomposites. The first part explains the peculiar structure of graphene, the main ways to synthesize graphene and the influence on electrical conductivity. In this first part, it is also explained how orientation and alignment of graphene platelets or the presence of a second filler can influence the percolation threshold or electrical conductivity of a monophase polymer nanocomposite. Finally, in this first part, we present some generalities on the enhancement of electrical properties by chemical treatments performed on the graphene. The aim of the second part of this review is to show the effect of the incorporation of graphene into immiscible polymer blends on the microstructures and on the electrical properties. Especially, we focus on the concept of selective localization of nanoparticles into a blend: how to predict the localization of graphene and how to tailor the localization by chemical and kinetics factors. Several graphs were drawn, based on the data of 73 publications, to exhibit the influence of different parameters on the electrical conductivity (in $S.cm^{-1}$) of graphene based polymer blend nanocomposites. Finally, the last part of this review is dedicated to the electrical applications of graphene-based polymer blend nanocomposites.

1. Introduction

The emergence of graphene nanoparticles and its remarkable properties entailed the production of new conductive polymer nanocomposites [1]. Due to its ultrahigh electrical performance, graphene has emerged as a promising nanoparticle for preparing high performance polymer nanocomposites. Its 2D structure have a potential to form a 3D network with reduced filler loading in a polymer matrix compared to a spherical filler like carbon black. It replaces microscopic fillers which need high amounts to obtain good performances with sometimes a degradation of mechanical properties [2]. Graphene showed its efficiency in several kind of polymer matrix which manifested an improvement of their mechanical, electrical, and thermal properties [3]. However, graphene is an expensive material and a random dispersion of graphene into a single polymer matrix led to relatively high percolation threshold. Several methods are also used to decrease the filler content that will be presented in this review. Part I of the present review summarizes the structure and electronic properties of graphene. It also explains the concept of percolation threshold and the influence of different graphene parameters on percolation threshold. Finally, part I summarizes how can chemical modification enhance the percolation. Another interesting way to reduce percolation threshold is to play with the morphology of the polymer composite material. The idea is to disperse graphene into immiscible polymer blends and especially localize graphene fillers in the minor phase or at the interface of co-continuous polymer blends to reduce the percolation threshold [4-7]. Part II explains how to change the morphology of graphene based polymer blends to improve electrical conductivity. Finally, some applications are exposed in part III of the present review.

2. Graphene: electrical properties and percolation

2.1. Electronic structure and electrical properties of graphene

2.1.1. Electronic structure of graphene and their derivatives

Graphene is considered as a multifunctional material thanks to its excellent mechanical, electrical and thermal properties. It owes this particularity to its 2D honeycomb structure only composed of carbon

* Corresponding author.
E-mail address: aurelie.taguet@mines-ales.fr (A. Taguet).

https://doi.org/10.1016/j.carbon.2024.119055
Received 19 September 2023; Received in revised form 20 February 2024; Accepted 17 March 2024
Available online 23 March 2024
0008-6223/© 2024 The Authors. Published by Elsevier Ltd. This is an open access article under the CC BY-NC license (http://creativecommons.org/licenses/by-nc/4.0/).

atoms and some hydrogen atoms notably at the edge of sheets. Since the discovery of 2D materials and graphene, lots of articles broached the graphene electronic subject around 25,000 since the 2000's. Understand the benefit of incorporating graphene into polymer matrices, it is important to be aware of intrinsic physical properties of graphene. In this review, the electrical conductivity of the graphene is investigated. Its structure without defects gives a high electrical conductivity of 10^6 S. cm^{-1} and a high electron mobility of 250,000 cm^2. V^{-1}. s^{-1} [8]. Each carbon atom forms three σ bonds with neighboring atoms by overlapping of sp^2 orbitals. Each carbon atom has one p_z electron and the p_z orbital overlaps form a band of filled π orbitals (valence band) and a band of empty π* orbitals (conduction band) [9]. Electrons follow the "zigzag" structure to move on the graphene structure and this gives a corner shape of the bands (the Dirac cone) which touch at the K point. There is a zero density of states but no band gap. The armchair structure leads to a behavior similar to a semiconducting behavior at the M point (Fig. 1 a, b). The number of layers stacked in the final graphene has supposed to play an important role in the final electrical behavior [10]. Single layer (monolayer) and bilayer graphene perform a zero-gap semiconductor with single type of holes and electrons. This kind of gap forms a Dirac cone where valence and conduction bands are joined in one point named K point which results into an effective zero mass [11]. At this point, the energy-momentum relation dispersion becomes linear described by the relativistic equation (1). In a conventional semi-conductor, an effective mass m and energy E are ascribed to electrons as defined by equation (2) [12]:

$$E = p \times v_f \tag{1}$$

$$E = \frac{p^2}{2m} \tag{2}$$

p is the momentum and v_f is the fermi velocity. Equation (1) shows that at the K point, electrons in graphene sheet behave like massless relativistic particles and entail a Quantum Hall Effect (QHE) at room temperature that is normally observed at ultralow temperature for metals [13]. The transport of electrons is considered like a ballistic transport [14]. These particularities give to graphene its exceptional electron mobility and electrical conductivity. Since monolayer is a no band gap, it makes its use impossible for digital electronic. However, the bilayer is more versatile because a transverse electrical field is enough to open the gap (Fig. 1c, d, e) [15]. This possibility to control interaction between the relativistic particles allows to alter these properties for several applications [16]. For multilayer, the valence and conduction bands begin to be separate. Zhu et al. [17], show that holes mobility is directly dependent on temperature variation. Different behaviors were observed between monolayer, bilayer and trilayer graphene deposed on SiO_2 substrate. The mobility of holes for monolayer decreased when the temperature increased. It is due to scattering by thermally excited surface polar phonons of the SiO_2 substrate. On the contrary, concerning bilayer and trilayer, the mobility increases proportionally to the temperature (Fig. 1 f, g, h). Coulomb scattering determined this dependence [18].

For most electrical applications, which use graphene, it is necessary to open an energy gap. A surface modification by the way of oxidant treatment or nanopatterning can induce an open energy gap [20]. For nanocomposite application, graphene under its oxide form (graphene oxide, GO) is most suitable in order to have a high affinity with polymers and a better dispersion in an organic matrix. Functional groups are grafted on GO basal plane and edges. It can interact with the polymer matrix. However, this graphene treatment drives down the electrical properties and GO is also insulating [21]. Indeed, the basic electronic structure of graphene is totally disrupted, and defects appear on the basal plane which prevent electron transport and it results in the remaining sp^2 domains and the formation of sp^3 domains (induced by bonded oxygen functional groups). The electronic properties of GO depend on the oxidation level and chemical composition. Chemical or thermal reduction of GO (rGO) allows to remove most of the oxide groups and recover a high electrical conductivity. For thermal reduction, oxide groups are decomposed into CO_2 and H_2O and the critical temperature to obtain rGO with the highest conductivity is from 200 °C under nitrogen atmosphere [22]. Fig. 2 shows that, thanks to oxidation and reduction mechanisms, the electrical conductivity may be tuned by controlling the oxygen content. However, GO reduction never totally restored the pristine graphene. Control oxidation degree means control electron mobility and electrical conductivity. Chang et al. [23]

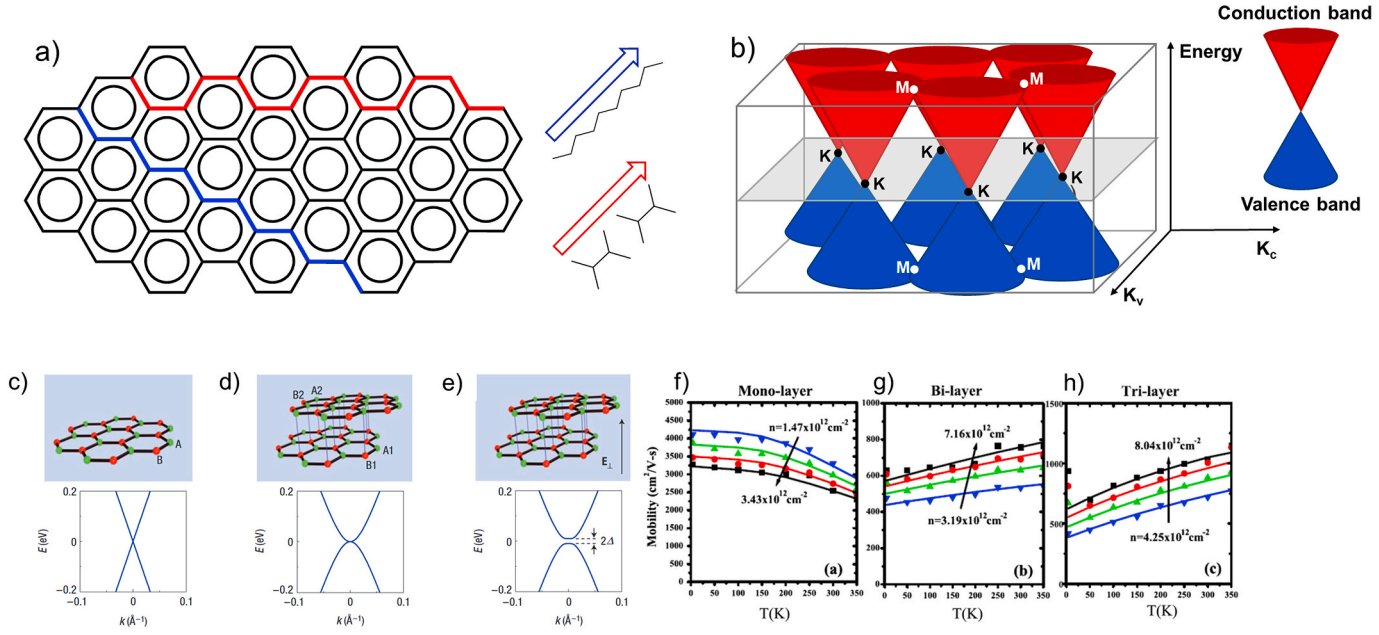

Fig. 1. (a) Electron transport mechanism, (b) Schematic model of graphene band structure (c) Lattice structure and energy diagram for Graphene monolayer Dirac point (d) Graphene bilayer zero gap semiconductor, (e) Graphene bilayer under electric field [19]; Holes mobility versus temperature with different carrier density for (f) graphene monolayer (g) graphene bilayer (h) graphene trilayer [11,18]. Reproduced from Refs. [18,19]with permission. (A colour version of this figure can be viewed online.)

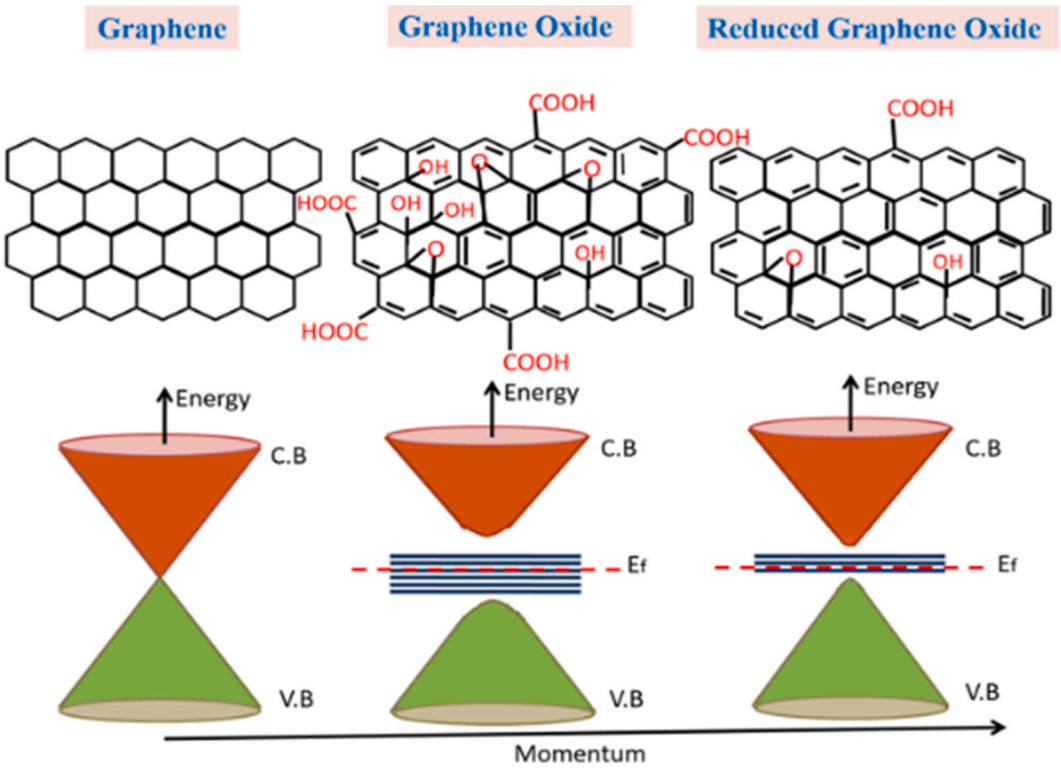

Fig. 2. Lattice structure and corresponding energy band diagrams of graphene, GO, rGO (CB: conduction Band, VB: Valence Band, Ef: Fermi energy) [24]. Reproduced from Ref. [24] with permission. (A colour version of this figure can be viewed online.)

compared the GO reduction at 150 °C and different times of annealing under nitrogen. Results proved that the bandgap energy changes according to the annealing time. Indeed, for 20, 90, 260 min thermally reduction time, reduced GO have a band gap energy of 1.5, 1, 0.5 eV, respectively. For GO, electrons need too much energy to reach conduction band with a band gap of 2.2 eV, and it is insulating. Reduced graphene oxide (rGO) is considered as a semiconductor or semimetal due to the low band gap of 1 eV or 0.5 eV (Fig. 2). This is the desired nanoparticles required to develop electrically conductive nanocomposite.

2.1.2. *Effect of graphene synthesis on electrical conductivity*

The electrical property of graphene depends on the synthesis used as shown in Fig. 3. Indeed, production method affects the final sp^2 structure and impressive properties of graphene are achieved for the highest quality material [25]. A high electrical conductivity is possible for a graphene sheet with low defects and few layers. Chemical vapor deposition (CVD) is a "bottom-up" process in which the synthesis of the bulk material starts with small entities. This method is known to produce high-quality graphene. It consists in depositing carbon atoms from gas on a metallic substrate at high temperature. Chemical-vapor-deposition (CVD) gives a large area graphene sheet and a high electrical conductivity around 10^4 S.cm^{-1} [26]. Despite these excellent properties, the preparation cost of this method is expensive. Mechanical exfoliation is another way to produce high quality graphene sheets easily. Contrary to CVD, this method is a "top-down" process. From graphite and via a mechanical strength induced by tape [27], it is possible to isolate few layers of graphene. An electrical conductivity of 10^4 S.cm^{-1} was also obtained. However, this method allows to synthesize small quantities of graphene sheets. Consequently, for industrial operations, it is not a suitable synthesis.

With CVD, exfoliation and reduction of graphite oxide technique appears as current graphene production used in industry. Several methods were used to oxidize graphite such as *Brodie* [28], *Staudenmaier*

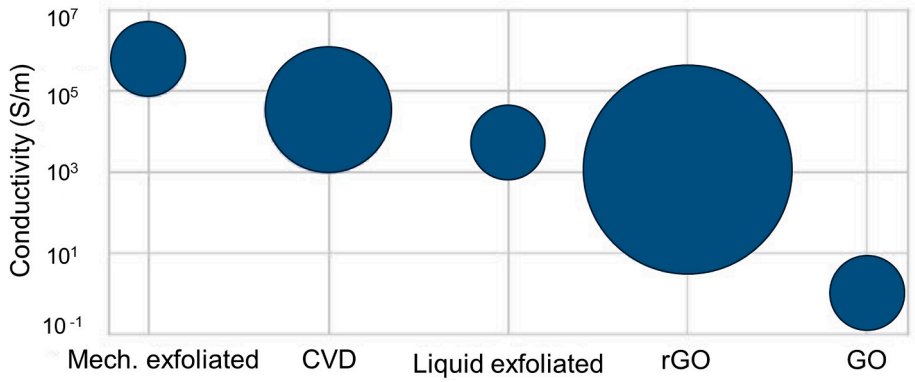

Fig. 3. Electrical conductivity according to the graphene method production [39]. Reproduced from Ref. [39] with permission. The measured conductivities of the available graphene sources. (A colour version of this figure can be viewed online.)

[29] and then *Hummers and Offeman* methods [30]. For example, graphene produced via graphite oxide is based on the oxidation of graphite by using Hummers' method and then sonication to exfoliate graphite oxide sheet in order to obtain insulating GO. This Hummers' method consists in insertion of strong acids and oxidizing reagents that create oxygen functional groups on the basal plane and at the edges of graphite [31]. Graphite is immersed in a H_2SO_4, $NaNO_3$ and $KMnO_4$ solution. The first step of Hummers' method is the intercalation of H_2SO_4 molecules and HSO_4^- ions between graphene layers. The oxidizing agent Mn_2O_7 replaced the intercalant acid species in a second time [32]. The exothermic oxidative action of these species leads to the formation of hydroxylates, carboxylates and epoxy groups. The *C*–O covalent bonding increases the distance between the graphitic layers. Bourlinos et al. [33] measured by XRD an interlayer raise from 0.34 to 0.68 nm after oxidation by Brodie's method. As indicated previously, graphene oxide can be reduced by thermal treatment (TrGO) or chemical treatment (CrGO) with reducing agents such as hydrazine to form rGO [34,35]. Thermal treatment (at high temperature) generally performs a better conductivity compared to the chemical treatment. Illustrating this fact, Vianelli et al. [36]prepared a rGO film by a thermal treatment at 940 °C in a high vacuum (10^{-6} mmbar) and measured a conductivity of 10^3 S.cm^{-1}. Chemical reduction with hydrazine was studied in the same article, a conductivity of 5.10^1 S.cm^{-1} was measured. Thermal reduction gives an electrical conductivity around 2 orders of magnitude higher than the chemical reduction.

From GO structure, arc discharge method allowed to synthetize high electrical conductivity graphene sheets as shown in Wu et al. study [37]. The electrical conductivity measurements presented promising results such as a conductivity of 2.10^3 S.cm^{-1}. In insulating environment as polymer, the same behavior is observed. Ghislandi et al. [38] compared three different methods to obtain graphene. Graphite was oxidized firstly by Hummers' method and reduced thermally or chemically. Another method was to produce graphene by dispersing graphite in water under ultrasonication. After incorporation in polystyrene, the highest electrical conductivity was obtained for the graphene that was chemically reduced (0.15 S.cm^{-1} at low percolation threshold of 0.9 % wt). With the ultrasonication the electrical conductivity is lower and the percolation threshold is much higher. It proves by using the same based material (graphite in this article), that the type of synthesis will have an impact on the electrical property of the graphene/PS nanocomposite.

2.2. Percolated graphene network

In an insulating polymer matrix, nanoparticle percolation is an essential parameter to reach desired electrical properties. The concept of percolation has to be distinguished from that of dispersion (agglomerates are broken to their smallest size) and distribution (spatial arrangements of the particles) [40]. Fig. 4 explains those three concepts. The large aspect ratio of graphene and its high electrical conductivity make it one of the best candidates for a performant nanocomposite at a low percolation threshold. The percolation threshold is identified by an abrupt increase of the electrical conductivity at a fixed filler content, as seen in Fig. 5a. Properties are dramatically modified near the percolation threshold [41]. The main objective for nanocomposite is to obtain a low percolation threshold corresponding to a network formation at a low volume fraction of fillers. The percolation threshold can be calculated with equation (3) [39,42]:

$$\sigma_c = \sigma_{gr}\left(\psi_{gr} - \psi_C\right)^t \quad (3)$$

σ_c is the conductivity of the composite, σ_{gr} corresponds to the graphene conductivity, ψ_{gr} is the volume fraction of graphene, ψ_c is the percolation volume fraction and t is the critical exponent (normally t~1.33 for 2D materials).

The dispersion, the distribution of the fillers, the aspect ratio and the size of the fillers have a direct impact on the percolation. The percolation theory said that, below a critical concentration, nanoparticles are considered to be individually isolated in the insulating matrix. When the nanoparticle concentration increases, the probability to have a connection between graphene nanosheets increases [43].

Mun et al. [44] reported that percolation threshold of polymer/-graphene nanocomposites are below 3 wt% which is significantly below the polymer/carbon black nanocomposites, but above the polymer/-carbon nanotube nanocomposites [45,46]. Moreover, in the same article, they compared solvent casting and melt mixing, and revealed that solution blending, thanks to sonication step, led to lower percolation threshold due to a disaggregation of nanoparticles (Fig. 5).

Numerous articles were published with different techniques to achieve a low percolation threshold with one type of filler by using functionalization, double percolation, triple percolation via multiphase immiscible polymer, or with the incorporation of a second filler [47–49]. Tkalya et al. tried to vary the state of dispersion of graphene

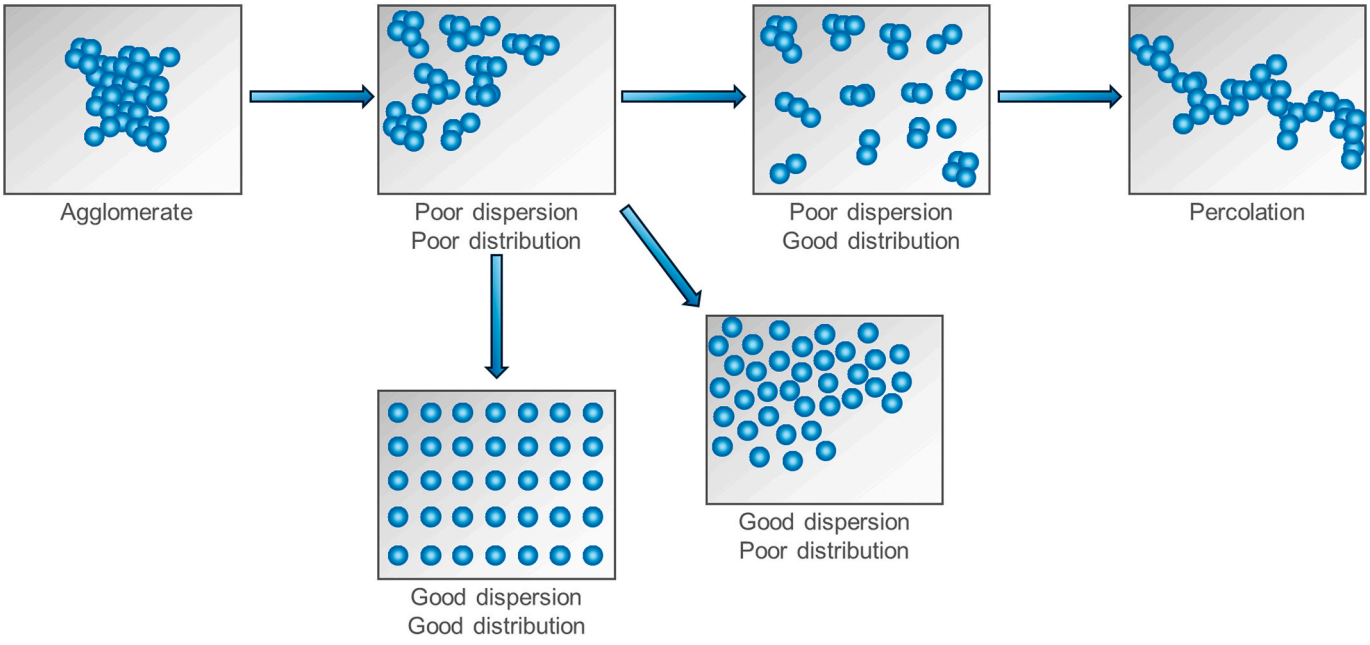

Fig. 4. Scheme to explain the differences between dispersion, distribution and percolation. (A colour version of this figure can be viewed online.)

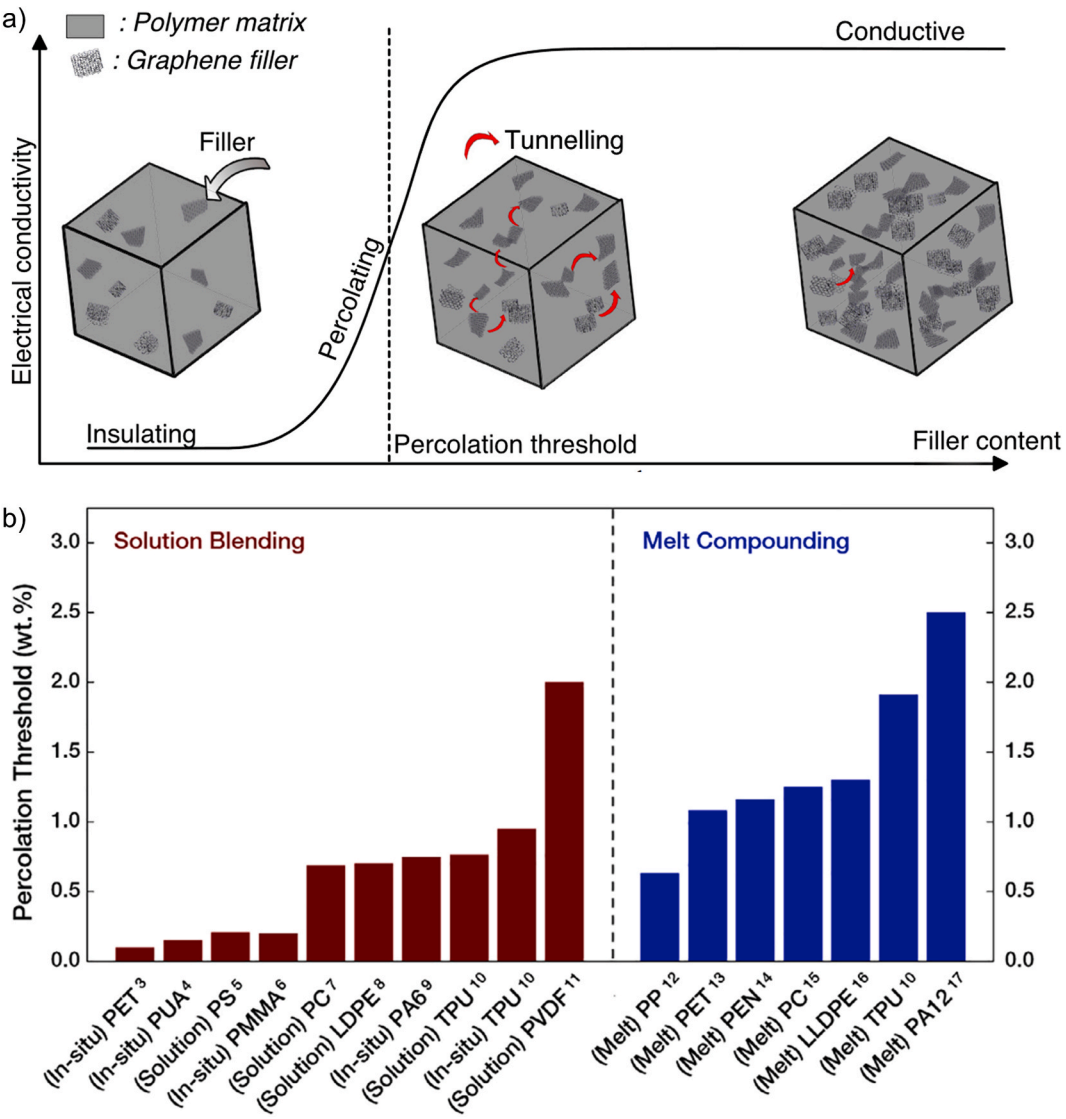

Fig. 5. (a) Schematic composite behavior at different nanoparticle contents, and corresponding evolution of the electrical conductivity [39], (b) Electrical percolation threshold values for polymer/graphene nanocomposites. Comparison between solution blending and melt blending [44]. Reproduced from Refs. [39,44] with permission. (A colour version of this figure can be viewed online.)

into a PS matrix in order to decrease the percolation threshold [50]. Nanocomposites were prepared from PS matrix and aqueous graphene dispersion. The state of dispersion for graphene was varied by changing the conditions of sonication. By measuring and theoretically predicting the percolation threshold, they observed that not only the stability of the aqueous graphene dispersion (Graphene nanosheets reaggregation due to their van der Waals interaction) and the degree of exfoliation play a crucial role, but also the polydispersity of size of the graphene platelets (measured by DLS).

2.2.1. Physical interactions to enhance percolation and electrical conductivity

2.2.1.1. Second filler aid percolation. Some articles show that restacking graphene nanosheets can be removed by incorporating a second carbon filler such as carbon black (CB) or carbon nanotubes (CNT) [49,51]. In Fig. 6a a model is proposed that can explain how CNTs are intercalated between graphene sheet and prevent restacking. A synergistic effect can be visualized between CNT and graphene. This second filler prevent restacking of graphene nanosheets and increases the electrical conductivity. Before CNT incorporation, the conductivity was $1.8.10^3$ S.cm^{-1} and after incorporation of 20 wt% of CNT in CNT-GO solution, the conductivity reaches $2.7.10^3$ S.cm^{-1} [52]. CNTs can form bridges between graphene nanosheets that make the network formation easier at a low percolation threshold (Fig. 6b).

In the same way, *Zhang* et al. [53], compared the effectiveness of both functionalized graphene (f-G) and functionalized multi-walled CNT (f-CNT) nanoparticles added in a poly (ether sulfone), PES matrix. A ternary composite f-CNT-f-G/PES was prepared by solvent casting. Various ratios of f-CNT/f-G were incorporated in PES matrix at an amount of 5 wt%. The electrical conductivity increased progressively when graphene was replaced by CNT in the composite. Indeed, a lower electrical conductivity was measured for the nanocomposites containing only one of the two fillers. A ratio f-G:f-CNT of 1:3 displayed the best performance (Fig. 6c). Moreover, a percolation threshold as low as 0.22 vol% was reached for the f-G-f- CNT (Wf-G/Wf-CNTs = 1:1)/PES composite. It proves that CNT makes easier the electron transport through graphene sheets. The synergistic effect for enhancing electrical conductivity is also approved. With the same idea, Maiti et al. [51] used hybrid fillers: MWCNT and graphene nanoplatelets (GNP) (at a 2:3 ratio) at an amount from 0.3 to 1 wt% in a PC polymer matrix and achieved an extremely low percolation threshold of 0.072 wt% for the (2:3) MWCNT:

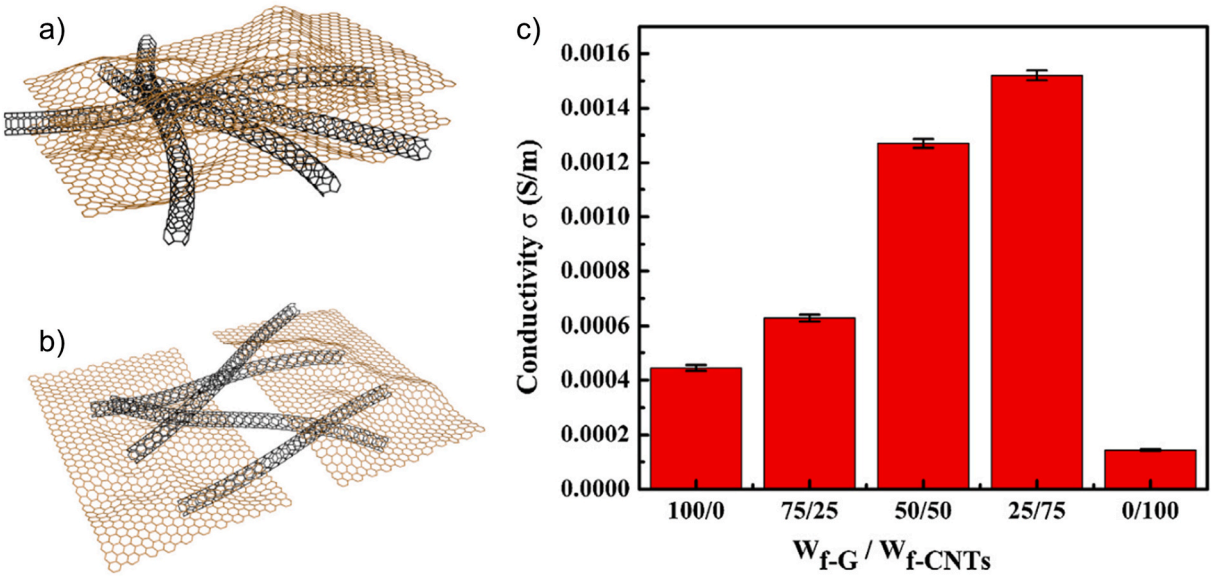

Fig. 6. (a) CNT between graphene sheets prevent restacking, (b) Bridging effect of CNT to graphene nanosheets [52], (c) Electrical conductivity of PES filled hybrid fillers at different weight ratio of f-G/f-CNTs for a filler content of 5 wt% [53]. Reproduced from Refs. [52,53] with permission. (A colour version of this figure can be viewed online.)

GNP loading.

Concurrently, Chakraborty et al. [54] used a non-conductive second filler (silica) which was effective to help for the graphene dispersion in a PS matrix. Silica nanoparticles prevent graphene nanosheet restacking or agglomerate during solvent casting. These nanoparticles are intercalated between graphene nanosheets and allow to remove weak van der Waals interaction (Fig. 7a). This better dispersion has a direct impact on electrical conductivity (Fig. 7b). 2.5 vol% of graphene was incorporated in PS matrix and gave a conductivity of 10^{-12} S.cm^{-1}. For the same amount of graphene with 12 vol% of silica, the electrical conductivity reached 1.10^{-2} S.cm^{-1}. This proves the real interest in having the best possible dispersion.

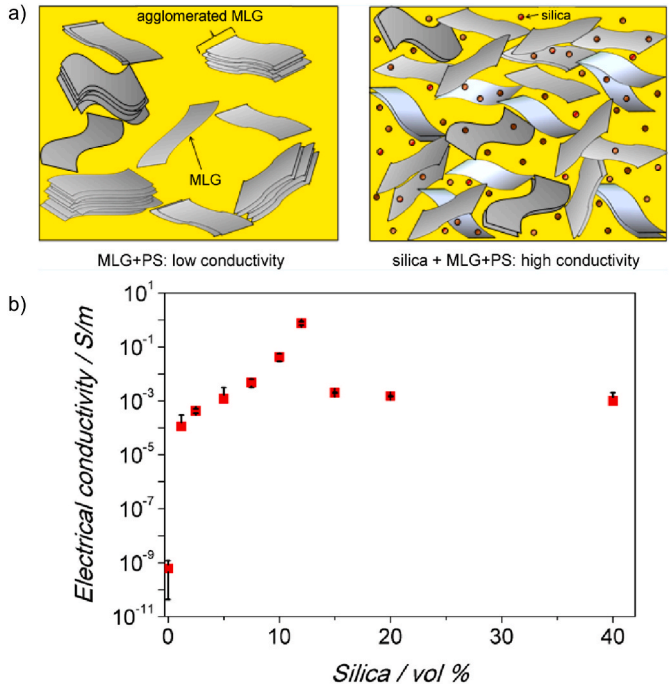

Fig. 7. (a) Silica nanoparticles intercalation between graphene sheets for dispersion aid, (b) Silica impact on electrical conductivity [54]. Reprinted (adapted) with permission from Ref. [54]. Copyright 2023 American Chemical Society. (A colour version of this figure can be viewed online.)

2.2.1.2. Graphene sheets aligned composites (AGC). The filler orientation is another factor that can influence mechanical, thermal, and electrical properties. Aligned graphene composites (AGCs) is an effective way to reach a low percolation threshold [55]. These AGCs behave like an anisotropic material and lead to an improvement of the properties in one direction. Several methods were investigated to align fillers, under electric [56] or magnetic fields [57], mechanical stretching [58], unidirectional freeze-casting [59], liquid crystal [60], or solvent evaporation induction [61]. Wu's et al. [62] introduced graphene nanoplatelets (GNP) in an epoxy matrix. An electric field was applied to GNP fillers in order to align them. After 20min under the apply electric field, the graphene sheets alignment was clearly visible as shown in Fig. 8a and b. This anisotropic behavior is effectively confirmed since the electrical conductivity in the direction of fillers is 2–3 orders of magnitude higher than along the transverse direction [62]. Moreover, the percolation threshold decreases with the electric field. Indeed, without alignment the percolation threshold was 0.55 vol% and with an electric field, it reaches 0.22 vol% for an electrical conductivity of 10^{-7} S.cm^{-1}. The end of each graphene sheet presents opposite charge that tend to attract themselves which facilitates the contact between sheets.

Le Ferrand et al. [63] prepared magnetically responsive reduced graphene oxide (*m*-rGO) via an adsorption of superparamagnetic iron oxide nanoparticles (SPION) onto graphene oxide flakes. The attachment of SPIONs was assisted by a bovine serum albumin (BSA). Hydrazine was further used to convert GO into rGO. The presence of polar organic groups in the surface thanks to adsorbed SPIONs and BSA prevents from the reaggregation of graphene flakes and make easier the dispersion in polar solvent. The *m*-rGO flakes were incorporated in two fluids (gelatin from bovine and poly (2-acrylamido-2-methyl-1-propanesulfonic acid, PAMPS) to form hydrogels. The magnetic synthetized *m*-rGO can be aligned thanks to a simple magnet. These hydrogels exhibit a liquid-to-solid transition while orienting the *m*-rGO flakes when applying a magnetic field as low as 50 mT. The flakes orientation was fixed in the hydrogel thanks to its state transition liquid-to-solid by decreasing temperature (Fig. 8d). It is also possible to control the spatial distribution of *m*-rGO flakes into the hydrogel while applying magnetic fields. The authors fabricated

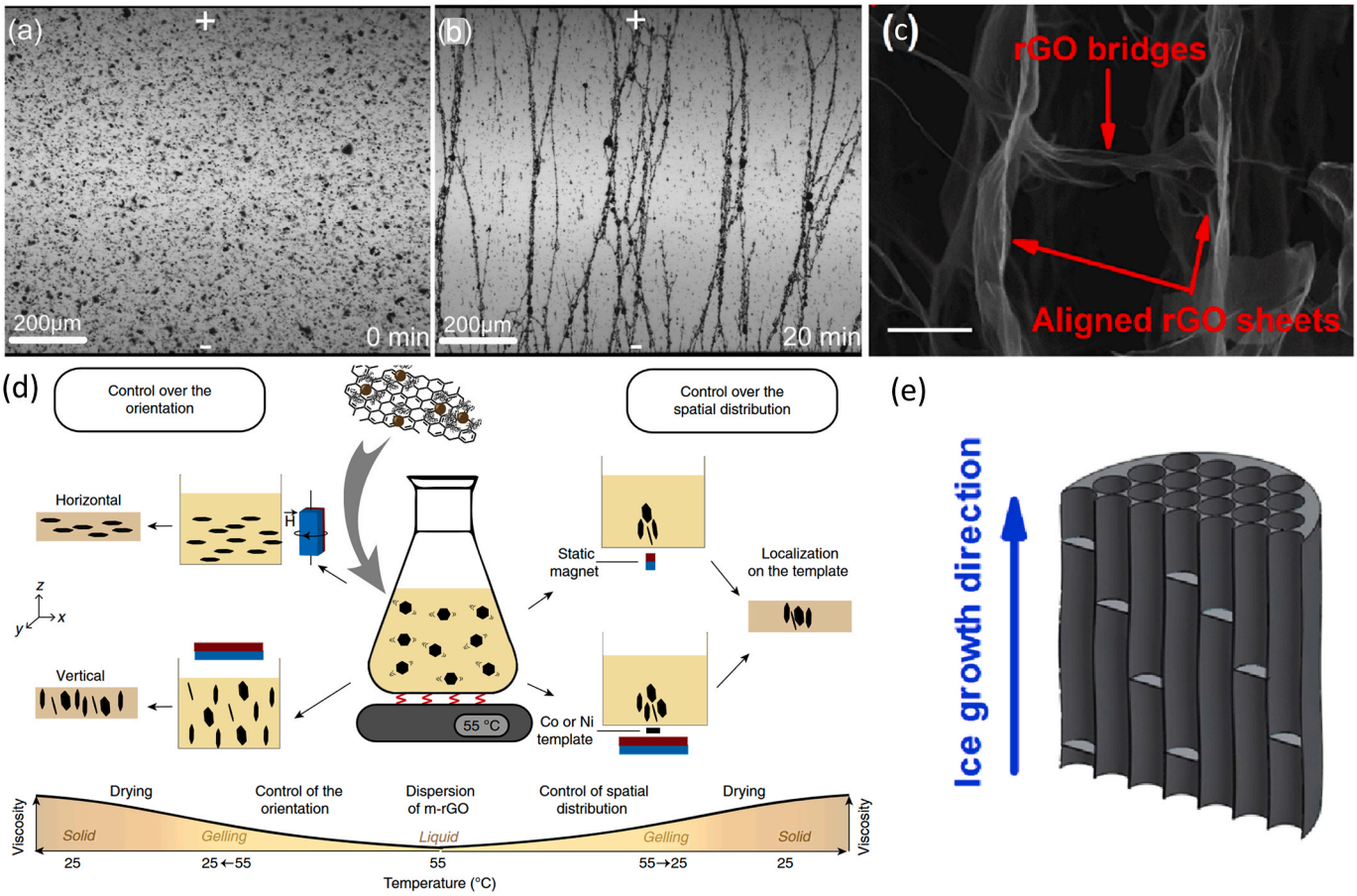

Fig. 8. (a) Randomly oriented GNP without applied field, (b) Aligned GNP after the electric field was applied for 20min [62], (c) 3D interconnected structure of UGA [59], (d) Alignment of graphene sheets by applying a magnetic field [63], (e) Schematic representation of the ice growth direction [59]. Reproduced from Refs. [62, 63] with permission and reprinted (adapted) with permission from Ref. [59]. Copyright 2016 American Chemical Society. (A colour version of this figure can be viewed online.)

oriented nanocomposites with an amount of 2 vol% of *m*-rGO, and an electrical conductivity of 2.10^{-2} S.cm^{-1} was reached. The percolation threshold was as low as 0.75 vol%. Finally, Wang et al. [59] proposed another method which manifested an extremely low percolation threshold. Unidirectional graphene aerogel (UGA)/epoxy nanocomposite was prepared. The freeze-casting method followed by the thermal reduction was presented. Graphene sheets were also aligned in the ice growth direction (Fig. 8e) which gave the anisotropic electrical properties of UGA/epoxy material. This method gives the best results for the percolation threshold by creating a 3D interconnected structure with aligned graphene sheets and graphene bridges (Fig. 8c). Knowing that the conductivity of epoxy is 10^{-12} S.cm^{-1}, with the addition of 0.01 vol % of graphene, an increase of 8 orders of magnitude in conductivity was measured. The ultralow percolation threshold obtained in this study reaches 0.007 vol% for an electrical conductivity of 10^{-1} S.cm^{-1}.

2.2.1.3. The effect of size and aspect ratio of graphene on percolation and electrical conductivity. Nanoparticle size was also an important factor to build a network at a low percolation threshold. Gao et al. [64] suggested to analyze the effect of different graphene aspect ratios on the mechanical, electrical, and thermal properties of PLA. Nanocomposite materials were carried out by a melt compounding method. Two kinds of graphene were tested: GNP-S (small aspect ratio) and GNP-L (large aspect ratio) with a diameter of 1 µm and 15 µm, respectively. Obviously, both allowed to improve the electrical conductivity of PLA matrix. An increase of electrical conductivity started at 7 wt% for the GNP-L while it started at 13 wt% for the GNP-S which proved that larger graphene platelets are more suitable to reduce the percolation threshold without treatment (Fig. 9a). However, it must be noticed that not only the length of the platelets but also the number of platelets (thickness) was varying between GNP-S and GNP-L.

Han et al. [65] used freeze casting method to synthetize graphene aerogel as it was presented in the paragraph I.2.1.2. As well as graphene sheets are aligned (UGA) thanks to this method, three different sizes of sheets were investigated. The average areas of GO used as precursors are 1.1 µm^2 (*S*-GO), 838 µm^2 (L-GO), (UL-GO) 1595 µm^2 to obtain then (small) *S*-UGA, (large) L-UGA and (ultra large) UL-UGA. Fig. 9b, clearly displays an enhancement of 10 orders of magnitude for the electrical conductivity compared to the neat epoxy. Three different percolation threshold values can be seen and a real gap is highlighted between *S*-GO and L-GO. The values of percolation threshold are 0.154, 0.033, 0.0066 vol% for *S*-GO, L-G, UL-GO, respectively. It shows that a higher sheet area is more suitable to reach lower percolation threshold. Large sheets need a lower quantity of nanoparticles to create an interconnected network.

He et al. [66], prepared nanocomposites of polypropylene (PP)/graphene in twin screw extruder by comparing five platelets with different aspect ratios: 8 (PG-8), 400 (PG-40), 1000 (PG-100), 1300 (PG-030), 1500 (PG-G5). PG-8, PG-40 and PG-100 display the same thickness (100 nm) but different diameters. The concentration of graphene was fixed at 12 wt%. PG-8 has no effect on electrical conductivity, as the electrical conductivity is close to the neat PP: 10^{-13} S.cm^{-1} (Fig. 9c). On the other hand, Fig. 9c shows a significant increase of the electrical conductivity when the diameter is larger. The thickness is lower for PG-030 than for PG-40 and their diameter are equal. The

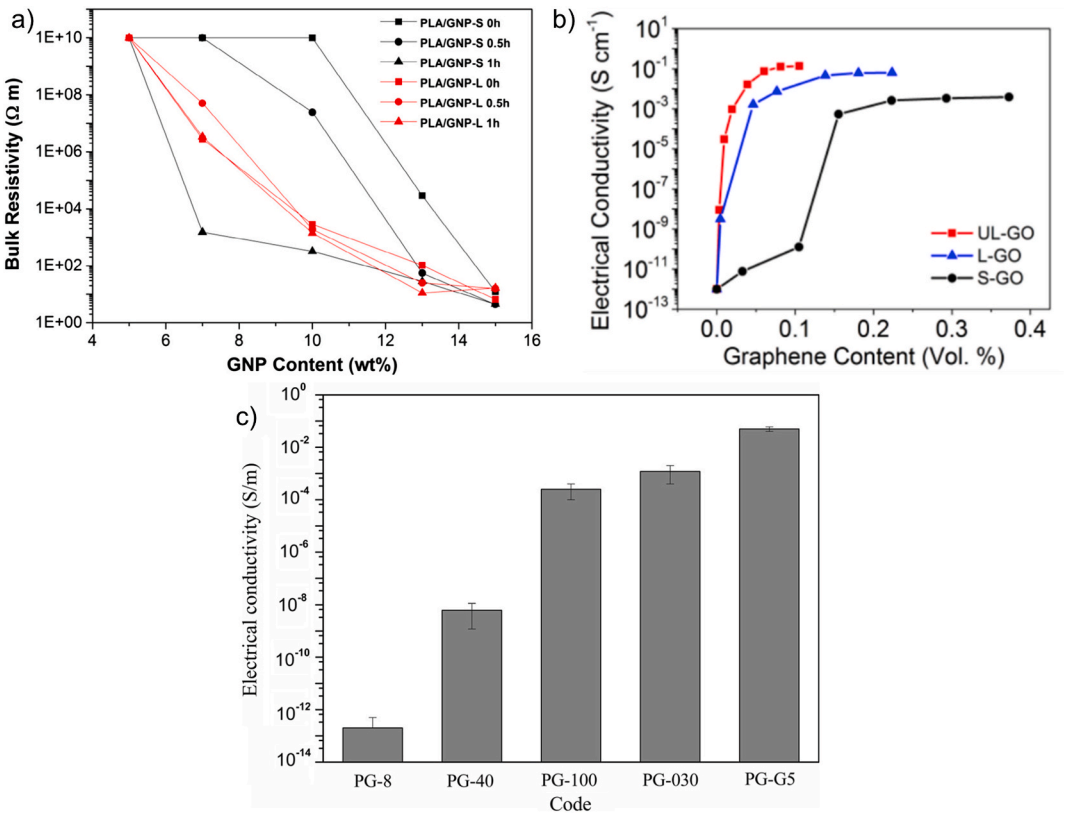

Fig. 9. (a) Electrical conductivity of epoxy matrix filled with different aspect ratio of reduced graphene oxide and different annealing times [64], (b) Electrical conductivity of PLA matrix filled with different sheet sizes of graphene nanoplatelets according to the annealing time [67], (c) Electrical conductivity of PP matrix filled with different aspect ratio of graphene sheets [66]. Reproduced from Refs. [64,66,67] with permission. (A colour version of this figure can be viewed online.)

difference of the electrical conductivity proved that the thickness plays an important role for improving conductivity of the nanocomposite. To summarize, a larger diameter and a thinner thickness, that give the highest aspect ratio, allow to transport more easily electrons between platelets and to drive down the percolation threshold. This part proves also that to produce performant nanocomposite, larger graphene particles are preferred to smaller particles.

2.2.2. *Chemical interaction to enhance percolation and electrical conductivity*

Graphene functionalization is one of the ways to improve affinity with the polymer matrix and to get a better dispersion and a lower percolation threshold. Non-covalent functionalization allows to modify graphene behavior in a system by physical interaction with other molecules such as surfactants. Covalent functionalization is another possibility which allows to attach organic molecules by chemical bond formation on graphene. On the one hand, to keep the graphene electronic structure intact with sp^2 domains, it is preferable to use non-covalent functionalization. This method is based on molecule adsorption by π-π interaction between molecules bearing aromatic rings and graphene [68]. The non-covalent functionalization is used for pristine graphene because of its low surface reactivity. On the other hand, the chemical functionalization is particularly attractive, shows good processability and a real enhancement of nanoparticle/matrix interaction. The covalent functionalization occurs mainly on the oxygenated groups of graphene oxide such as epoxides and/or hydroxyls [69]. Chemical modification of graphene by covalent functionalization entails inevitably the formation of sp^3 regions for the functionalized zone. If we consider graphene oxide (GO), the structure contains both sp^2 (with π orbitals) and sp^3 (π orbitals replaced by σ orbitals) regions [70,71]. This modification removed π electron vs the initial organization of carbons, which is responsible to the low energy band gap between the conduction band and valence band. Consequently, the carrier density, the electron mobility and electrical conductivity are affected. Even after a reduction of GO, disorders are still present in the structure.

To enhance graphene dispersion in polar polymer matrix, two covalent functionalization ways, "grafting from" and "grafting to", are effective. It consists in modifying graphene structure by fixing polymer chains. "Grafting from" involves the use of graphene as an initiation site to grow a polymer. "Grafting to" consists in a chemical reaction between graphene with functional groups and a polymer [72]. "Grafting from" is more suitable for producing a high graft density but this process is less easy to implement than "grafting to" [73].

2.2.2.1. "Grafting to" method. The "grafting to" method is performed in two steps: firstly, the polymer chain is synthesized and then it is appended with the reactive graphene functional groups via esterification, amidation, click chemistry, nitrene chemistry or radical addition [74]. This method is a versatile approach for grafting polymers on graphene surface. The steric hindrance limits the production of graphene grafted with high molecular weight polymer contrary to the "grafting from" method. It is then preferable to use low molecular weight for "grafting to" method [75]. Park et al. [76] used a covalent functionalization carried out by grafting alkyl chains and benzyl moieties on graphene oxide surface that forms functionalized graphene oxide (FGO). Visual observations of cast films and optical micrographs show a better dispersion of graphene in PE matrix. Indeed, PE is a non-polar and hydrophobic polymer that makes difficult the dispersion of GO which is hydrophilic. This improvement is directly benefit for the electrical property of the nanocomposite as shown by the measurement of the film surface resistance (Fig. 10a and b). Indeed, at 3 wt% of nanoparticles for LLDPE, the resistance strongly decreases by going from 10^{12} Ω with TRG (thermally reduced graphene) to 10^6 Ω with FGO. Other ways to functionalize with PE chains with two different paths

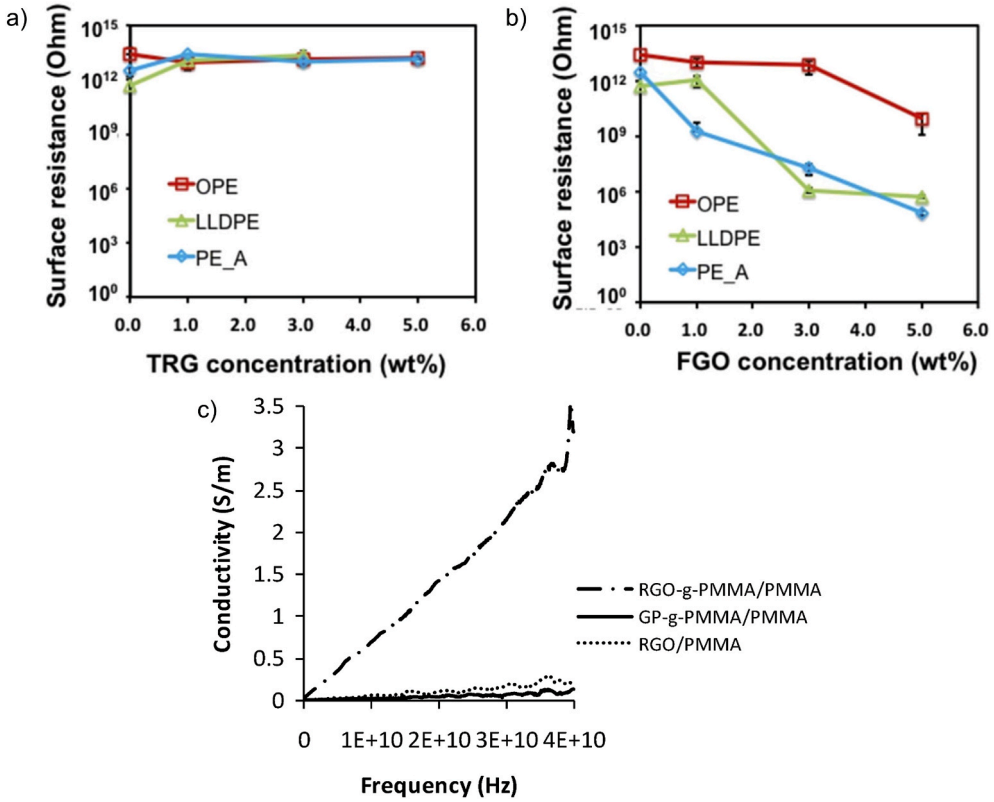

Fig. 10. Surface resistance of PE matrix filled by (a) thermal reduced graphene oxide (TrGO) or by (b) functionalized graphene oxide (FGO) [76], (c) Electrical conductivity of nanocomposite PMMA filled different rGO structure [84]. Reproduced from Refs. [76,84] with permission. (A colour version of this figure can be viewed online.)

were tested by Guimont et al. [77], but with graphite instead of graphene. In the first way, a radical grafting reaction was carried out by using benzoyl peroxide approach in the presence of PE chains. The second way used azide end functionalized route. Graphite oxide was used as starting material and after each radical reaction the electrical conductivity of the powder was highest than graphite oxide due to the solvothermal reduction at 150 °C for 6 h. Highest grafting level was identified for the benzoyl peroxide route. With a high level of grafting and a better electrical property (1 order of magnitude) of the functionalized graphite powder, this approach could be suitable for the elaboration of PE/PE-g-rGO nanocomposite.

The same PE matrix was used by *Castelain* et al. [78] but with another strategy. They functionalized graphene via click chemistry method and tried to disperse it in a polyethylene matrix in order to obtain a nanocomposite by solvent casting in xylene solution. Three different click reactions were carried out such as copper-catalyzed alkyne-azide (CuAAC), thiol-ene, thiol-yne, and the functionalized graphene are named respectively GAA, GTE and GTY. The degree of functionalization (mmol of PE grafted per g) was estimated thanks to Thermal Gravimetric Analysis (TGA) by comparing mass loss. TGA shows that GTY presents the largest functionalization degree. This result can be explained by the fact that thiol-yne allows the incorporation of two polymer chains. After graphene modification, Raman spectroscopy of GTE shows the lowest defect level which is logical since the TGA shown that GTE has the lowest functionalization degree so most of the sp^2 domains are intact. Indeed, the measured electrical conductivity of GTE is relatively high (12.6 $S.cm^{-1}$) and closed to the starting graphene (25 $S.cm^{-1}$). The other modified GTY and GAA graphenes have lower electrical conductivities of $1.52.10^{-4}$ $S.cm^{-1}$ and $3.35.10^{-4}$ $S.cm^{-1}$, respectively. Raman characterization can explain the impact of functionalization on electrical property. Effectively, according to the type of functionalization, I_d/I_g ratio value changed [79]. Ratio of I_d/I_g changed strongly with the alkyne pretreatment from 1.5 (graphene) to 1.1. The other functionalization also modified ratio value with 1.75 for GAA, GTY and 1.9 for GTE. The addition of chemical modification inevitably leads to a drop in the electrical conductivity. The creation of defects by new covalent bonds disrupts sp^2 graphene structure which entailed a decrease of the electrical conductivity. The greater amount of polymer coated on the graphene sheet and chemical modification performed on graphene prevents electron to circulate along the graphene structure. Moreover, graphene used at started material presents too many defects even before chemical modification. Indeed, I_d/I_g graphene ratio must be lower than 1.5. The profile of the graphene spectra seems to be similar to the insulating graphene oxide [80,81]. Its electrical conductivity of 25 $S.cm^{-1}$ is low compared to several studies [82,83]. It is then expected to lead to low electrical performance for the nanocomposite. To illustrate the impact of these properties on the final nanocomposite, modified graphenes were mixed with an insulating HDPE matrix. The results show that GTE-HDPE nanocomposite is the only composition which can display an electrical conductivity measurement equal to 10^{-7} $S.cm^{-1}$ for a graphene content of 0.74 wt% knowing that the electrical conductivity of HDPE is 10^{-14} $S.cm^{-1}$. For the other modified graphenes, nanocomposites are insulating. The high degree of covalent functionalization for GAA and GTY destroyed too much the graphene sp^2 structure that leads to an insufficient electrical conductivity for improving final property of the nanocomposite. In the case of pristine graphene, the insulating property of the nanocomposite is due to the bad dispersion in the matrix. This article shows that the control of covalent functionalization degree and dispersion at the same time are the main issues to obtain the best material.

Another way to functionalize graphene and improve its dispersion is by grafting polymer chains on its basal or edge sheets. *Vuluga* et al. [84] prepared rGO from GO grafted with PMMA and obtained relatively high electrical conductivity. They mixed GO with poly (methyl methacrylate) end-capped by an alkoxyamine ($PMMA\text{-}ONR_2$) in a water/toluene

biphasic solution. At 50 °C, the alkoxyamine was removed and PMMA macroradicals were grafted on the sp^2 carbons of GO that was simultaneously reduced into rGO and transferred to the organic phase leading to a homogeneous distribution. The conductivity of the PMMA/rGO (5 wt %) was low and reached 2.10^{-3} S.cm^{-1} at 40 GHz due to the poor dispersion (Fig. 10c), while after the functionalization, the electrical conductivity of PMMA/rGO-g-PMMA (5 wt%) reaches $3.4.10^{-2}$ S.cm^{-1} at the same frequency. This proves that the biphasic process allows to start from a homogeneous dispersion of exfoliated GO on which PMMA can graft and maintain this crucial exfoliation state during GO reduction in order to enhance the dispersion and the final electrical property. More recently, *Lalire* et al. [85] showed the possibility to combine covalent functionalization (by grafting onto method) and electrical conductivity of graphene-like powder. The copolymer of methyl methacrylate and hydroxyethyl methacrylate P (MMA-*co*-HEMA), P (MMA-*co*-HEMA) copolymer, was grafted by an esterification with carboxylic acid present in GO structure and alcohol function from HEMA. Different strategies were carried out with a soft route with nitric acid oxidation and strong oxidation with Hummers' method. The soft route, even with the copolymer functionalization, allowed to maintain electrical property. The strong route required a reduction step thanks to hydrazine hydrate and the functionalization of the copolymer increased the resistivity but maintained sufficient electrical conduction.

2.2.2.2. "Grafting from" method. Similarly, to "grafting to" method, "grafting from" method is a covalent functionalization. This kind of functionalization can disrupt the sp^2 structure of graphene and also decrease the high electrical conductivity of graphene. In some cases, it is necessary to graft molecules with suitable electrical property to hope produce performant electrical nanocomposite. Actually, a recent study of Aguilar-Bolados et al. [86] tested a "grafting from" method which corresponds to an atom transfer radical polymerization using activators regenerated electron transfer (ARGET-ATRP). Graphene oxide was used as the started material. This method is a subclass of ATRP process, the most common is SI-ATRP. In this article [86], the impact of the graphene oxide modification with poly (monomethyl itaconate) (PMMI) by ARGET-ATRP method on electrical conductivity of the nanoparticle was studied. PMMI molecule has a high electrical conductivity and when it is grafted on graphene, the electrical conductivity goes to $5.04.10^{-2}$ S.cm^{-1}. This value is high compared to GO powder which achieved an electrical conductivity of 10^{-8} S.cm^{-1}. It proved that this kind of method is suitable for electrical application such as for electrode.

2.2.3. Graphene functionalized by surfactant species

A lack of articles has shown that the real efficiency of covalent functionalization of graphene for electrical applications is currently not assured since the covalent modification of graphene leads to a destruction of the sp^2 structure and consequently disrupts the electrical conductivity [87].

Non-covalent functionalization can also improve the dispersion of graphene in the polymer without disrupting the sp^2 structure of graphene thanks to physical interaction between graphene and surfactants. As first glance, this kind of functionalization can allow to obtain high electrical conductivity. However, results of Lotya et al. [88] showed that the conductivity of their graphene functionalized with sodium dodecylbenzene sulfonate (SDBS) decreased by adding surfactant. Another study of Mohamed et al. [50] contradicts these observations by incorporating graphene functionalized with surfactants such as SDBS and showed that electrical conductivity of graphene/rubber nanocomposite increased. The natural rubber displayed an electrical conductivity equals to $1.51.10^{-14}$ S.cm^{-1} while the nanocomposite rubber/graphene without surfactant (pure graphene) reached $3.56.10^{-12}$ S.cm^{-1}. The graphene/SDBS, enhanced the electrical conductivity of 6 orders of magnitude with a value equal to $3.04.10^{-6}$ S.cm^{-1}. It seems that the SDBS surfactant stabilizes the graphene dispersion. By comparing these two articles of Lotya et al. [87] and Mohamed et al. [88], it proves that it is preferable to use modified graphene, even if it decreases its electrical conductivity, with high stabilization in polymer matrix than to use pure graphene with high electrical conductivity but with a low stabilization in polymer matrix with aggregated graphene.

Other methods are known such as functionalization with plasma or with chlorine which are more appropriate to not disturb the structure of graphene [89].

3. Graphene/multiphase polymer blends nanocomposites

3.1. Polymer blend morphology

Improving the electrical conductivity can be achieved by localizing filler in one component or at the interface. The latter morphology can be explained by the double percolation concept. This concept was for the first time proposed by Sumita et al. [90] for carbon black particles in a co-continuous polymer blend which proved an improvement of the electrical conductivity. Then, several investigations were based on double percolation with different fillers such as carbon nanotube, carbon fiber and graphene [91–93]. The understanding of fillers migration mechanism and the morphology of polymer blends is essential to predict graphene localization and performance.

3.1.1. Thermodynamic for binary polymer blends

Polymer blends are obtained by mixing two or more polymers in order to acquire new material with improved properties. The first element to take into account is the miscibility of these polymers to know if the mixture will be heterogeneous or homogeneous, in other words, immiscible or miscible, respectively. It can be predicted by calculating the free Gibbs energy, given by equation (4):

$$\Delta G_m = \Delta H_m - T\Delta S_m \quad (4)$$

ΔG_m is the free energy of mixing per unit volume, ΔH_m is the enthalpy and ΔS_m the entropy of mixing. For a homogeneous system, ΔG_m is negative but most of the times, polymer blends are immiscible and give ΔG_m positive due to a negligible entropy. Indeed, number of molecular configurations are restricted, and the entropy is also extremely low [94]. By mixing two polymers, miscible polymers lead to one-phase morphology. Whereas, immiscible and in some cases partially miscibility polymers show two-phases morphology. Immiscible polymer blends are the suitable morphology for nanocomposite systems with ultralow percolation thresholds. Hence, next parts of this article will deal with immiscible polymer blends only.

3.1.2. Effect of different parameters on polymer blending

3.1.2.1. Binary polymer blends. By changing the polymer proportions, it is possible to control the blend morphology. Indeed, in a binary polymer blend, the increase proportion of one phase allows to go from a dispersed phase/matrix morphology to co-continuous phases morphology. One polymer phase at lower proportion tends to be dispersed into droplets in the major phase, leading to a "sea-island" morphology. The co-continuous behavior is illustrated by a phase inversion interval at which volume fraction values form a perfect co-continuous morphology (Fig. 11a). The length and the position of the dual phase region in Fig. 11a, depend on several parameters such as the polymer viscosity and elasticity and their interfacial tension [95]. When the volume fraction value is higher than the phase inversion interval, the dispersed/matrix morphology is observed again. A coalescence phenomenon can explain the morphology evolution [96]. The transition from nodules shape (dispersed phase) to continuous domains is possible using four steps as shown in Fig. 11b.

It is possible to predict the phase inversion interval. One of the simplest models was described by Paul and Barlow [98] which allows

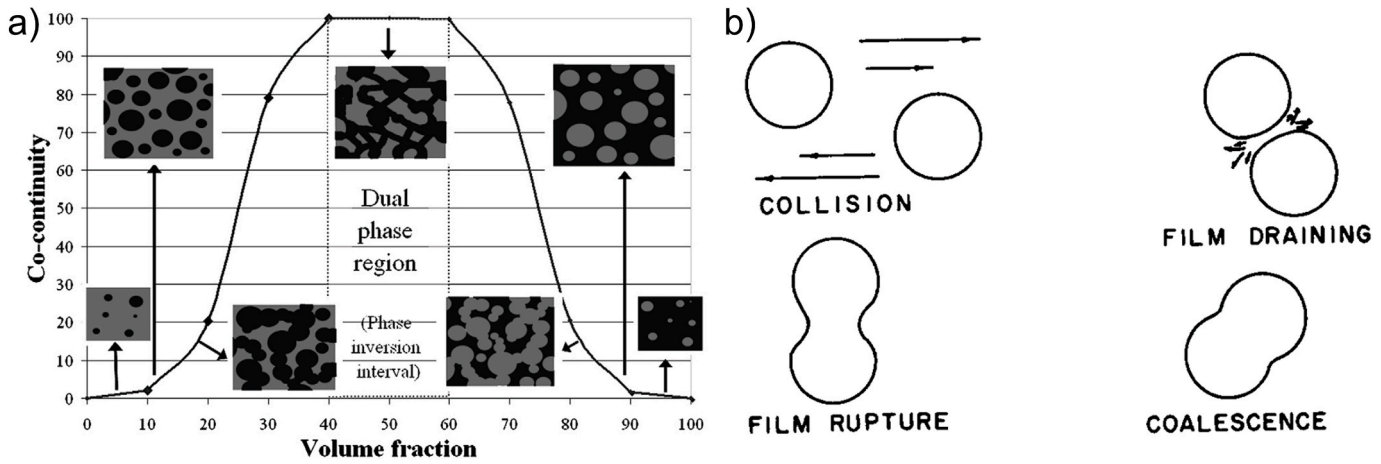

Fig. 11. (a) Morphology evolution versus volume fraction of one phase in an immiscible binary polymer blend [97], (b) Coalescence phenomenon illustration [96]. Reproduced from Refs. [96,97] with permission. (A colour version of this figure can be viewed online.)

estimating the phase inversion point from the viscosity ratio (Fig. 12). By using this simple model, two-phase polymer blends show that for components of equal viscosity, phase inversion occurs at a volume fraction of 0.5. If the viscosity of one component differs significantly from the other, the phase inversion point is shifted towards compositions richer in the high viscosity phase [99]. This is due to the fact that the less viscous component tends to encapsulate the more viscous one. However, other models exist that include the mixing conditions, the capillary instabilities, the phases elasticity [100].

Another important parameter for phase inversion is the interfacial tension. As shown by Bhadane et al. [101] in the case of a PP/EPDM blend with low interfacial tension, a small difference in the viscosity ratio of the two phases does not affect the morphology. Moreover, lower interfacial tension leads to a broader composition range of co-continuous structures.

3.1.2.2. Ternary polymer blends. Like binary polymer blend, ternary polymer blend morphology is depending on interfacial tension, viscosity, and proportion of each polymer phase. For ternary polymer blend, one phase tends to be located between the two others which gives a complete wetting (Fig. 13a). Another morphology is the partial wetting

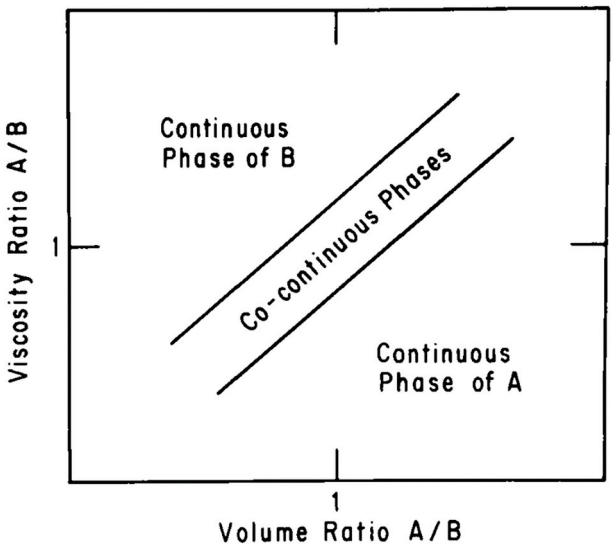

Fig. 12. Relation between the volume range of a co-continuous structure and the viscosity ratio [102]. Adapted from Ref. [102] with permission. (A colour version of this figure can be viewed online.)

where all phases are in contact to each other. Both morphologies can be predicted by the spreading coefficient theory defined by Harkins equation (5):

$$\lambda_{ij} = \gamma_{jk} - \gamma_{ik} - \gamma_{ij} \quad (5)$$

λ_{ij} is the spreading coefficient which defines the tendency of polymer i to encapsulate polymer j in polymer matrix k. γ are the interfacial tensions. A positive λ_{ij} corresponds to a complete wetting where polymer i spreads over polymer j, leading to a matrix/core-shell morphology such as in Fig. 13a. A negative value of the three spreading coefficients ($\lambda_{ij}, \lambda_{ik}, \lambda_{jk}$) gives a partial wetting behavior (Fig. 13b). Ravati et al. [97] studied the case of a PS/PMMA/HDPE blend, for which the spreading coefficient $\lambda_{PS/PMMA}$ is positive (2.6 mN m^{-1}). Considering this value, we can predict that PS spreads over PMMA. This is confirmed by the FIB-AFM image of a PMMA/PS/HDPE (40/20/40) polymer blend (Fig. 13c). The proportion plays an important role to determine the morphology (Fig. 13d). Indeed, by modifying the proportion of the three polymers (PMMA/PS/HDPE), four sub-morphologies can be observed such as matrix/core-shell dispersed phase, tri-continuous, matrix/two separate dispersed phases and bi-continuous/dispersed phase morphologies. To reach a tri-continuous structure, the third minor polymer phase can be a copolymer which has a certain affinity with the two other phases to act like a compatibilizer, or a polymer for which thermodynamic allows it to be localized at the interface of the two other major polymers.

Besides thermodynamic considerations, final morphology of a ternary blend can also be dictated by viscosities of each polymer phase [103]. The ideal tri-continuous structure depends on the viscosity ratio between each component. Different viscosity ratio between two polymer phases can totally change the morphology of the polymer blend [104]. The lowest viscosity phase tends to encapsulate the highest viscosity phase [105].

3.2. Nanoparticles influence the blend morphology

As known and developed in several reviews, articles and books bearing with polymer blend nanocomposites, nanoparticles can greatly affect the final morphology of the material [106,107]. All types of nanoparticles have an influence on the final morphology. Nanoparticles can cause a refinement, a coarsening, an irregular shape or a co-continuity (Fig. 14A). It depends on their size, shape, aspect ratio and surface chemistry. As shown by Cai et al. [108] who used TiO_2 nanoparticles in a PA6/PS polymer blend, a variation of nanoparticle loading affects the continuity of the PA6 phase and the morphology of the entire system (Fig. 14B).

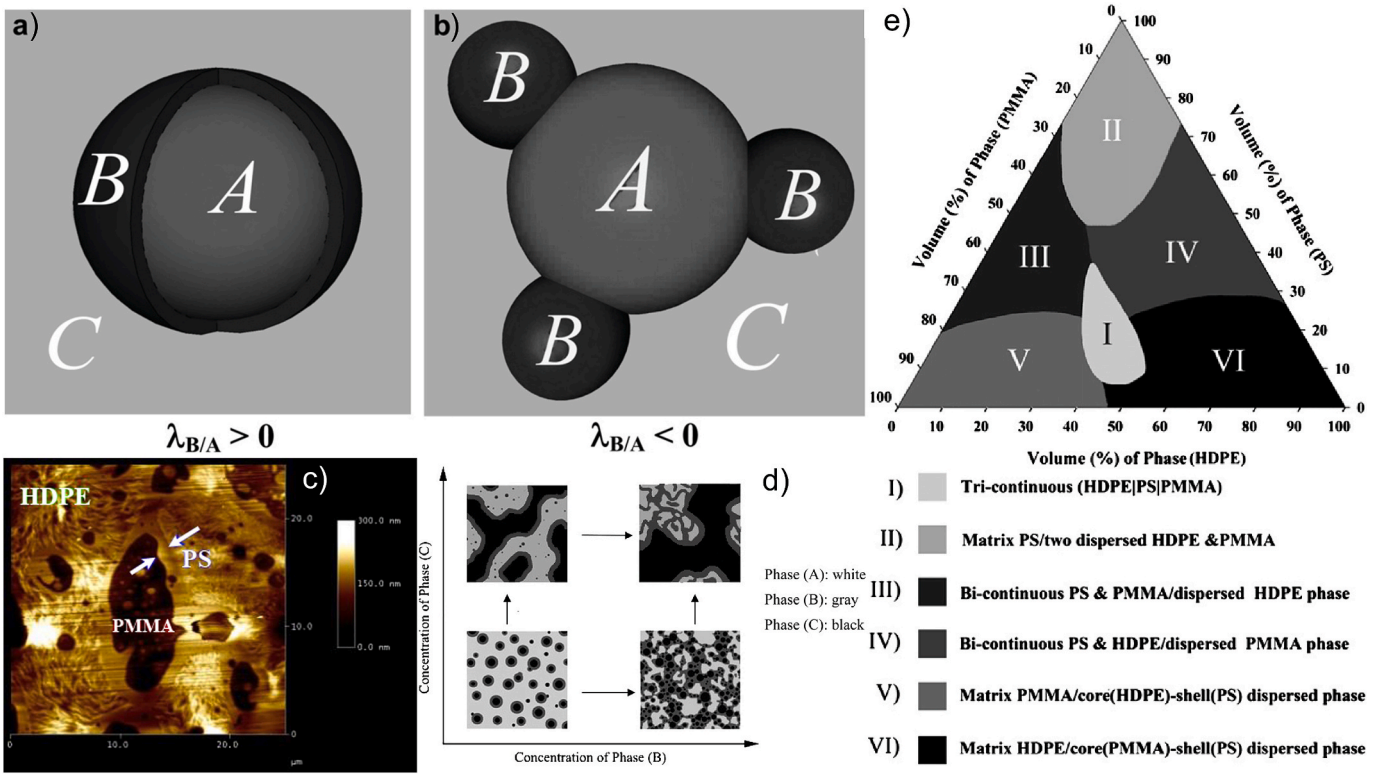

Fig. 13. Schematic representation of (a) complete wetting: the case that one phase locates between two other phases, and (b) partial wetting: the case that all phases are in contact with each other. (c) FIB-AFM image of complete wetting morphology for ternary 40/20/40 HDPE/PS/PMMA blend showing the layer of PS at the interface of HDPE and PMMA. (d) Evolution of the morphology in a ternary A/B/C blend demonstrating complete wetting as a function of the concentration of phases B and C. Phase A concentration is held constant. (e) Triangular concentration diagram showing the composition of the various ternary HDPE/PS/PMMA blends [97]. Reproduced from Ref. [97] with permission. (A colour version of this figure can be viewed online.)

The final morphology is greatly influenced by the localization of the nanoparticles, and especially the localization of graphene in the present case. Whereas this localization is itself influenced by several parameters depending on the polymers, the graphene, and the process. Indeed, a localization of nanoparticles at the interface can suppress the coarsening mechanism. This phenomenon was observed several times with a localization at the interface of graphene or even with other nanoparticles like silica which stopped the coarsening during the annealing [109,110].

Regarding the co-continuous morphology, generally speaking, the polymer amount at which phase inversion occurs is expanded when nanoparticles are added. In other words, the zone of co-continuity in a graph bearing both polymer continuity percentages versus polymer amounts is larger. In the next parts we will first explore the thermodynamic prediction of graphene localization in an immiscible polymer blend. Then, kinetics parameters will be considered to explore the localization. Finally, we will focus on the influence of graphene on the co-continuity of binary blends.

Nanoparticles have also an impact on the matrix viscosity. Usually, whatever the nanoparticle surface treatment or aspect ratio, the viscosity of the matrix/nanoparticle composite is intended to increase. Improvement of modified filler-matrix interaction normally leads to an increase of the viscosity polymer due to chain entanglement [111]. However, some authors reported a decrease of the viscosity of the matrix when graphene, and especially rGO were added. Indeed, Shen et al. [112] showed the evolution of the complex viscosity before and after adding 5 wt% of rGO in PLA and EVA matrix (Fig. 15). They explained this decrease by a possible chemical interaction between unremoved oxygen-containing groups on rGOs and PLA chains. Besides the possible degradation of the matrix during the melt-compounding or the presence of solvent which increase free volume, the viscosity reduction was already explained in the literature by several mechanisms [113,114]. These phenomena have already been reported a few times and are generally encountered with nanoparticles with low charge quantity in polymer matrices and is called “Non-Einstein like” behavior [115,116]. The low surface friction of graphene or graphite can also induce a viscosity reduction due to an interfacial slippage between polymer chains and the graphite surface [117]. It was also demonstrated with nanoparticles grafted with single PS chains mixed in PS matrix and a low friction of the nanoparticle was associated to the viscosity reduction [118]. Despite the improvement of the matrix-filler affinity, the low surface friction can lead to viscosity decrease. Other explanation is a selective adsorption mechanism described as a physisorption of the highest molar mass polymer chains onto the nanoparticle surface with a surrounding lower molar mass molten matrix [119].

3.3. *Selective localization of graphene filler*

Graphene localization depends on thermodynamic parameters (wetting coefficient or wettability parameter), kinetic effects (mixing sequence, mixing time, shear rate) and rheological properties (viscosity of each polymer phase). The final properties of filled polymer blends are largely influenced by the graphene localization. That is why studies about phenomenon which reign around graphene behavior in multiphase structures are necessary. Theoretically, to significantly reduce the percolation threshold, achieve a co-continuous structure with filler localized at the interface is essential [120].

3.3.1. *Thermodynamic predicts the graphene localization*

3.3.1.1. Prediction of the graphene localization with wetting parameter. The graphene localization in a polymer blend can be predicted by

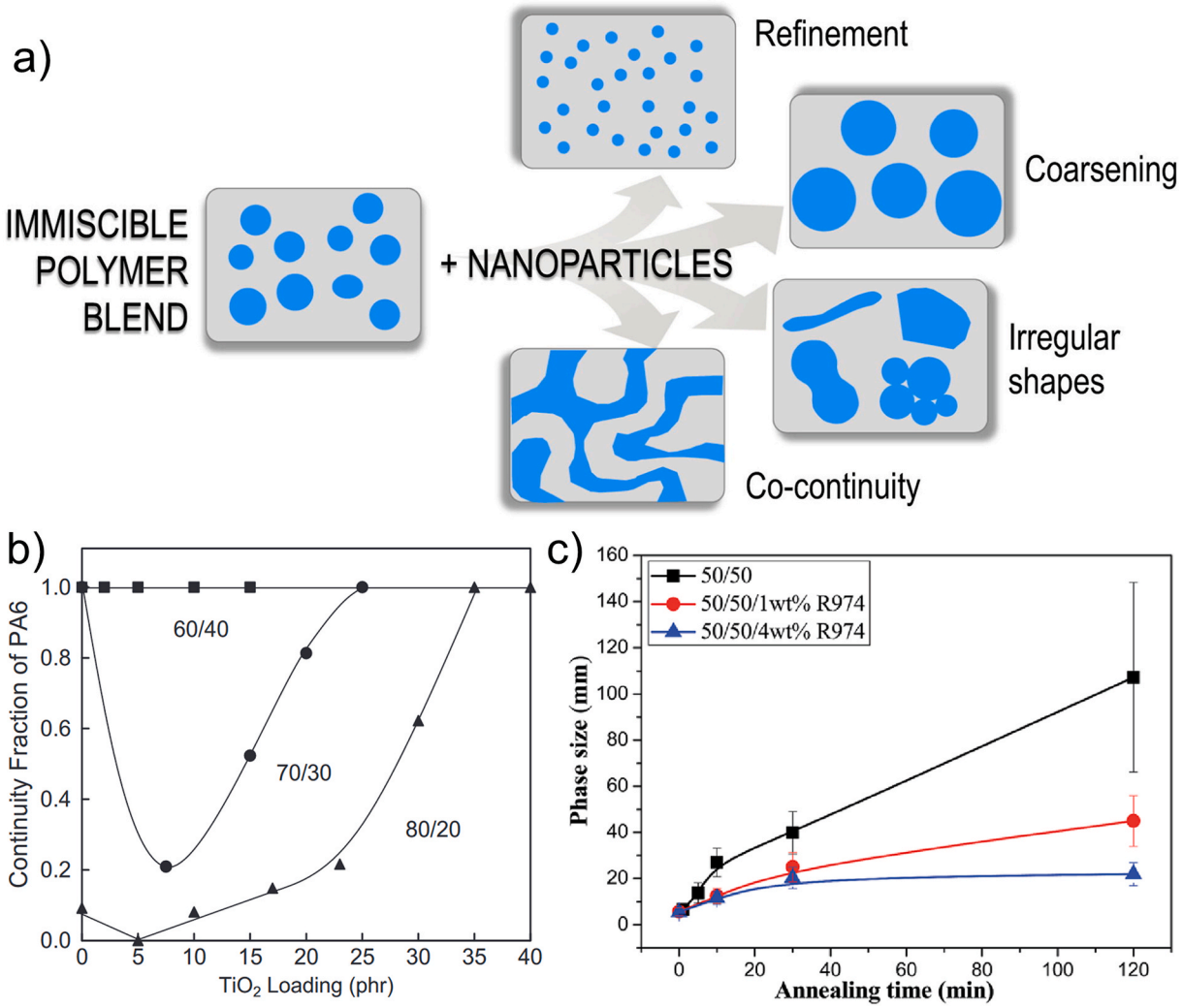

Fig. 14. (A) Schematic of different nanoparticles effect on morphology [107] (B) Dependence of the PA6 continuity fraction on TiO_2 content for PS/PA6/TiO_2 mixtures with various weight ratios of PS to PA6 [108], (C) Phase sizes of pure and nano-SiO_2 particle filled 50/50 PP/PS blends after annealing at 190 °C for various time [109]. Reproduced from Refs. [107–109] with permission. (A colour version of this figure can be viewed online.)

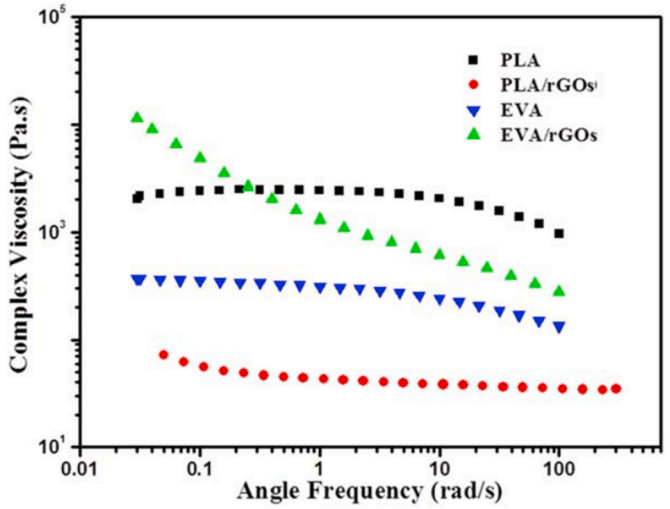

Fig. 15. Variation of complex viscosities of the PLA, EVA, PLA/rGOs, and EVA/rGOs. The content of rGOs is 5 wt% [112]. Reproduced from Ref. [112] with permission. (A colour version of this figure can be viewed online.)

calculating the wetting parameter. The Young's equation (equation (6)) allows to estimate the thermodynamic equilibrium [121]:

$$\omega_a = \frac{\gamma_{g-A} - \gamma_{g-B}}{\gamma_{A-B}} \tag{6}$$

γ_{x-y} is the interfacial tension between two components, g corresponds to graphene, A and B are polymers. The graphene localization can be predicted according to the wetting parameter, as shown Table 1.

Interfacial tension between the two polymers is classically calculated from the surface tension of the two polymers using the Wu's harmonic mean average equation given in equation (7):

$$\gamma_{ij} = \gamma_i - \gamma_j - 4\left(\frac{\gamma_i^d \gamma_j^d}{\gamma_i^d + \gamma_j^d} + \frac{\gamma_i^p \gamma_j^p}{\gamma_i^p + \gamma_j^p}\right) \tag{7}$$

Table 1
Graphene localization in a co-continuous structure of an immiscible polymer blend.

Wettability coefficient ω_A	Graphene localization
$\omega_A < -1$	Polymer A
$-1 < \omega_A < 1$	AB Interface
$\omega_A > 1$	Polymer B

Table 2
Surface energy of polymers and graphene at different temperatures.

Material	Surface energy at room temperature	Surface energy at 240 °C
PA6	37.34	22.94
PEO	25.58	14.40
Graphene	54.37	32.82

d and *p* represent dispersive and polar contributions of the surface tensions.

Whereas, the interfacial tension between the filler and one polymer is classically calculated from the surface tension of the two components using Wu's geometric mean equation (not shown here) [122]. However, generally speaking, there are lots of different ways to estimate the interfacial tension between two polymers [123], especially ones taking into account the melting state and the processing temperature [124]. The surface tension of the filler can be estimated by different methods more or less reliable [125], that we will discuss in the paragraph II.3.1.2.

This model seems to be promising to predict the localization. However, discrepancies are inevitable between experimental and theoretical approaches since predictions are based on thermodynamic calculations. Indeed, kinetic and processing parameters are essential to take into account. These factors alter inevitably the migration of graphene and its final localization. For polymer blends with high interfacial tension, graphene nanoparticles can be localized at the interface to reduce the interfacial tension and obtain a stable thermodynamic system.

Hadaeghnia et al. [126], predicted the localization of graphene nanoparticles in a blend of PA6/POE by thermodynamic calculation (wettability coefficient). Surface tensions were first measured by contact angle at room temperature (Table 2) and interfacial tension were determined with Wu's mean and harmonic equations (Table 3). The extrapolation of the surface energy at 240 °C, showed a decrease for each component. Interfacial tensions of graphene/polymer showed a better affinity of graphene for PA than POE. The Young's equation was used to determine wettability coefficient and to predict localization of graphene.

By comparing Tables 1 and 3, graphene should be located at the interface with more affinity with PA6. However different morphologies were observed and did not matched with the thermodynamic predictions due to kinetic factors. For a ratio of 60/40 (PA6/POE), in the case of a POE masterbatch (graphene was previously melt mixed with POE), small amounts of graphene were located at the interface and the rest in the POE. In the case of a PA6 masterbatch, graphene was located in the PA6 phase. This article proved that considering only thermodynamic parameter can be limited to get the final morphology. Other factors must be taken into account and techniques to determine surface energy of each material are important and must be considered.

Table 3
Interfacial tension and wettability coefficient to predict graphene localization.

Method	$\gamma_{PA6/Graphene}$	$\gamma_{POE/Graphene}$	$\gamma_{PA6/POE}$	ω
Mean harmonic equation	3.75	7.25	3.50	−0.99
Mean geometric equation	1.91	3.78	2.03	−0.92

3.3.1.2. Interfacial tension calculation method. As shown in the previous section, to predict wetting parameter, we must estimate the surface energy of each component used in the system. To estimate interfacial tension between a polymer and graphene, one favored method is the contact angle measurement [127]. It is important to note that several parameters must be fixed and checked at each measurement to obtain an efficient contact angle comparative study. Indeed, environment, type of substrate, and liquid used can change the wettability of the graphene sheet [118,128,129]. Since graphene is a 2D material and does not have a bulk phase, the surface energy cannot be applied to an isolated graphene monolayer. Graphene must be grown or transferred on a substrate to perform the contact angle measurement. The type of liquid used for the measurement allows to determine polar or dispersive components. The water generates polar interaction and non-polar liquid such as diiodomethane generates dispersive interactions. The substrate which is used to deposit graphene has an influence on the surface energy and the wettability [130]. Indeed, numerous articles tried to measure the contact angle of graphene on different substrates (Table 4). Graphene has a wetting-transparency behavior regarding the interaction between water and underlaying substrate that can also perturb the contact angle measurement and then give a wrong value of graphene surface energy. That's why it is important to fix parameters in order to be in the same conditions. The contact angle does not allow to access the surface energy directly. Several models must be used like Owens and Wendt [131], Fowkes [132], or Li and Neumann [133] to determine the surface energy from the contact angle. However, these contact measurements can be influenced by airborne contaminants adsorption [134].

Van Engers et al. [135] directly measured adhesive forces and surface energies of a CVD-grown graphene in dry nitrogen, water, and sodium chlorate by using a modified surface force balance presented schematically in Fig. 16a and b. Graphene sheets are mounted on two cylindrical lenses. The measurement can give a precise value of the mechanical pull-force by using Hooke's law: $F_{adh} = k_{spring}.d_{jump}$.

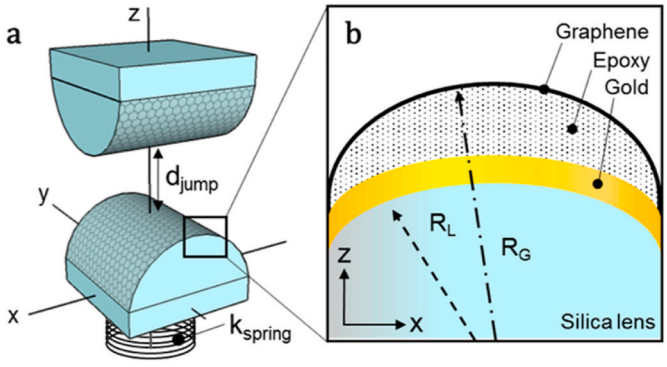

Fig. 16. (a) Schematic illustration of the crossed-cylinder, (b) Scheme of multilayer geometry consisting of a smooth sheet of single layer graphene (SLG) or few layer graphene (FLG) glued onto epoxy, supported by a gold-covered silica lens of curvature R_L = 10 mm. Because of thickness inhomogeneity in the epoxy layer (exaggerated in the figure), the actual surface curvature (R_G) differs from R_L [135]. Reprinted (adapted) with permission from Ref. [135]. Copyright 2017 American Chemical Society. (A colour version of this figure can be viewed online.)

Table 4
Different surface energy measurements by contact angle according to the substrate and the graphene synthesis.

Graphene synthesis	Graphene substrate	Surface energy of graphene (mJ/m^2)	Surface energy of substrate (mJ/m^2)	Ref.
Chemically exfoliated flakes	Silicon	46.7	–	[128]
CVD	Copper	62.2	–	[129]
CVD	PDMS	40.4	24.1	[130]
CVD	Glass	48.8	72.6	

k_{spring} is the spring constant and d_{jump} is the distance of the jump out.

Then, the Johnson, Kendall, and Roberts (JKR) relation allows to determine the surface energy γ from the F_{adh} (8):

$$\gamma = \frac{F_{adh}}{3\pi R_G} \quad (8)$$

F_{adh} is the pull-force, R_G is the actual surface curvature. Contact angle method gives a graphene energy surface around 50 mJ/m^2. However, by surface force balance (SFB) method and with JKR theory the obtained surface energy is around 115 mJ/m^2. This large disparity between those values questions the validity of the SFB method.

3.3.1.3. Surface energy of different graphene structure to predict the affinity with polar and apolar polymers. Modification of graphene via oxidation, or functionalization entails variation of its surface energy and also entails variation in thermodynamic prediction. Wang et al. [128] measured contact angle and calculated surface energy with Young's equation for three materials: graphite, graphene and graphene oxide. Graphite exhibited a surface-energy of 54.0 mJ m^{-2}, graphene: 46.7 mJ m^{-2} and graphene oxide: 62.1 mJ m^{-2}. The presence of functional groups on graphene entails an increase of the polarity and also an increase of the surface energy. This was proved by Bai et al. [136,137], by comparing C/O ratio with XPS and the surface energy. Three powders GNP, GO and rGO were analyzed that display a C/O ratio of 50.7, 10.3 and 1.5, respectively. Surface-energies associated are 29.42 mJ m^{-2}, 31.2 mJ m^{-2}, and 46.6 mJ m^{-2} for GNP, rGO and GO, respectively. The polarity component δ_p follows the reverse evolution of C/O ratio values. These evolutions will have an impact on nanoparticles affinity with polymer matrices. If the polarity changes, that induces a modification of the surface energy. It leads to a modification of the affinity between nanoparticles and polymer and also of the interfacial energy. Effectively, PLA has a surface energy of 41.48 mJ m^{-2} and PS of 29.54 mJ m^{-2}. PLA shows a higher polar component than PS due to the presence of oxygen group on PLA. In these articles, rGO seems to be located at the interface of the co-continuous PLA/PS blend. On the contrary, GNP nanoparticles are located in the PS matrix. These behaviors are logical, the most polar GO nanoparticles tend to be located at the interface. On the contrary, GNP, the less polar nanoparticle, tends to penetrate in the PS matrix due to a better affinity, a smaller interfacial energy with PS.

To resume, uncertainties of surface tension measurements and the existence of numerous models to calculate interfacial tension can lead to differences between the reality and the predictions. Moreover, it is necessary to investigate the mechanism of graphene migration and all the parameters that can influence the final graphene localization.

3.3.2. Mixing sequence and time effect

Kinetics parameters must be considered for the final localization of nanoparticules into a blend. This is especially linked with the migration mechanisms of NPs (and graphene in our present case) that are briefly described previously. To bring into play those migration mechanisms, it is possible, during the melting step, to vary the sequence of mixing of the three components (two immiscible polymer and one nanoparticle). Four mixing sequences are possible.

- Polymers and nanoparticles are mixed simultaneously.
- Nanoparticles are added to the pre-mixed molten blend.
- Nanoparticles are pre-mixed with the polymer with which they have the best affinity. And the second polymer is further added.
- Nanoparticles are pre-mixed with polymer with which they have the lowest affinity. And the second polymer is further added.

Liebscher et al. [138] showed that the mixing sequence, mixing time and screw speed of a melt blending process have a real impact on graphene nanoplatelets (GNPs) localization in a PC/SAN polymer blend prepared by melt mixing. 1 wt% of GNPs were added into a co-continuous PC/SAN blend. Thermodynamic predicted that GNPs preferred the PC phase. When GNPs were pre-mixed in PC phase, results showed that they remained in PC matrix after blending with SAN. On the other hand, when graphene was pre-mixed with SAN before adding PC, it tended to migrate through the interface to join the PC phase depending on the mixing speed and mixing time. Longer mixing time and higher rotation speed resulted in smaller GNP platelets dimension. This improves the transfer through the interface to the PC phase. When mixing conditions are softer, some GNPs can stay at the interface. This result is in good agreement with the previous results of the same team [139].

With the same idea, Aguiar et al. [140] studied the mixing sequence effect on the graphene localization in a polymer blend composed of 80/20 PLA/PCL. In this study, graphene nanoplatelets (GNP) were added at a rate of 0.5 wt%. Regarding the parameters that influenced the final localization: (1) $\eta_{PLA} > \eta_{PCL}$, (2) T_m (PLA) $\gg T_m$ (PCL) and (3) GNP should prefer the PCL dispersed phase regarding the wetting parameter. As shown in Table 5, whatever the mixing sequence, GNP were almost all the time localized in the PCL phase (except for the formulation with a pre-mixed in PLA). Since there is not a real difference on the interfacial tension between GNP/PCL and GNP/PLA, and since the interfacial tension between PLA and PCL is low (0.19 mJ m^{-2}), the graphene did not stay in the most viscous phase such as in the case of the system described by Plattier et al. [141] for 60/40 co-continuous PP/PCL filled with carbon black ($\gamma_{PP/PCL}$ = 3.2 mJ m^{-2}). Indeed, GNP had a high tendency to be encapsulated by the PCL phase and to migrate into this low viscosity PCL phase. However, for a pre-mixing of PLA/GNP, where PLA presented a weaker affinity with GNP, finally, nanoparticles were observed in both phases. This was explained by the graphene geometry which exhibited a rapid transfer through the interface.

Tu et al. [142] prepared PE/PP and graphene nanocomposites by melt-compounding. A fraction of 60/40 (PE/PP) was tested and several weight % of graphene were incorporated in this blend according to the type of the mixing sequence in order to determine a percolation threshold. The microstructure of the blend (either co-continuous or PE matrix/PP dispersed phase) is not clearly discussed. Wetting parameter shows that graphene prefers the PE phase. The impact of the mixing sequence on nanocomposite electrical performance was clearly demonstrated (Fig. 17). A premixing with the PP matrix gives the lowest percolation threshold (around 2 wt%) compared to a mixing with all components together (around 3 wt%). Moreover, the electrical conductivity was higher for the premixing with PP with a value of 7.35.10^{-7} S.cm^{-1} compared to 3.18.10^{-8} S.cm^{-1} in the case of premixing with PE. The sequence of (Graphene/PP)/PE leads to a graphene localization at the interface and in one matrix phase, this is why percolation threshold decreases. Mixing sequence has an impact on electrical performance for the melt blending process. But finally, it is thermodynamic laws that guide us in the choice of the mixing sequences. According to the thermodynamic, a specific mixing sequence will be privileged to allow the localization of nanoparticles at the interface.

Göldel et al. [139] studied the transfer through the interface of a co-continuous PC/SAN blend of two kinds of carbon based NPs (carbon nanotubes, CNT and carbon blacks, CB). They showed that the migration depends on mixing time and aspect ratio of nanoparticles. The conclusion of this study is that nanoparticles with high aspect ratio are easier to transfer through the interface than particles with low aspect ratio.

Table 5
Graphene localization according to the mixing sequences at a constant proportions PLA/PCL (80/20 wt%) and 0.5 wt% of graphene [140].

Melt mixing sequence	Graphene localization
PLA/PCL/GNP (all together)	PCL
(PLA/PCL) + GNP	PCL
(PLA/GNP) + PCL	PLA and PCL
(PCL/GNP) + PLA	PCL

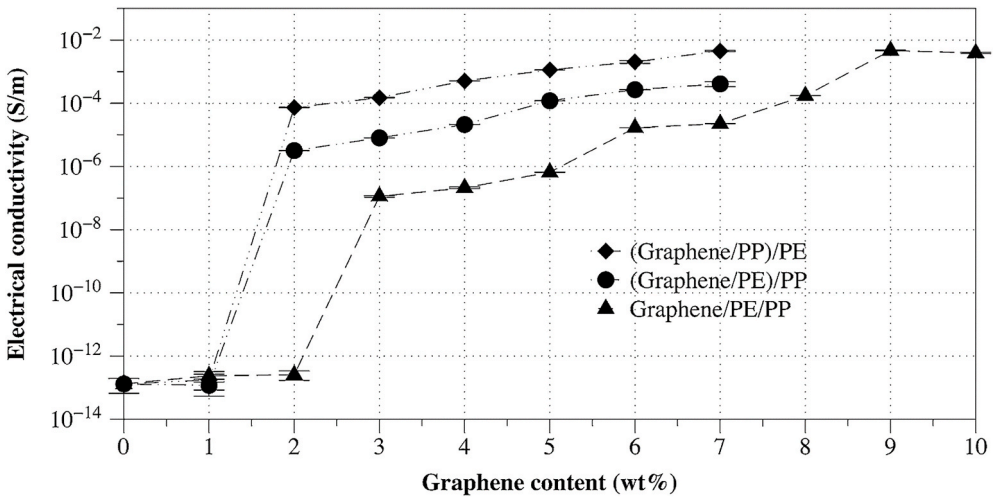

Fig. 17. Electrical conductivity PE/PP/graphene nanocomposites according to the mixing sequence and the graphene content [142]. Reproduced from Ref. [142] with permission. (A colour version of this figure can be viewed online.)

Meaning that low aspect ratio CB have a high tendency to localize at the interface whereas high aspect ratio CNT goes to the PC phase. At the end of the article [139], they proposed a table classifying the transfer speed of several NPs versus their aspect ratio. Stacked microparticles of graphite belong to the group of slow transfer fillers whereas graphene belongs to the intermediate transfer speed (CNT belonging to the fast transfer group). *Kou* et al. [143], tried also different mixing times of graphene nanoplatelets (GNPs) dispersed in a PLA/EVA immiscible polymer blend by melt-blending. Electrical measurements confirmed that mixing time impacts electrical property of the nanocomposite. Effectively, according to the mixing time and the nanoparticles migration, a range of time can be defined corresponding to the graphene localization at the interface before the transfer of graphene to the other polymer phase. This localization favors the contact between graphene and also decreases the percolation threshold at the same time.

Another study of Bai et al. [136] showed the impact of kinetics factor such as mixing sequence and mixing time on graphene localization by preparing nanocomposites with co-continuous PLA/PS and graphene (GNP) via a melt blending process. Knowing that graphene thermodynamically preferred the most viscous PS phase, different mixing sequences displayed different graphene localization. When GNPs were pre-mixed with PLA and then melt-compounded with PS matrix, a high number of GNPs were found at the interface (Fig. 18a). This is due to the high viscosity of PS and relatively large lateral dimensions of GNPs that entrapped the GNPs at the interface. And it is shown that in that case, GNPs remained at the interface even after 60 min of annealing.

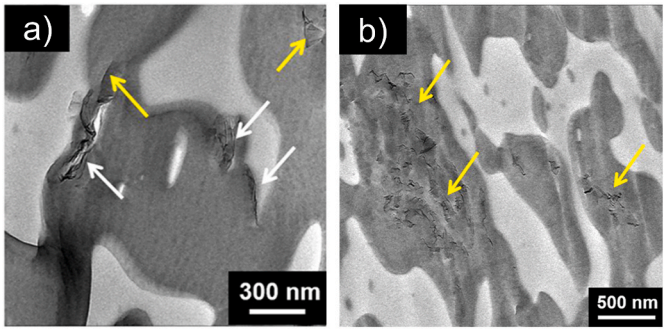

Fig. 18. (a) (PLA/GNP) + PS mixing, (b) (PS/GNP) + PLA mixing; GNP at the interface are indicated by white arrows and GNPs in the matrix by yellow arrows [136]. Reprinted (adapted) with permission from Ref. [136]. Copyright 2018 American Chemical Society. (A colour version of this figure can be viewed online.)

However, for (GNP/PS) + PLA mixing sequence, GNPs remained in the PS phase (Fig. 18b).

This study highlights that in the case of a relatively high interfacial tension blend ($\gamma_{PLA/PS}$ = 2.39 mJ m^{-2}), and with a more viscous preferred phase, it is possible to kinetically trap graphene nanoplatelets at the interface via the control of the melt-mixing sequences, mixing time and shear rates. Then, it is in good agreement with Göldel et al. results shown above [139]. Even though, the electrical conductivity measurements were relatively low (10^{-6} S.cm^{-1} with 0.5 wt% of GNPs), this seems promising for antistatic applications.

More recently, Hadaeghnia et al. [126] compared thermodynamics predictions and kinetics factor and showed that kinetics factors governed the nanoparticles localization. A blend of polyamide 6 (PA6) polyolefin elastomer (POE) and graphene was performed by melt blending. This article proves also that graphene localization is strongly dependent on mixing-sequence.

3.3.3. *Geometrical factor and migration mechanism*

The migration mechanism of nanoparticles depends on many factors such as the shape, size and chemical surface of the nanoparticles but also on the polymer parameters and on melt properties of the polymer blend. Migration through the interface can be illustrated by the motion of fillers in one component, followed by a contact between nanoparticles and blend interface. And in a second step, the nanoparticles are transferred from the first to the second phase. This phenomenon requires driving forces thanks to thermodynamics effects, diffusion, and hydrodynamic stress. Elias et al. [144] illustrated three possible mechanisms, in the case of silica. Brownian motion is one of the three possible mechanisms and depends strongly on polymer viscosity and nanoparticle size. The time required to travel a distance equal to the nanoparticle diameter can be predicted by equation (9). In the case of 2D nanoparticle like graphene, the corresponding rotary diffusivity is determined by equation (10) [145]:

$$t_d = \frac{D^2}{4D_{ro}} \quad (9)$$

$$D_{ro} = \frac{3K_B T}{4\eta_s D^3} \quad (10)$$

D_{ro} is the rotary diffusivity, t_d is the required time for a nanoparticle to travel a distance equal to its diameter D, η_s is the viscosity of the polymer, K_B is the Boltzmann constant and T is the temperature. However, this Brownian motion contribution to the migration of platelets shape nanoparticles is very small due to the high viscosity of the polymer

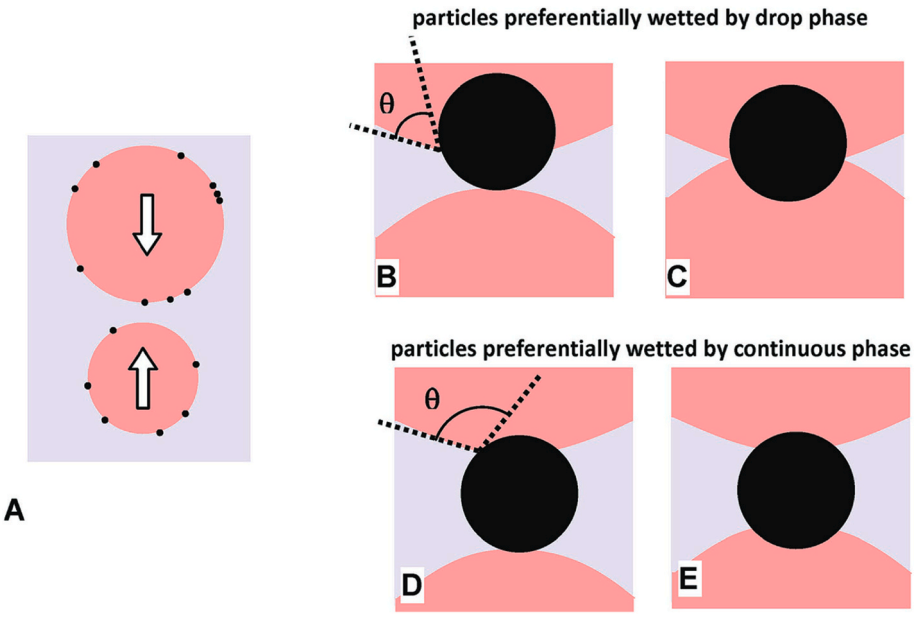

Fig. 19. (A) Droplets containing adsorbed particles on their surfaces will collide, (B) Particles prefer to be wetted by the dispersed phase, $\theta < 90°$, (C) Coalescence phenomenon,(D) Particles prefer to be wetted by the continuous phase, $\theta > 90°$, (E) A bridge is formed [145]. Reproduced from Ref. [145] with permission. (A colour version of this figure can be viewed online.)

matrices.

Another mechanism is the shear-induced migration. During the melt-process, there are collision between droplets of the minor polymer phase and the nanoparticles, that can lead to an incorporation of the NPs into the droplets.

The third mechanism is called "bridging-dewetting" (shown in Fig. 19). Bridging effect is defined as nanoparticles adsorbed on two approaching droplet surfaces, and then these particles are trapped between two drops (Fig. 19e). Other phenomena, when NP is moving into the blend, are explained in Fig. 19.

Few studies addressed graphene migration mechanism at the polymer blend interface. *Kou* et al. [143], proposed a migration process in four steps (Fig. 20). Graphene nanoparticles seem to firstly drain the polymer blend interface. The film drainage time depends on the contact length between nanoparticle and interface. Perpendicular orientation of the nanoparticle according to the interface direction allows faster migration rates. The displacement velocity (noted V) can be predicted for nanoparticle at the interface: $V = \frac{F}{\xi L}$. With F the thermodynamic driving force, and ξ is the friction coefficient and L is the contact length.

As discussed previously, Göldel et al. [139] explain the transfer through the interface for low and high aspect ratio fillers based on the orientation of the filler and the difference of interfacial tension of polymers and fillers.

3.3.4. *Polymer viscosity ratio*

The importance of the polymer viscosity ratio was already exposed in the previous parts. To study the influence of this factor it is necessary to get rid of other factors and especially the sequence of mixing. It seems that when carbon blacks (CB) are added to a relatively high interfacial tension co-continuous PP/PCL premixed blend, the CB have a high tendency to stay in the most viscous phase, even if it is not the preferred one [141]. In the case of a lower interfacial tension blend, when graphene is added to the pre-mixed 80/20 PLA/PCL blend, the influence of viscosity ratio is less important as graphene reaches the less viscous and preferred PCL phase. The impact of viscosity on nanoparticle (and more specifically graphene) migration are currently not sufficiently exposed. Indeed, it is difficult to realize an experiment to explain nanoparticle migration in which only viscosity parameter is changing and the other parameters (thermodynamic, kinetic) are unchanged. Some articles have attempted to prove the importance of polymer viscosity on the migration and localization of nanoparticles. Fenouillot et al. [146] explained also that it is difficult to decouple thermodynamic, kinetic effects and viscosity. Since 2009, this problematic is still topical.

With other types of nanoparticles such as carbon blacks, an article from Feng et al. [147] tried to study the impact of viscosity on CB localization by testing three different PMMA matrix with three different molecular weights. Polypropylene (PP), PMMA and CB were added at

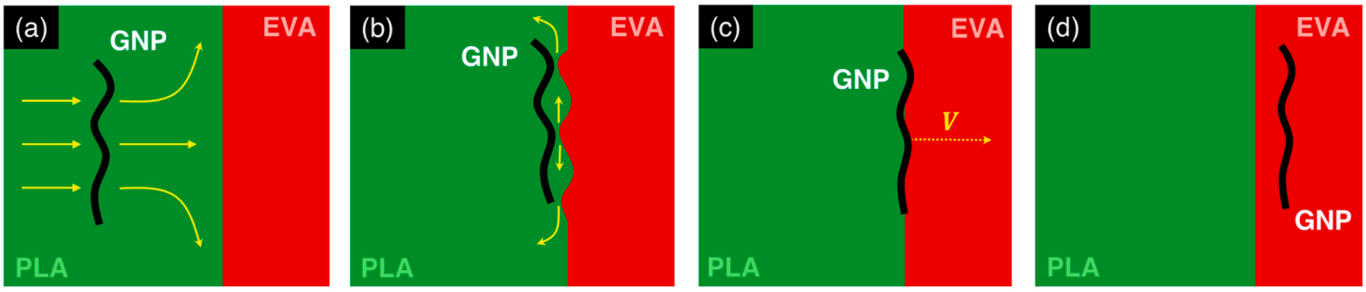

Fig. 20. Scheme of the four steps of graphene migration from the PLA (less preferred) phase to the EVA (more preferred) phase: (a) migration from PLA matrix to interface, (b) film drainage of the departing phase at the interface, induced by the attractive interactions between graphene and EVA, (c) the displacement of the three-phase contact line at the filler surface, and (d) eventual particle migration across the interface into the preferred EVA phase [143]. Reproduced from Ref. [143] with permission. (A colour version of this figure can be viewed online.)

the same time in a Haake mixer. Thermodynamically, CB preferred PMMA phase. It was observed that at a low PMMA viscosity with a viscosity ratio (η_{PP}/η_{PMMA}) of 1, CB was located in PMMA matrix. When PMMA viscosity increased, CB particles tended to be located at the interface and in the PP matrix for the highest PMMA viscosity. However, shape and size of particles have also an impact on the migration and on the localization so in the case of graphene, the result could not be the same.

3.3.5. *Graphene functionalization or janus nanoparticles to influence localization in polymer blend*

3.3.5.1. Graphene functionalized by copolymer. This subsection relates chemical modification methods on graphene allowing its migration at the interface in order to minimize the percolation threshold. Graphene is often oxidized as a pre-functionalization because oxygen groups allow the grafting of molecule or polymer chains by creating covalent bond, for example via esterification between carboxylic acid of GO and hydroxyl group or an amidation between epoxide group of GO and amine [148,149].

Tan et al. [150] tried to graft poly (styrene-*co*-methyl methacrylate) (P(St-*co*-MMA)) copolymer on graphene thanks to a mini-emulsion polymerization. The high surface reactivity of GO was used to facilitate the functionalization. GO was firstly functionalized with γ-methacryloxypropyl trimethoxysilane (MPS) which could ensure a covalent grafting of the copolymer chains (Fig. 21a). The presence of MPS was proven by FTIR with the Si–*O*–C stretching vibrations at 1090 cm^{-1}. The obtained product is P(St-co-MMA)-g-GO which was then reduced by hydrazine to obtain a conductive P(St-co-MMA)-g-rGO. This modified graphene was incorporated in a PMMA/PS blend (1/1 vol) in order to check its impact on electrical conductivity of the nanocomposite. To prove the interest functionalizing graphene with this copolymer, P(St-*co*-MMA)-*g*-rGO was compared to rGO regarding the electrical conductivity of the polymer blend nanocomposite. Fig. 21b displays an increase of the electrical conductivity of PMMA/PS blend thanks to P(St-co-PMMA)-g-rGO addition. Indeed, the electrical conductivity at 0.4 %vol is 4 orders of magnitude higher for P(St-co-MMA)-g-rGO/PS/PMMA ($\sigma = 10^{-7}$ S.cm^{-1}) than for rGO/PS/PMMA ($\sigma = 10^{-11}$ S.cm^{-1}). About the percolation threshold, it is estimated at 0.35 %vol and 0.02 %vol for rGO and P(St-co-MMA)-g-rGO, respectively. Thanks to SEM characterization, the migration of grafted graphene to the interface becomes undeniable (Fig. 21 c,d). It explains why the electrical conductivity increases.

In order to localize graphene at the interface and enhance properties of the nanocomposite, Kol et al. [151] dispersed graphene oxide and graphene oxide functionalized with aminosilane (GOAS) (Fig. 22a) in a PP/PA blend. Graphene oxide is known to be a good compatibilizer in immiscible polymer blends due to its polarity structure, and hydrophilicity property [152]. However, an oxidized structure is not suitable to reach a performant nanocomposite in electrical or thermal conductivity fields. In this article, GOAS tend to have more affinity with PA matrix. Another advantage is the reduction of GO during the blending that allows to reduce GOAS to obtain rGOAS. The localization of rGOAS was verified by HRSEM (Fig. 22c). GOAS were premixed with PP matrix by melt blending to form PP-rGOAS and then PA was added by melt blending. By adding PA, rGOAS tend to migrate at the interface of PA/PP blend after 15 min of mixing whereas rGO (without functionalization) tends to remain in the PP phase. The percolation of rGOAS is proved by rheological measurements (Fig. 22b). A solid-like behavior takes place around 2 wt% of nanoparticles which proves that rGOAS is located at the interface and facilitate the percolation.

An amphiphilic graphene oxide (AGO) was already carried out [153]. The possibility to localize AGO at the interface of a polymer blend constituted of a polar and a non-polar polymer can be an effective way. *Pu* et al. [154] tried this experiment and found effectively a preferential localization at the interface of the AGO in a LLDPE/EVA polymer blend. GO was functionalized with diphenylmethane 4,4-diisocyanate MDI and benzyl-2-hydroxy-*N*,*N*-dimethylethaammonium bromide to obtain AGO nanoparticles. Several mixing sequences were tested and the LLDPE/EVA/AGO simultaneous mixing allowed a localization at the interface of

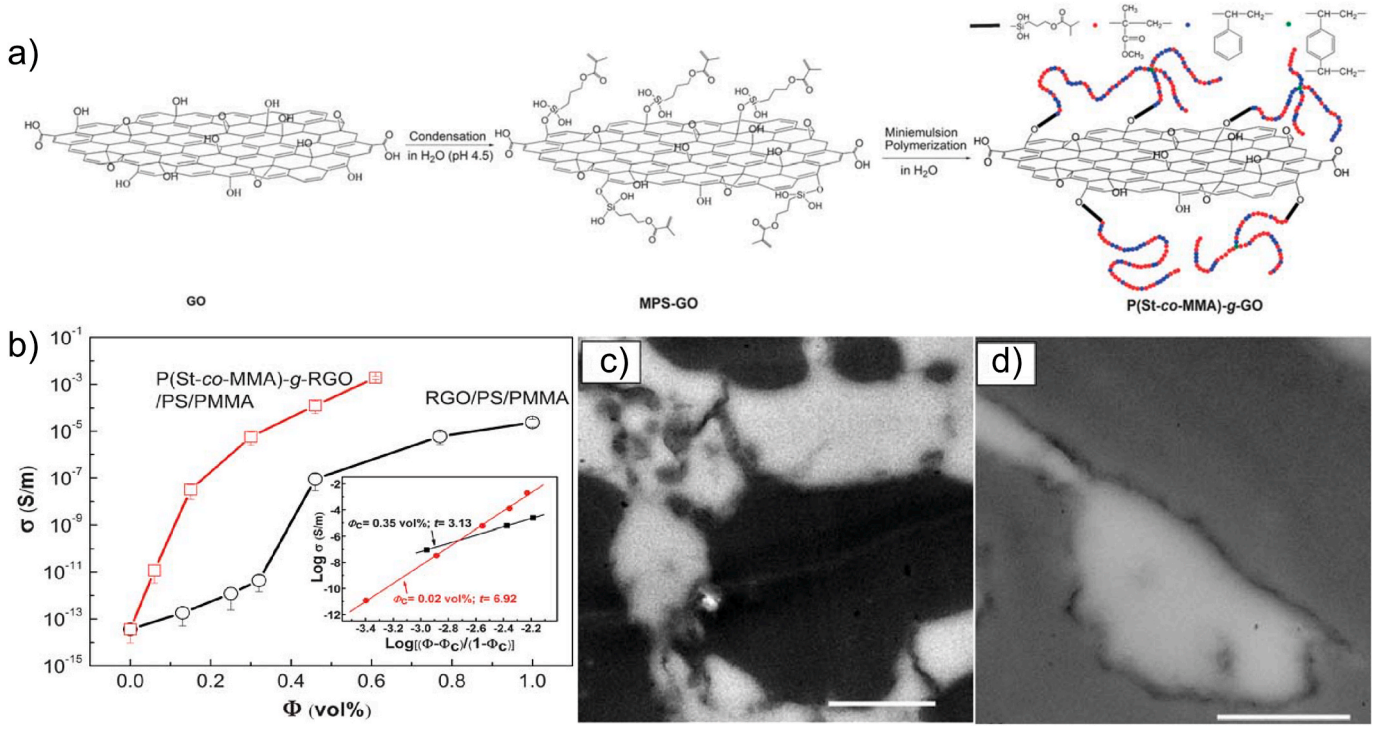

Fig. 21. (a) Synthesis of P(St-co-MMA)-g-GO, (b) Electrical conductivity of rGO/PS/PMMA and P(St-co-MMA)-g-rGO/PS/PMMA according to filler content in % volume, TEM micrographs of: (c) rGO in PMMA/PS blend at 0,46 %vol, (d) P(St-co-MMA)-g-rGO in PMMA/PS blend at 0.46 %vol (the scale bars represent 1μm) [150]. Adapted from Ref. [150] with permission. (A colour version of this figure can be viewed online.)

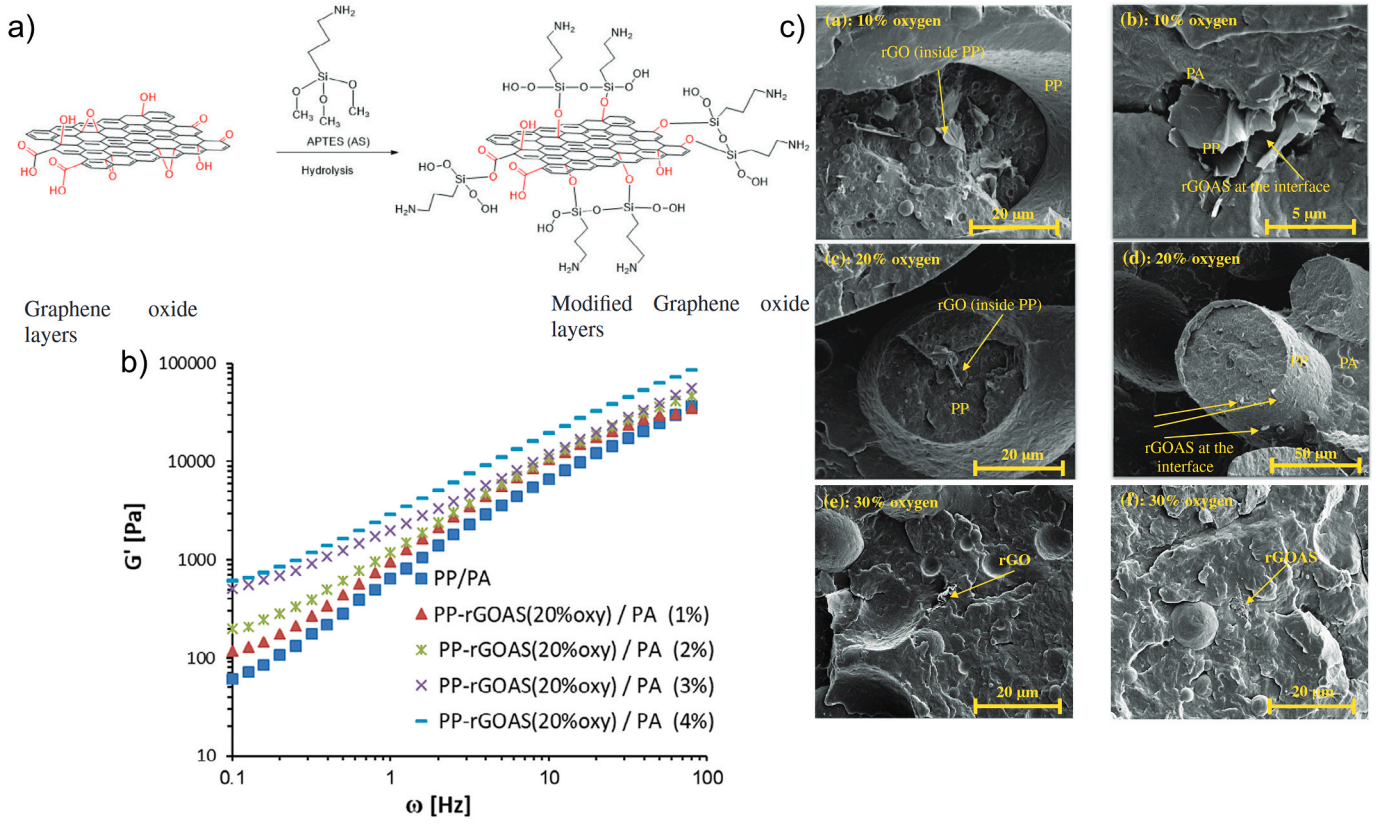

Fig. 22. (A) Functionalization of GO with aminosilane (GOAS), (B) Rheological properties (G′ vs ω) of PP-rGOAS (20% of oxygen from the oxidation step)/PA at different weight loadings, (C) SEM images of rGO and rGOAS in PP/PA blend [151]. Reproduced from Ref. [151] with permission. (A colour version of this figure can be viewed online.)

AGO nanoparticles. The interest localizing AGO at the interface was given directly by tensile measurement such as an enhancement of the yield strength. Another study, of Kar et al. [155] proved that modified graphene were localized at the interface and could give better mechanical properties contrary to a random dispersion in one polymer phase.

3.3.5.2. From graphene to janus graphene nanoparticles. In the previous part, molecules or copolymers reacted with one of the GO oxygen groups like epoxide, carboxylic acid in order to be grafted randomly on the edge

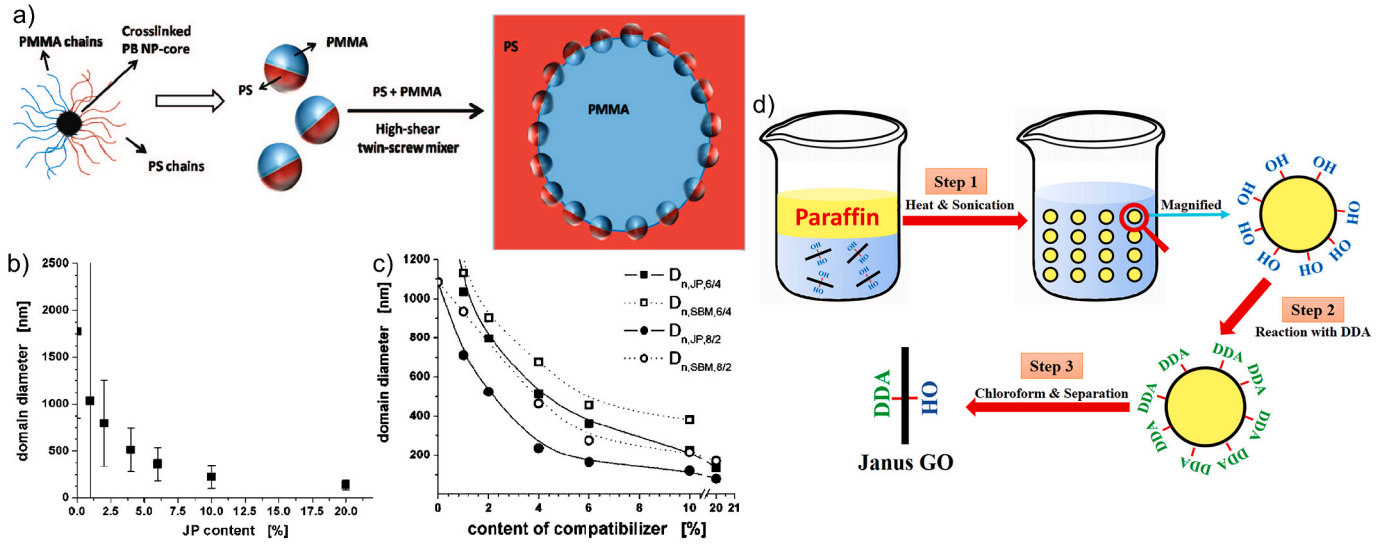

Fig. 23. (A) Schematic representation of Janus particles and their adsorption at the blend interface of a PS/PMMA blend, (B) PMMA domain diameter as a function of the content of Janus particles for a PS/PMMA (6/4) blend, (C) Evolution of the PMMA domain diameter as a function of the content of compatibilizer for different types of stabilizers, SBM and Janus particles, and varying blending ratios as indicated in the graph [157] (D) Pickering emulsion for JGN synthesis [161]. Reprinted (adapted) with permission from Ref. [157]. Copyright 2008 American Chemical Society. Adapted from Ref. [161] with permission. (A colour version of this figure can be viewed online.)

or side of sheets. The objective was to improve the affinity of the modified GO to locate them at the interface of a polymer blend while playing with the mixing sequences. Janus nanoparticles are particles at the nano-scale that have two or more distinct physical properties, namely one hydrophilic hemisphere and one hydrophobic one. In the case of a polymer blend, adding Janus particles offers the possibility to match the chemistry of each part of the particle to that of the blend components [156]. *Walther* et al. [157] proved that Janus nanoparticles can saturate the interface of a polymer blend, compatibilizing it with much more efficiency then copolymers. Their Janus particles are the result of a crosslinked polybutadiene nanoparticle core surrounded by 13 chains of each PMMA and PS (Fig. 23A). In this article, the compatibilizing effect of Janus particles (JPs) compared to that of a terpolymer polystyrene-*block*-polybutadiene-*block*-poly (methyl methacrylate) (SBM) with a 60/40 and an 80/20 PS/PMMA polymer blends was analyzed. If the nanoparticle has a compatibilizing role by placing at the interface of the immiscible blends, the higher the quantity of compatibilizer, the smaller the size of the dispersed domains. This evolution has been verified in more recent publications [158,159]. Fig. 23B illustrates the precedent affirmation. JPs were placed at the interface of the PS/PMMA blend and avoid coalescence of the dispersed phase. It shows that the greater the JPs loading, the more difficult it is for the dispersed phase to coalesce. Fig. 23C shows that JPs are more efficient compatibilizer then SBM as the PMMA dispersed phase diameter is lower. Janus nanoparticles are very promising fillers for nanocomposite constituted of polymer blends with the objective to thermodynamically localize them at the interface of a polymer blend [155]. Janus graphene nanoparticle (JGN) is a functionalization of graphene which can be defined by a nanoparticle with asymmetric properties. For example, graphene sheets can be hydrophobic for one of the sheet side and hydrophilic for the other. Several methods were developed to obtain Janus graphene nanoparticles like the Pickering emulsion (Fig. 23D) [160–163]. Nowadays, JGNs are mainly used for surface modification, sensing, electronics, biology, medicine, actuators. JGNs could also localize at the interface in order to decrease the electrical percolation threshold. However, JGNs require at this time further investigation to prove the efficiency of this modification for the graphene localization control, and also for the development of performant electrical nanocomposites. JGNs look promising to localize at the interface of a co-continuous polymer blend to improve electrical conductivity. However, there is no article in the literature dealing with this subject.

3.4. Impact of graphene localization in a co-continuous polymer blend structure on electrical conductivity

3.4.1. Double percolation phenomenon

Previous parts showed that graphene localization was influenced by several parameters. It also pointed out, that while varying those

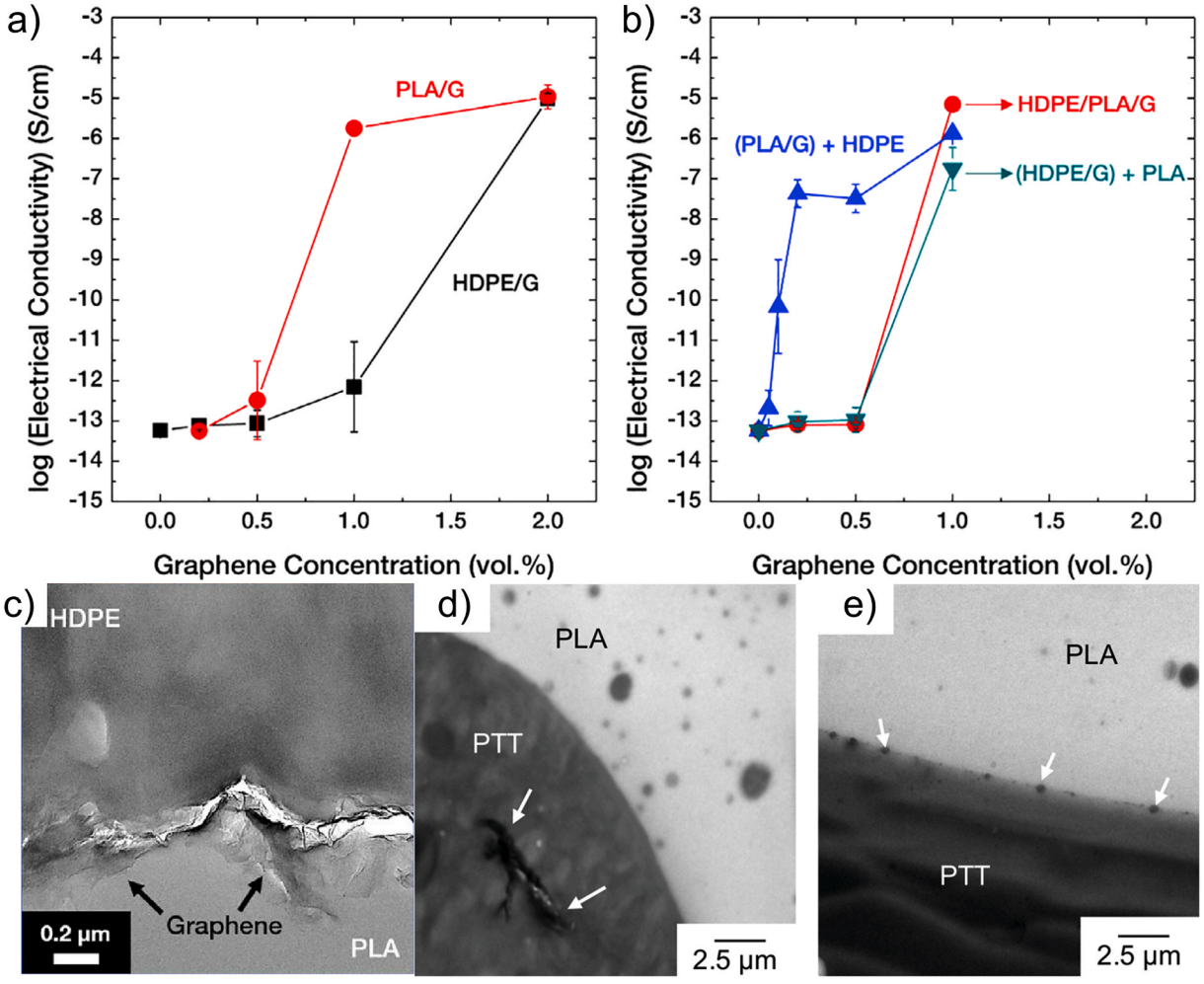

Fig. 24. Electrical conductivity of (a) PLA/G and HDPE/G and (b) HDPE/PLA/G, (PLA/G) + HDPE and (HDPE/G) + PLA as a function of graphene concentration [44], (c) SEM of (PLA/G) + HDPE nanocomposite [44], (d) TEM images of (PTT/G)/PLA and (e) TEM images of (PTT/rGO-PGMA)/PLA [164]. Reproduced from Ref. [44] with permission. Reprinted (adapted) with permission from Ref. [164]. Copyright 2021 American Chemical Society. (A colour version of this figure can be viewed online.)

parameters it is possible to take advantage of the interfacial localization of graphene and decrease the percolation threshold while increasing the electrical conductivity. This part illustrates the effect of the localization of graphene in the co-continuous blends on percolation threshold and electrical conductivity.

The concept of interfacial localization of graphene into a co-continuous polymer blend is called double percolation and was well explained by *Mun* et al. [44], who prepared two different co-continuous polymer blend nanocomposites by melt compounding HDPE/PLA/-Graphene and LLDPE/PLA/Graphene with a rate of graphene up to 0.4 vol% (1 wt%). For each nanocomposite, the impact of the morphology and mixing sequences on electrical conductivity was investigated. It must be noticed that graphene has a better affinity with HDPE and LLDPE than PLA. Fig. 24 a,b shows that percolation threshold decreases by mixing two polymers and creating a continuous interface. Indeed, percolation thresholds are between 0.5 and 1 vol%, and between 1 vol% and 2 vol% for PLA/G and HDPE/G, respectively. After adding a second polymer phase, it is possible to obtain a percolation at 0.05 vol% for a pre-mixed of G in PLA, and further adding of HDPE. This result is due to a specific localization of graphene nanoparticles at the PLA/HDPE interface. Graphene mixed with PLA tends to migrate toward the HDPE phase, then localized at the PLA/HDPE interface (Fig. 24c). The PLA/HDPE blend is the most interesting blend as the high interfacial tension between HDPE and PLA can lead to a large domain size and dispersed graphene sheets can cover the entire interfacial area as an interconnected network. More recently, Kultravut et al. [164] dispersed graphene (G) and reduced modified graphene oxide with a poly (glycidyl methacrylate) grafting (rGO-PGMA) in an immiscible PLA/PTT (poly (trimethylene terephthalate) polymer blend. Fillers were premixed in the PTT matrix by melt-blending. As shown in Fig. 24d graphene seems to be localized preferentially in the PTT matrix. By grafting PGMA on reduced graphene oxide, nanoparticles were transferred from PTT phase to the PTT/PLA interface. This nanoparticle transfer at the interface impacts directly the percolation threshold and the electrical conductivity. The percolation threshold decreases strongly in Fig. 24e.

3.4.2. *Correlation between graphene localization, polymer blend morphology stabilization and electrical conductivity*

In some articles, it was explained that fillers localized at the interface of a polymer blend can entail a phenomenon of suppression of the coarsening. The characteristic size variation of the polymer phase is stopped by the presence and the mechanical resistance induced by fillers localized at the polymer blend interface [165]. The coarsening can have an impact on the electrical performance of polymer nanocomposites [136].

The coarsening suppression was observed by preparing co-continuous nanocomposites with PLA/PS (51.2/48.8 wt%) and graphene nanoplatelets at 0.5 wt% (GNPs) via a melt blending method [137]. Mixing time, mixing sequence, and annealing time influence the graphene localization and then the electrical conductivity of a PLA/PS/GNP blend. Since GNPs preferred thermodynamically PS matrix, a pre-mixed of PLA/GNP was more suitable to place fillers at the interface (Fig. 18a). Moreover, when the mixing time was increased, fillers tended to migrate in the PS matrix whereas they stayed at the

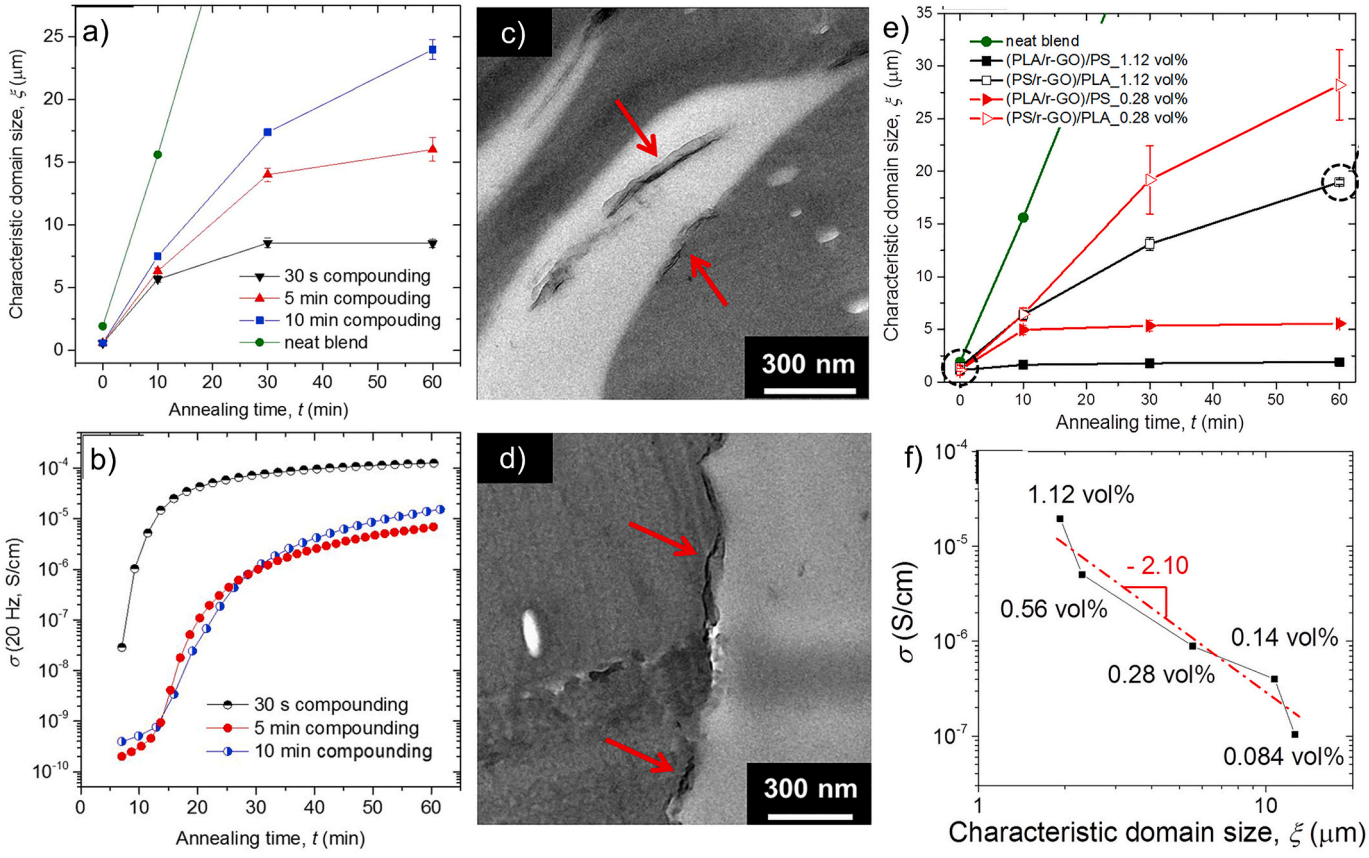

Fig. 25. PLA/PS/GNPs blend nanocomposites (a) Characteristic domain size (ξ) as a function of annealing time at 180 °C, for PLA/PS neat blend and (PLA/GNPs)/PS-0.5 wt % blend with melt-compounding times of 30 s, 5 min, and 10 min; (b) Electrical conductivity at $\omega_{AC} = 20$ Hz, as a function of annealing time at 180 °C, for (PLA/GNPs)/PS-0.5 wt % blend with different melt-compounding times; TEM micrographs of (PLA/r-GO)/PS-0.28 vol% [137]: (c) without annealing, (d) after 1 h annealing; (e) Characteristic domain size (ξ, as a function of annealing time at 180 °C for PLA/PS and different mixing sequence of PLA/PS/rGO at different filler contents (f) Relationship between DC conductivity (σ) and characteristic domain size (ξ) [136]. Reprinted (adapted) with permission from Ref. [136]. Copyright 2018 American Chemical Society. Reproduced from Ref. [137] with permission. (A colour version of this figure can be viewed online.)

interface with a small mixing time. Annealing process after melt compounding allowed the filler to be trapped at the interface via Brownian motion. A sufficient amount of GNPs at the interface led to a suppression of the blend coarsening. Thus, the evolution of the characteristic domain size during annealing can be used as an indicator to reflect the percentage of interfacial GNP. A smaller domain size was due to a higher percentage of interfacial graphene. Indeed, for 30 s of mixing and after 30 min of annealing at 180 °C, the domain size stopped to increase due to the suppression of the coarsening related to the high amount of graphene at the interface. Moreover, other mixing times were tested and the highest amount of GNP at the interface was for 30 s mixing time (Fig. 25a). This was confirmed by the electrical conductivity measurement. After 10 min of annealing, the electrical conductivity of the 30 s melt compounding was 3 orders of magnitude higher than for 5 or 10 min of melt compounding (Fig. 25b). The percolation threshold can be estimated at 5 min of annealing for 30 s of mixing time and at 15 min of annealing for 5 and 10 min of mixing time. Same results were observed in another study of Bai et al. [136], dealing with r-GO. A mixing of PLA/PS (48/52 vol%) + rGO by melt blending was carried out. GNPs were replaced by rGO in this article, but polymer matrices were the same. Fig. 25c shows some rGO remained in PLA matrix and others at the interface. Fig. 25 d proved the interest of the 1 h-annealing by transferring large quantities of fillers at the interface. (PLA/rGO) + PS was the ideal mixing sequence with rGO localization at the interface it was proven by a smallest characteristic domain size for this sequence (Fig. 25e). Fig. 25e also shows that with a higher amount of rGO, the coarsening is stopped at lowest annealing time due to higher amount of rGO at the interface. However, some rGO aggregates remained in PLA due to low impact of kinetics effect during the annealing. Moreover, it was supposed that there were van der Waals attractions between rGO and PS from the other side of the polymer blend interface, which keep fillers trapped at the interface. On the other hand, the coarsening flow facilitates the rGO interfacial trapping by moving fillers at a smallest distance of the interface. This article confirmed that a smallest characteristic domain after annealing means a greatest filler network by an increasing of electrical conductivity (Fig. 25f).

The same phenomenon was observed by Kurusu et al. [166] with a co-continuous structure composed of two polymers (EVA and LLDPE). Interfacial tension between those two polymers is relatively low (0.9 mN m^{-1}) and their viscosities are similar (around 500 Pa s at 100s^{-1}). Consequently, according to Fig. 12, a co-continuous structure is obtained at a volume ratio of 50/50 (EVA/LLDPE). In this study, regarding the wettability coefficient, even if the interfacial tension between graphene and LLDPE is close to that between EVA and graphene (3.8 and 2.8 mN m^{-1}, respectively), it is predicted that graphene tends to migrate to the EVA phase. Two masterbatches were carried out: graphene nanosheets (GN) were pre-mixed in EVA in one case and in LLDPE in other case. A smaller characteristic domain size and a higher electrical conductivity were obtained for the LLDPE masterbatch samples after annealing for amounts of graphene higher than 1.3 vol%. It is explained that graphene nanosheets localization at the interface in the case of LLDPE masterbatch should stop the coarsening (Fig. 26a). Graphene acts like a physical barrier between the polymer domains. This is confirmed by the electrical conductivity measurement (Fig. 26b) where the percolation threshold appears at a lower graphene quantity for LLDPE MB (masterbatch) between 1.3 and 2 vol%. A diminution of characteristic domain size or a suppression of its coarsening significates that graphene nanosheets are forming a percolated network which is benefit for an improvement of the electrical conductivity.

Recently, Kou et al. [167] studied a co-continuous polymer blend nanocomposite PMMA/SAN filled with graphene nanoplatelets. The co-continuity was obtained by a spinodal decomposition of a PMMA/-SAN homogeneous polymer blend. The spinodal decomposition was obtained by annealing well above the lower critical solution temperature. It allows to keep an equilibrium during the processing contrary to immiscible polymer blends which tends to lose their co-continuous structure. A co-continuous and spatially regular morphology in which conductive GNP fillers percolate entirely within the SAN-rich phase was obtained.

3.4.3. *Correlation between rheology and electrical conductivity*

Small Amplitude Oscillatory Shear tests (SAOS) performed on nanocomposites allow to identify networks formed by the nanoparticles. Indeed, at high frequencies, the viscosity is dominated by that of the matrix, whereas at low frequencies, the elastic contribution to the viscosity is dominated by the solid network formed by the nanoparticles. Moreover, it is well-known that nanoparticle aspect ratio plays a key role on the viscosity of the polymer at the melt state. Fig. 27 shows that rod and plate particles drastically increase the viscosity even at low amounts.

The rheological behavior in SAOS tests can inform on the formation of a network for graphene nanoplatelets. Indeed, a plateau of G' versus ω

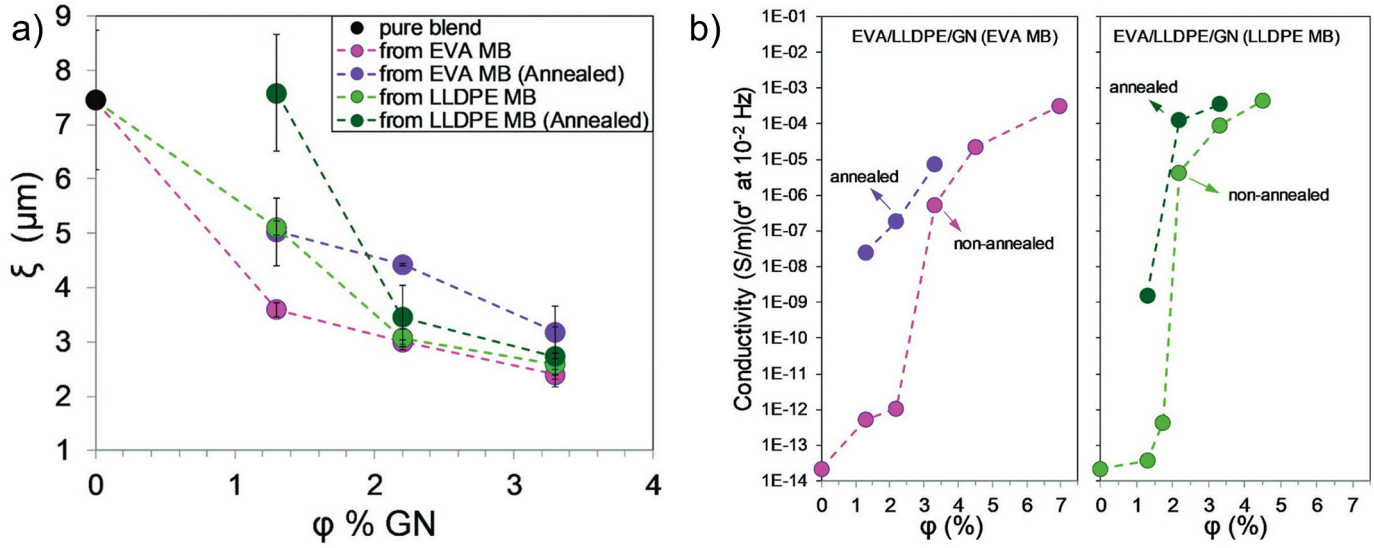

Fig. 26. (a) Characteristic domain size before and after annealing of each nanocomposite elaborated from different masterbatches, (b) Electrical conductivity before and after annealing for the samples prepared from either EVA or LLDPE masterbatch (MB) [166]. Reproduced from Ref. [166] with permission. (A colour version of this figure can be viewed online.)

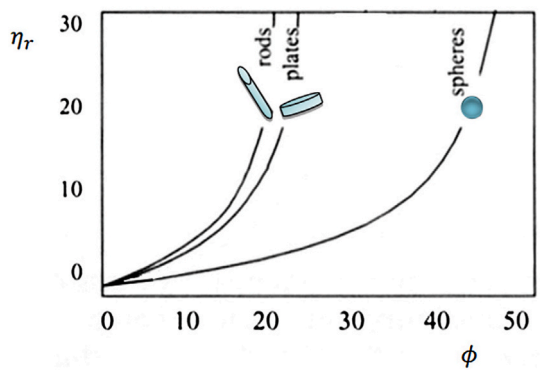

Fig. 27. Evolution of viscosity according to the shape and amount of nanoparticles [168]. Adapted from Ref. [168] with permission. (A colour version of this figure can be viewed online.)

at low frequency inquires on the formation of a network informing that the percolation threshold is potentially achieved, and that the electrical conductivity is high. And it is known that the localization of the graphene nanoplatelets plays a role on the formation of this network.

The suppression of coarsening during annealing is due to a stabilization of the system morphology. It proves that it is possible to make a link between stabilization of the morphology thanks graphene nanosheets and electrical conductivity. Indeed, Helal et al. [169] tried to find a correlation between rheological behavior and electrical behavior. They used a LLDPE/EVA blend filled with graphene nanoplatelets (GNP). These nanocomposites were prepared by melt blending via a twin-screw extrusion to obtain a co-continuous morphology for a 50/50 blend composition. Rheological tests were made on EVA/LLDPE/GNP blend nanocomposite and on single filled matrices (EVA/GNP, LLDPE/GNP). Results confirmed that the rheological percolation was lower for the blend nanocomposite (Fig. 28a and b). Rheological percolation was obtained when nanocomposites exhibited a pseudo-solid-like behavior at low frequencies represented graphically by a plateau on G' [110,170]. Rheological tests were carried out after the annealing at 160 °C during 2 h. G' was measured according to the angular frequency for each nanocomposite from different masterbatchs. For LLDPE masterbatch, the rheological percolation seems to be confirmed at around 1.3 vol % while for EVA masterbatch the zero slop at low frequencies is more pronounced at 1.3 vol % so the percolation threshold is lower than this value. Electrical conductivity and electrical percolation threshold were determined and compared to the rheological percolation threshold. After annealing, electrical percolation threshold for each nanocomposite reaches 1.21 and 0.5 vol% for LLDPE

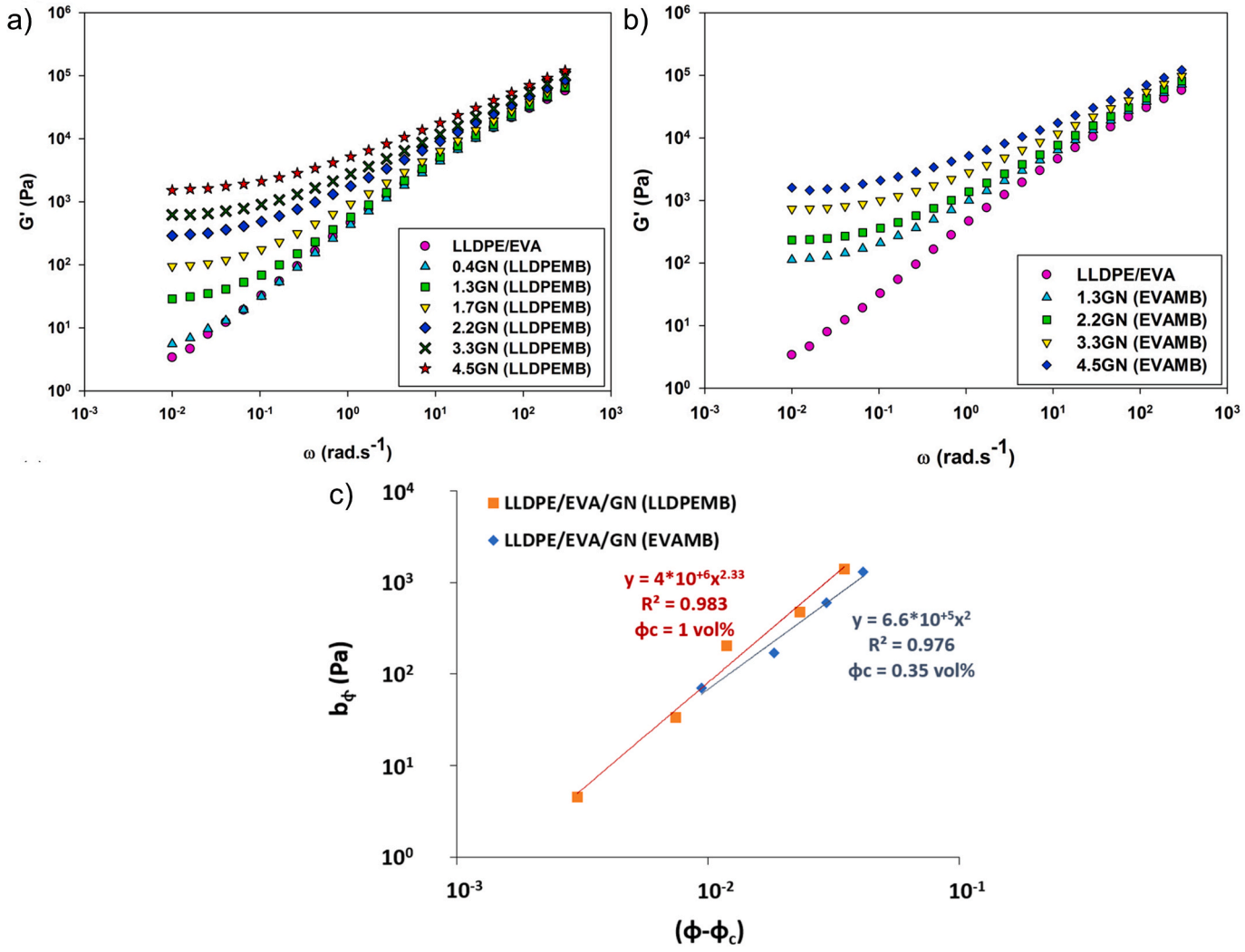

Fig. 28. SAOS tests performed at 160 °C after stabilization for 30 min on LLDPE/EVA/GN composites: (a) G′ for LLDPE MB, (b) G′ for EVA MB, (c) Electrical percolation threshold of the LLDPE/EVA/GN for a LLDPE masterbatch and EVA masterbatch [169]. Reproduced from Ref. [169] with permission. (A colour version of this figure can be viewed online.)

masterbatch and EVA masterbatch, respectively (Fig. 28c). These values are closed to those estimated for rheological percolation which proves that rheological characterization is useful to predict an improvement of the electrical conductivity.

In some cases, rheological and electrical percolation can show some different thresholds for the same nanocomposite. Indeed, Hu et al. [171] found for a PET/MWCNT (multiwalled carbon nanotube) nanocomposite different percolation threshold when measuring the conductivity and the rheological properties.

3.5. Comparison of the electrical conductivity of graphene/multiphase polymer nanocomposites

A high number of electrical conductivities σ in $S.cm^{-1}$ were collected from 73 publications in order to distinguish the effect of (1) the type of graphene (among expanded graphite, graphene nanoparticle (GNP), graphene oxide (GO), reduced graphene, reduced graphene oxide (rGO) and functionalized graphene), (2) the vol% of graphene, (3) the polymer matrix for monophasic nanocomposites (among several thermoplastics, amine modified carbon nanofibers (CNF), polydimethylsiloxane (PDMS), water-borne polyturethane (PU), cellulose fibers, styrene butadiene rubber (SBR) epoxy resin) (4) the type of binary polymer

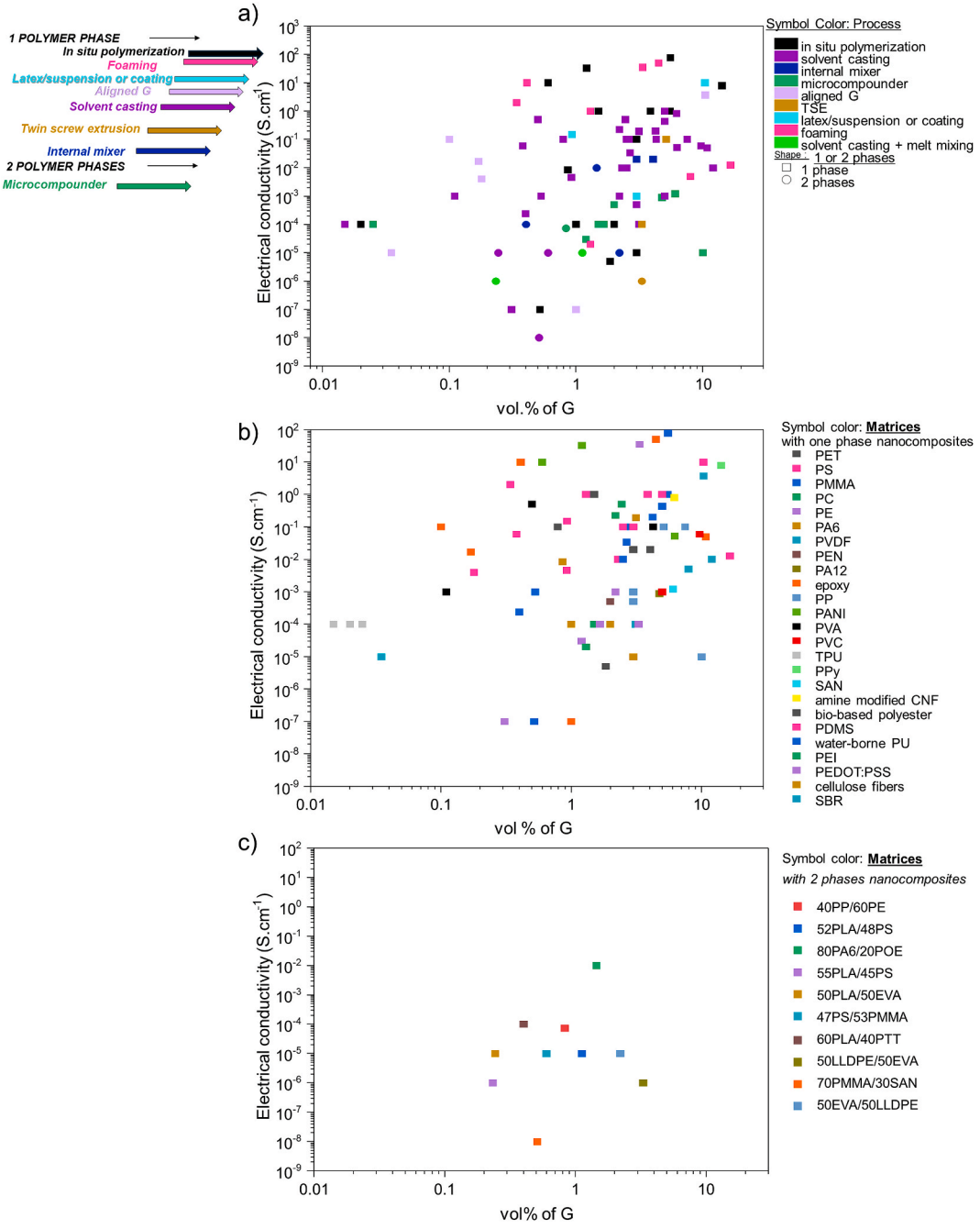

Fig. 29. Graphs representing the electrical conductivity versus vol% of graphene based on references [3,7,59,60,62,66,78,84,111,126,136,137,143,148,150,152,166,167,169,172]– [178,180–226]. (a) Effect of process and the number of polymer phases (one or two phases), (b) effect of the polymer matrices for one phase nanocomposites, (c) effect of the polymer matrices for two phases nanocomposites, (d) effect of the type of graphene or graphite used and (e) effect of the nanoparticle localization into the blend among the references dealing with polymer blends. (A colour version of this figure can be viewed online.)

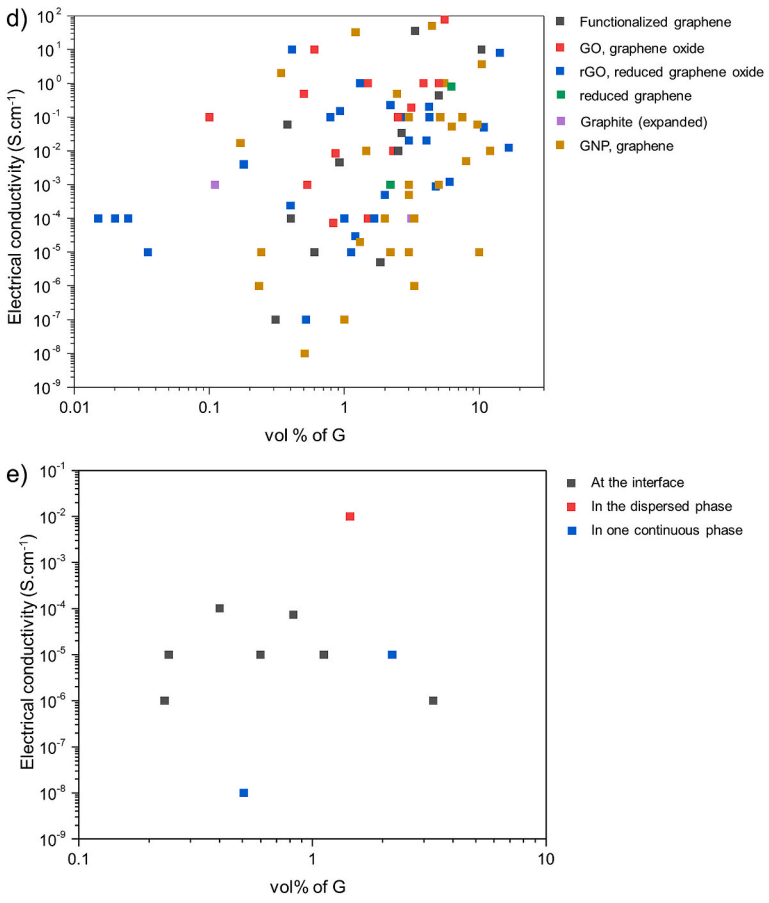

Fig. 29. (*continued*).

blends, their microstructure (co-continuous or matrix/dispersed phase) and the final localization of the nanoparticles in the blend (5) the processing used (among microcompounder, twin-screw extrusion (TSE), solvent casting followed by melt mixing, solvent casting, aligned graphene, internal mixer, in situ polymerization, latex/suspension or coating, and foaming). Regarding Fig. 29a, it is seen that very low amounts of graphene (0.015, 0.02 and 0.025 vol%) [172] in thermoplastic polyurethane (TPU) can lead to high electrical conductivity (measured as DC surface resistance and converted to σ); and that -in that case-solvent casting gives the lowest percolation threshold compared to melt blending or in-situ polymerization. Generally, foaming and in-situ polymerization give the best electrical conductivities thanks to the organization and orientation induced by those two processing. It was demonstrated that the conductive polyaniline (PANI) can be polymerized in situ leading to graphite exfoliation and high values of σ [173]. Poly (methyl methacrylate) (PMMA) was also synthesized in situ with high amounts of expanded graphite (8 wt% equivalent to 5.53 vol%) [174] leading to high electrical conductivity (77.7 S.cm^{-1}). Foams or expanded nanocomposites can be processed by creating a high density 3D hollow material containing interconnected graphene and infiltrated with a polymer [175–177]. Solvent casting is the third most efficient processing to lead to high electrical conductivities. This process allows to reach high amounts of dispersion of graphene. Regarding Fig. 29a, and expect the previous remarks, it is difficult to highlight a clear influence of each process on the final electrical conductivity. Fig. 29b allows to view all the polymeric matrices that were reported in those graphs. Fig. 29c represents again the electrical conductivity versus vol% of graphene differentiating the influence of the type of graphene used. Here again it is difficult to highlight a trend. Reduced graphene and graphite seem to be the worst nanoparticles to improve the electrical conductivity. Finally Fig. 29d represents σ versus vol% of G for polymer blends [7,126,136,137,143,150,166,167,178]. Legend differentiates the localization of the graphene NPs. The highest value of σ was obtained for an 80PA/20POE blend with 3 wt% of graphene nanoplatelets [179]. The authors explain that a peculiar microstructure was obtained for this formulation with graphene dispersed in POE domains with a small portion of graphene within the PA phase that creates bridges between two discrete POE domains. Regarding the other articles, while using immiscible polymer blends, authors often tried to dispersed graphene at the interface of a co-continuous system. However the best electrical conductivity measured was only 10^{-4} S.cm^{-1} that limits there final application [164].

3.6. *Impact of a third polymer phase in polymer blend nanocomposite on electrical conductivity*

The ultralow percolation threshold stays difficult to obtain in binary polymer blend structures. As it was presented in the previous section, graphene has to be localized at the co-continuous interface of the two polymers. However, a complete percolation of graphene nanosheets at the interface is not so easy regarding the processability. Another way is the incorporation of a third polymer phase that contains graphene (Fig. 30). This third polymer phase should localize at the interface of the two others, forming a tri-continuous morphology. This is the case of the complete wetting in (Fig. 13a) when one phase locates between two other co-continuous phases [48,227,228]. The interest of this ternary structure is to achieve an ultralow percolation threshold of nanoparticles. An article studied ternary blend nanocomposites with different types of nanoparticles for electrical applications [44].

Few publications deal with graphene in ternary polymer, such as Mun et al. [44] (Fig. 31A) or Parameswaranpillai et al. [229]. Mun et al. showed an ultralow percolation threshold (Fig. 31B,C) for a

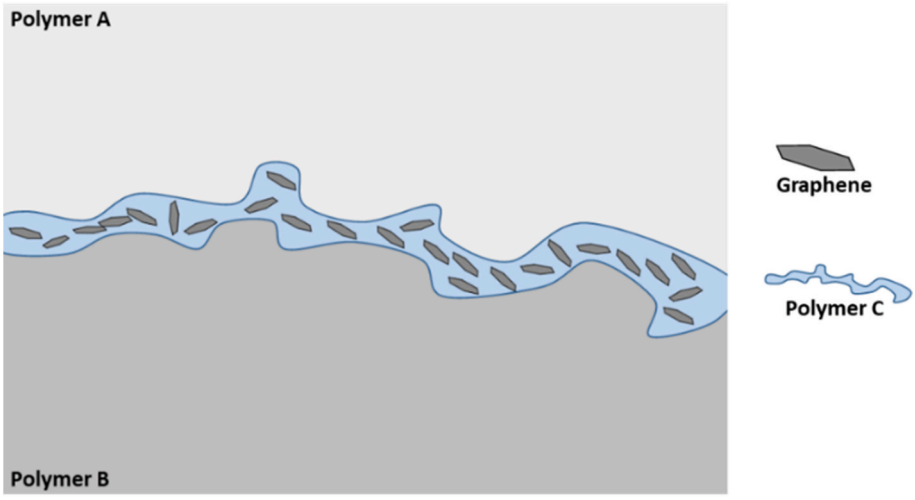

Fig. 30. Scheme of a ternary system with two major polymers (polymer A and B), and one minor polymer (polymer C) which contains graphene. (A colour version of this figure can be viewed online.)

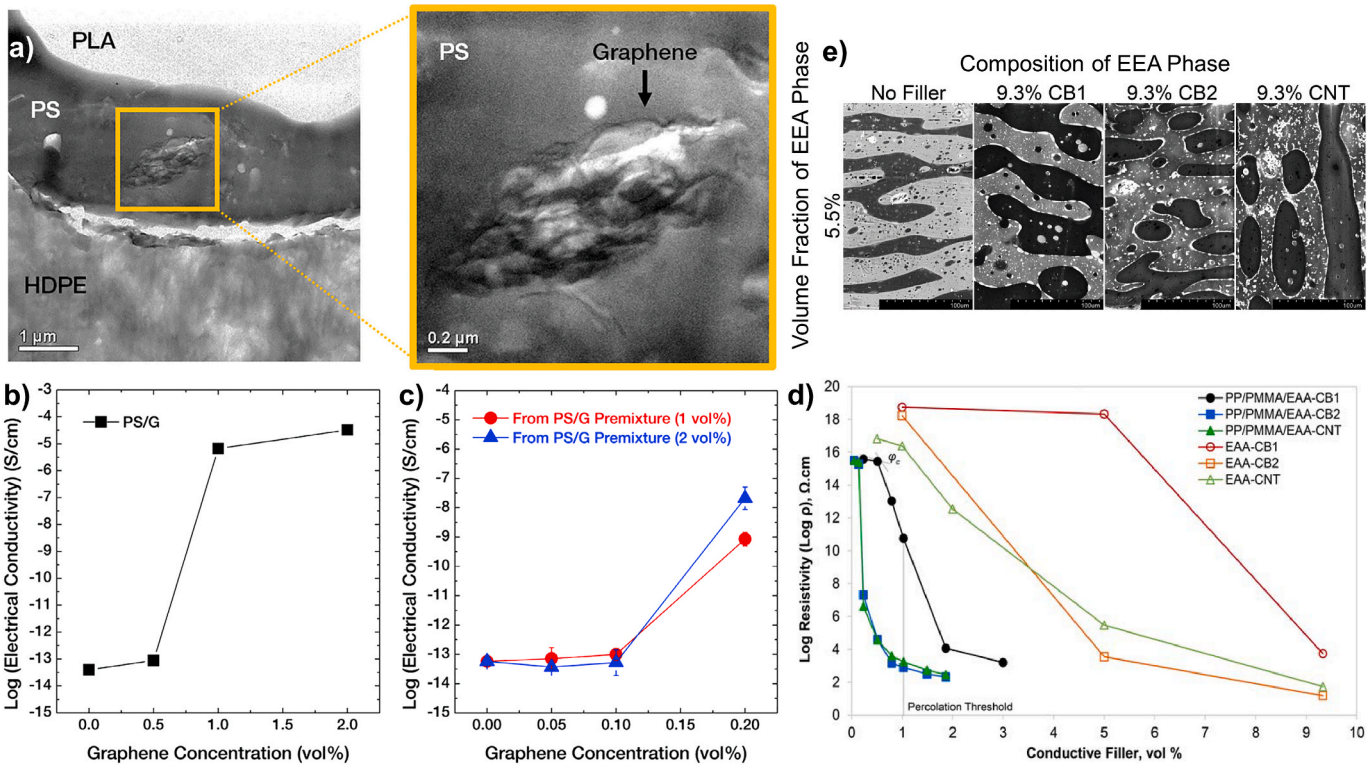

Fig. 31. PS/PLA/HDPE/G nanocomposites: (A) TEM images of (PS/G) + HDPE/PLA nanocomposites (0.2 vol%). The volume ratio of HDPE, PLA, PS/G is 40/40/20: Electrical conductivity of (B) PS/G premixtures and (C) (PS/G) + HDPE/PLA (50/50) [44]. PP/PMMA/EAA ternary blend with CB or CNT: (D) Comparison of the resistivity of the nanocomposites containing different fillers, (E) SEM images for different fillers and filler contents [230]. Reproduced from Refs. [44,230] with permission. (A colour version of this figure can be viewed online.)

nanocomposite of HDPE/PLA + (PS/G) (45/45/10). The percolation threshold was measured between 0.1 and 0.2 vol%. In the same study, as explained in the paragraph II.4.1, a nanocomposite of HDPE/PLA/G gave a percolation threshold around 0.5 and 2 vol% which is higher than that of the ternary blend. This proves the interest of using a system with two polymers matrix at equal volume and one minor polymer matrix which contains graphene. Effectively, the SEM image of Fig. 31A shows graphene sheets located at the interface or in the third minor polymer matrix. It facilitates the network of graphene sheets formation.

To compare, Brigandi et al. [230] studied a ternary nanocomposite with other carbon nanofillers such as carbon blacks (CB) and carbon nanotubes (CNT) in tri-continuous structure. Three phases of PP/PMMA as major polymers and EAA (ethylene acrylic acid) as the minor polymer, which encapsulates PP phases, are clearly visible in the SEM images of Fig. 31E. EAA containing conductive fillers corresponds to the bright domain and is located at the interface. The particularity of CB, CNT and graphene is their different aspect ratio: CB1<CB2<Graphene < CNT. High aspect ratio nanofillers such CNT and graphene entail high viscosity and difficulties to disperse it in the polymer matrix. In this article, electrical conductivity was analyzed to determine the percolation

threshold according to the type of conductive filler and also their aspect ratio. Nanocomposites containing fillers with the highest aspect ratio display the smallest percolation threshold around 0.2 vol% for CB2 and CNT whereas it is 1.0 vol% for CB1 (Fig. 31D). With the same nanocomposite structure but different matrices, graphene displays an ultra-low percolation threshold at 0.2 vol%. It proves that aspect ratio and blend morphology are essential to obtain performant nanocomposite at extremely low loadings.

The number of publications dealing with those co-continuous ternary blends containing graphene (or any other nanoparticles) remains low probably because it is hard to obtain those peculiar morphologies. Indeed, the final microstructure depends on several parameters such as polymer proportion, viscosity and interfacial tension and graphene parameters.

4. Polymer blend electrical applications

Polymer/graphene nanocomposites are also used in a large variety of applications and some reviews already addressed this topic [3, 231–236]. This part is only focused on polymer blend nanocomposite systems and their relative electrical applications. In general, electrical polymer blend nanocomposite can be used for the same application as the single polymer matrix nanocomposite. Effectively, the primary benefit of polymer blend is to reduce the percolation threshold. Targeted applications depend only on the material electrical conductivity whether it is a polymer blend or a single phase matrix.

According to the polymer blend morphology, polymer blend nanocomposite electrical property can be adjusted, and different applications are targeted. It depends if nanoparticles are localized in the dispersed phase or in the continuous phase. Polymer blend nanocomposite is promising for electromagnetic interference shielding (EMI shielding) or dielectric materials.

4.1. Dielectric applications

A dispersed phase/matrix microstructure is not suitable for electrical conductive nanocomposites especially if nanoparticles are localized in the dispersed phase. However, this morphology is suitable for the elaboration of dielectric materials for charge storage applications (Fig. 32a). The dielectric permittivity corresponds to the polarizability of a material in presence of an electric field. It allows the development of nano-capacitors for example. To determine the capability of a material to store charge, the real part ε' is determined from the relative dielectric permittivity complex form: $\varepsilon = \varepsilon' + i\varepsilon''$ [237]. It is also related to the charge polarization. The interfacial polarization occurs due to the accumulation of charge carrier at the interface of two materials with different electrical conductivities. Graphene oxide is an insulating nanoparticle which led to poor dielectric permittivity in polymer matrices due to their insulating behavior. In Fig. 32b, when epoxy was filled with GO, only a few polarizations occurred in the interface due to the electrical insulated nature of GO. The dielectric constant of epoxy/GO is very low. The imaginary part ε" is related to the capacity of a material to dissipate the current. Dielectric materials require conductive nanoparticles with non-contact between them to avoid current leakage. A localization in a dispersed matrix system or at the interface, like in Fig. 32a, allows a non-contact of nanoparticles. If the percolation is reached, current leakage occurred, and the material recover electrical conduction. Hence, an insulator-to-conductor percolating transition can be created by the increase of the filler content [238,239]. In the case of reduced graphene oxide dispersed in epoxy, the dielectric constant was increased compared to GO/epoxy, due to the large difference of conductivity between rGO and epoxy matrix that induced a lot of accumulation of charge carriers at their interface (Fig. 32c). Indeed, in addition to this high interfacial polarization, the probability of contact between rGO platelets is high and by increasing nanoparticle content, dielectric loss becomes high and leads to current leakage (Fig. 32c) because percolation is reached.

In the last case (Fig. 32d), rGO was functionalized with DGEBA to firstly improve interface and benefits from the formation of more micro-capacitors. Moreover, as for rGO/epoxy composites, the difference of electric conductivity between matrix and fillers entraps the free charges that accumulate at the interface. And finally, as no contact are present between fillers due to the functionalization, these conditions lead to good dielectric performances, that is to say high dielectric constant and low loss. Some articles report that graphene was functionalized by different ways to avoid contact between nanoparticles [238,239].

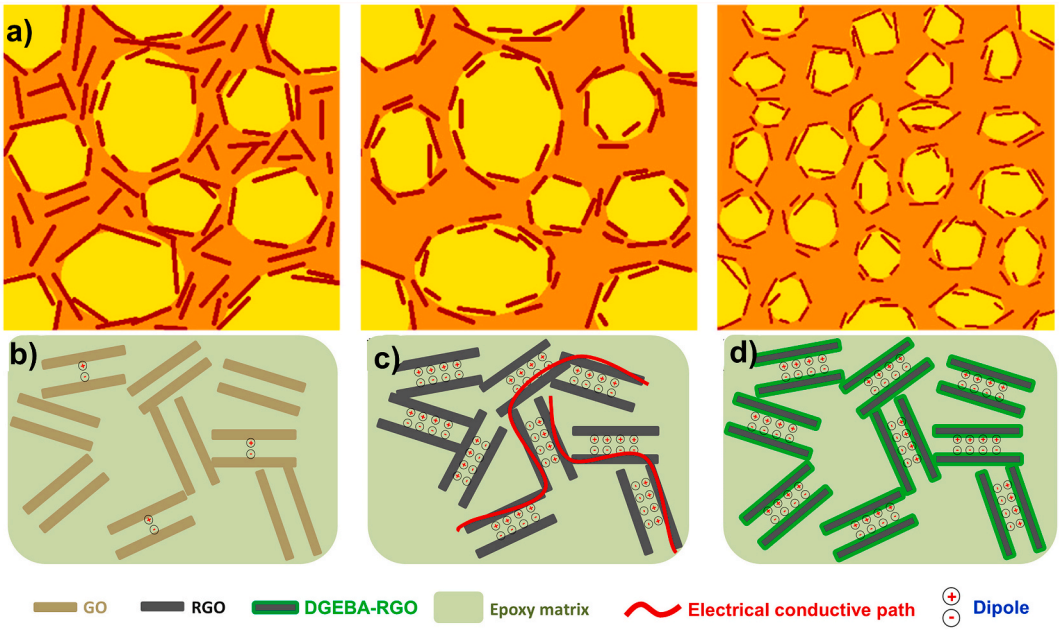

Fig. 32. (a) Matrix/dispersed phase microstructure with conductive nanoparticles from lowest to highest dielectric performance (from left to right) [240], (b) Graphene oxide filled epoxy matrix, (c) Reduced graphene oxide filled epoxy matrix (d) Functionalized graphene in epoxy matrix [239]. Reproduced from Refs. [239, 240] with permission. (A colour version of this figure can be viewed online.)

Other recent works report an increase in dielectric constant ε' while incorporating graphene into polymer blends. With 2 wt% of graphene oxide incorporated into a PMMA/cellulose acetate blend, the dielectric constant was improved from 2.25 to $2.25.10^3$ [241]. Saboor et al. [242] reported a higher dielectric constant when incorporating graphene into a PANI/SAN blend thanks to the accumulation of electric dipoles at the insulator conductor-interface. Goodarzi et al. [243] varied the GNP types (by varying the chemical functionalization) and GNP amounts in an 80/20 polystyrene/ethylene- α-octene copolymer (EOC) to vary the microstructure and then the dielectric properties. They reported the highest dielectric properties for the co-continuous PS/EOC blend containing 1.5 wt% of GNPs dispersed at the interface.

Finally, dielectric properties are very important in energy storage materials for applications such as battery, solar cell, chemical sensors and supercapacitors. Indeed, charge carriers, ionic conductivity and ion mobility are electrochemical properties that can be evaluated by measuring dielectric constant. Films based on (PVP-PVA)-5wt.% $NaHCO_3$ and 15 wt% rGO (reduced graphene oxide) were prepared and reached the highest dielectric constant value that allows a larger dissociation of dopant salt ions leading to ionic conductivity [244].

4.2. Electrically conductive applications

As described previously, co-continuous morphology is suitable for electrical conduction application which allows the formation of a percolated network. For sensors elaboration (thermal, strain, and chemical sensing), their efficiency is defined by the quality of the electrical conduction. A piezoelectric sensor allows to convert variation of mechanical stress in electrical signal. A mechanical contribution to the sensor will change the conductive path and a different electrical signal will be produced. This electrical signal variation is necessary for application in biorobotics or artificial muscles [245]. EMI shielding is also a target application for electrically conductive materials. This application requires material which can inhibit electromagnetic wave transmission to protect electrical devices from interference or for military airplane, boat stealth. EMI shielding can be effective through several mechanisms such as reflection (reflection Shielding Effectiveness, (SE_R), absorption (SE_A) and multiple reflection (SE_M) of the electromagnetic wave. The difference signal intensity of the wave before and after the contact with the material is converted in decibel unit. A minimum of 20 dB of attenuation is required to confirm that the material is performant. The performance is strongly linked to the electrical conductivity of the material. Conductive material led to electromagnetic waves reflection due to the mobility of charge carrier. Absorption mechanism is favored with a high dielectric constant material. The complete efficiency protection is the addition of these three mechanisms: $SE_T = SE_A + SE_R + SE_M$. In the case of polymer blend, the co-continuous morphology is crucial for the improvement of EMI shielding which favors graphene percolation and

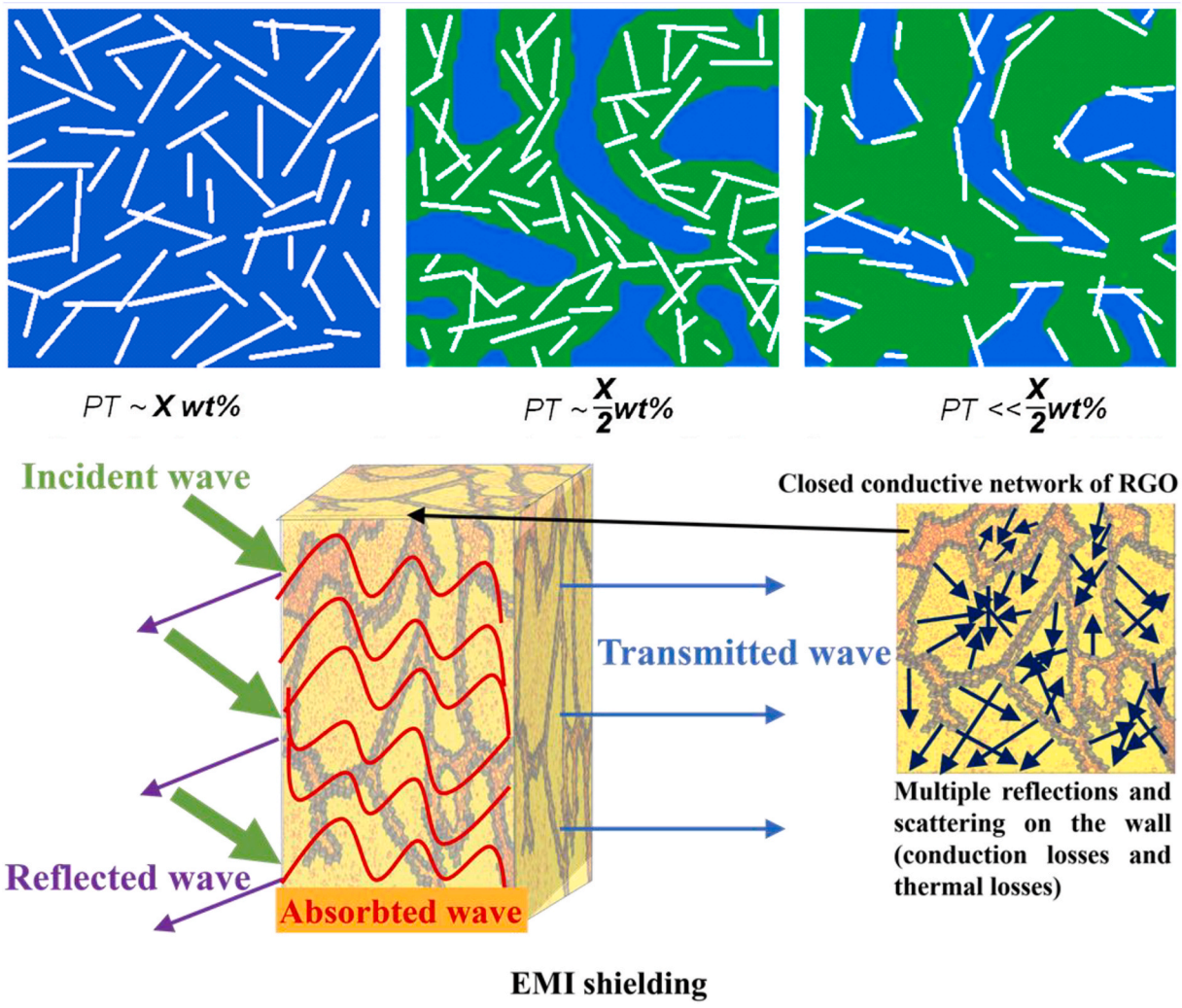

Fig. 33. (a) From one matrix to co-continuous structure with conductive nanoparticles from highest to lowest percolation threshold (from left to right) [240], (b) EMI shielding mechanisms with multiple reflection thanks to the co-continuous structure [246]. Reproduced from Refs. [240,246] with permission. (A colour version of this figure can be viewed online.)

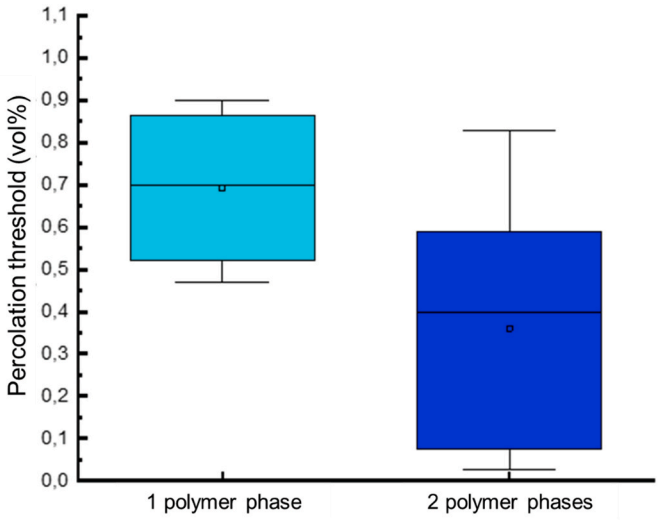

Fig. 34. Percolation threshold according to different number of polymer phases in a nanocomposite graphene/polymer elaborated by melt blending and compared with box plot [39,44,142,169] [200,215,260]. (A colour version of this figure can be viewed online.)

the high conductivity of the material (Fig. 33a). Moreover, the percolated network allows EM wave reflection due to the electrical conductivity, but also multiple reflection as shown Fig. 33b due to the closed-cell network [246]. EMI shielding can be improved, as Dou et al. [48] demonstrated, by using a multiphase structure with three polymers matrix (PVDF, HDPE in major proportions and PS is the minor phase). The localization of MWCNT nanoparticles in the minor phase favors nanoparticle percolation and the formation of a strong network. This strong closed-cell network shows also a high wave absorption.

Polycarbonate//ethylene methyl acrylate (EMA)/graphene nanocomposites were prepared and exhibit total EMI shielding of −52 dB for 15 phr graphene loading, which indicates that these nanocomposites can be used for commercial applications and can also be used against electromagnetic pollution as effective lightweight shielding materials [247]. SAN/PANI/few layer graphene nanocomposites were developed and exhibited interesting EMI shielding response (24.3 dB) at 0.1 wt% loading of graphene. This was attributed to the network formation of both PANI and graphene in the SAN matrix [242].

Even if the number of applications for graphene based polymer blend nanocomposites remains low, it is probable that it will grow up in the next years in the domain of textile and biomedical. Graphene can replace carbon nanotubes that are hazardous, either in conductive textiles [248,249] but also for flexible devices in biomedical domain [250]. Moreover, there is a growing interest for biochars as new conductive particles from biogenic carbon and dispersing this kind of particle into polymer blends can allow to get interesting electrical or dielectric properties [251].

5. Conclusion

Graphene has proven to be an excellent candidate for the development of conductive materials thanks to its structure. The way of synthesis for graphene production greatly impacts the properties of graphene. That's why it is important to control the graphene structure before its use for development of electrical nanocomposites. Despite this high potential in electrical nanocomposite development, the dispersion of graphene in polymer matrices is still a challenge. The large lateral size and small thickness of graphene nanosheets favor the restacking and the formation of aggregates in polymer matrix due to π-π interaction. This phenomenon tends to increase the percolation threshold. Several strategies were exposed in this review to counter this problematic by using chemical or physical methods such as covalent or non-covalent graphene functionalization, nanoparticles alignment. But these techniques can disturb the graphene structure or require implementation steps that are difficult to use at an industrial scale. Polymer blend with two polymer phases appears like an innovative way for development of electrical nanocomposites with a low graphene quantity due to the control of nanoparticles localization in this immiscible system. Several publications show the interest of this morphology with different type of fillers or matrices [252–256]. The localization depends on many parameters such as the thermodynamic, the mixing sequence, the mixing time, the nanoparticle aspect ratio and the polymer viscosities. Controlling graphene localization requires taking these parameters into account and also adjusting these conditions depending on the nature of the nanoparticles and polymers. The best performances are shown with a localization of nanoparticles at the interface of an immiscible polymer blend. Effectively, the lowest percolation threshold is obtained with interfacial localization and confirmed by rheological analyses and electrical measurement which can be correlated.

A third polymer phase can be added in the polymer blend which is filled with graphene. In Fig. 34, polymer blend with three polymer phases do not appear due to a low number of articles regarding this system. However, it is mentioned previously that a percolation threshold as low as 0.1 vol% can be reached for these co-continuous systems. Hence, those systems, with a third polymer phase, are very promising. The reduction of percolation threshold is essential for industrial applications. Obtaining a performant material with excellent electrical properties at a small proportion of graphene is a big challenge. In fact, the production costs are low, but performances are high. In this context, polymer/graphene nanocomposites have established itself as the future materials in aeronautic, energy storage and other fields … This material already appears in aeronautic for electromagnetic shielding, in energy storage for supercapacitors production thanks to a fast discharge/charge of graphene/polymer electrodes [51,52,257–259]. Indeed, this kind of material combines flexibility, high electrical conductivity and high specific surface area which makes it the best nanocomposite for electrode and for a coating.

At this moment, several aspects like the graphene migration in polymer matrix or the transfer mechanism at the interface are still not completely understood and must be studied to hope an improvement in the production and properties of graphene-based polymer blend nanocomposites.

CRediT authorship contribution statement

Thibaut Lalire: Writing – original draft, Validation, Methodology, Investigation, Formal analysis, Data curation, Conceptualization. **Claire Longuet:** Writing – original draft, Validation, Supervision, Project administration, Methodology, Investigation, Formal analysis, Conceptualization. **Aurélie Taguet:** Writing – review & editing, Writing – original draft, Validation, Supervision, Project administration, Methodology, Investigation, Formal analysis, Conceptualization.

Declaration of competing interest

The authors declare that they have no known competing financial interests or personal relationships that could have appeared to influence the work reported in this paper.

Data availability

Data will be made available on request.

References

[1] X. Sun, C. Huang, L. Wang, L. Liang, Y. Cheng, W. Fei, Y. Li, Recent progress in graphene/polymer nanocomposites, Adv. Mater. 33 (2021) 2001105, https://doi.org/10.1002/adma.202001105.

[2] H. Pang, L. Xu, D.X. Yan, Z.M. Li, Conductive polymer composites with segregated structures, Prog. Polym. Sci. 39 (2014) 1908–1933, https://doi.org/10.1016/j.progpolymsci.2014.07.007.

[3] B. Sreenivasulu, B. Ramji, M. Nagaral, A review on graphene reinforced polymer matrix composites, Mater. Today Proc. 5 (2018) 2419–2428, https://doi.org/10.1016/j.matpr.2017.11.021.

[4] P.J. Brigandi, J.M. Cogen, R.A. Pearson, Electrically conductive multiphase polymer blend carbon-based composites, Polym. Eng. Sci. 54 (2014) 1–16, https://doi.org/10.1002/pen.23530.

[5] L. Bai, S. He, J.W. Fruehwirth, A. Stein, C.W. Macosko, X. Cheng, Cocontinuous conductive polymer composites with interfacial graphene, in: Annu. Tech. Conf. - ANTEC, Conf, Proc., 2017, pp. 810–813.

[6] C. Tu, K. Nagata, S. Yan, Key factor of graphene localization on electrical conductive properties of graphene filled polyethylene/polypropylene composites during melt blending, J. Mater. Sci. Res. 6 (2017) 1, https://doi.org/10.5539/jmsr.v6n3p1.

[7] C. Tu, K. Nagata, S. Yan, Dependence of electrical conductivity on phase morphology for graphene selectively located at the interface of polypropylene/polyethylene composites, Nanomaterials 12 (2022) 509, https://doi.org/10.3390/nano12030509.

[8] E.V. Castro, K.S. Novoselov, S.V. Morozov, N.M.R. Peres, J.M.B.L. dos Santos, J. Nilsson, F. Guinea, A.K. Geim, A.H.C. Neto, Biased bilayer graphene: semiconductor with a gap tunable by the electric field effect, Phys. Rev. Lett. 99 (2007) 216802, https://doi.org/10.1103/PhysRevLett.99.216802.

[9] V. Georgakilas (Ed.), Functionalization of Graphene, Wiley-VCH Verlag GmbH & Co. KGaA, Weinheim, Germany, 2014, https://doi.org/10.1002/9783527672790.

[10] J. Phiri, P. Gane, T.C. Maloney, General overview of graphene: production, properties and application in polymer composites, Mater. Sci. Eng. B Solid-State Mater. Adv. Technol. 215 (2017) 9–28, https://doi.org/10.1016/j.mseb.2016.10.004.

[11] A. Mehmood, N.M. Mubarak, M. Khalid, R. Walvekar, E.C. Abdullah, M. T. Siddiqui, H.A. Baloch, S. Nizamuddin, S. Mazari, Graphene based nanomaterials for strain sensor application—a review, J. Environ. Chem. Eng. 8 (2020) 103743, https://doi.org/10.1016/j.jece.2020.103743.

[12] M. Wilson, Electrons in atomically thin carbon sheets behave like massless particles, Phys. Today 59 (2006) 21–23, https://doi.org/10.1063/1.2180163.

[13] K.S. Novoselov, Z. Jiang, Y. Zhang, S.V. Morozov, H.L. Stormer, U. Zeitler, J. C. Maan, G.S. Boebinger, P. Kim, A.K. Geim, Room-temperature quantum hall effect in graphene, Science 315 (2007) 1379, https://doi.org/10.1126/science.1137201.

[14] X. Du, I. Skachko, A. Barker, E.Y. Andrei, Approaching ballistic transport in suspended graphene, Nat. Nanotechnol. 3 (2008) 491–495, https://doi.org/10.1038/nnano.2008.199.

[15] A.C. Ferrari, F. Bonaccorso, V. Fal'ko, K.S. Novoselov, S. Roche, P. Bøggild, S. Borini, F.H.L. Koppens, V. Palermo, N. Pugno, J.A. Garrido, R. Sordan, A. Bianco, L. Ballerini, M. Prato, E. Lidorikis, J. Kivioja, C. Marinelli, T. Ryhänen, A. Morpurgo, J.N. Coleman, V. Nicolosi, L. Colombo, A. Fert, M. Garcia-Hernandez, A. Bachtold, G.F. Schneider, F. Guinea, C. Dekker, M. Barbone, Z. Sun, C. Galiotis, A.N. Grigorenko, G. Konstantatos, A. Kis, M. Katsnelson, L. Vandersypen, A. Loiseau, V. Morandi, D. Neumaier, E. Treossi, V. Pellegrini, M. Polini, A. Tredicucci, G.M. Williams, B. Hee Hong, J.H. Ahn, J. Min Kim, H. Zirath, B.J. Van Wees, H. Van Der Zant, L. Occhipinti, A. Di Matteo, I. A. Kinloch, T. Seyller, E. Quesnel, X. Feng, K. Teo, N. Rupesinghe, P. Hakonen, S. R.T. Neil, Q. Tannock, T. Löfwander, J. Kinaret, Science and technology roadmap for graphene, related two-dimensional crystals, and hybrid systems, Nanoscale 7 (2015) 4598–4810, https://doi.org/10.1039/c4nr01600a.

[16] A. Abbasi, H. Rezania, Electrical conductivity of undoped bilayer Graphene: beyond nearest neighbor approximation, Chem. Phys. (2019), https://doi.org/10.1016/j.chemphys.2019.05.011.

[17] W. Zhu, V. Perebeinos, M. Freitag, P. Avouris, Carrier scattering, mobilities, and electrostatic potential in monolayer, bilayer, and trilayer graphene, Phys. Rev. B Condens. Matter 80 (2009), https://doi.org/10.1103/PhysRevB.80.235402.

[18] S. Das Sarma, S. Adam, E.H. Hwang, E. Rossi, Electronic transport in two-dimensional graphene, Rev. Mod. Phys. 83 (2011) 407–470, https://doi.org/10.1103/RevModPhys.83.407.

[19] J.B. Oostinga, H.B. Heersche, X. Liu, A.F. Morpurgo, L.M.K. Vandersypen, Gate-induced insulating state in bilayer graphene devices, Nat. Mater. 7 (2008) 151–157, https://doi.org/10.1038/nmat2082.

[20] J.-A. Yan, L. Xian, M.Y. Chou, Structural and electronic properties of oxidized graphene, Phys. Rev. Lett. 103 (2009), https://doi.org/10.1103/PhysRevLett.103.086802.

[21] S. Stankovich, D.A. Dikin, R.D. Piner, K.A. Kohlhaas, A. Kleinhammes, Y. Jia, Y. Wu, S.T. Nguyen, R.S. Ruoff, Synthesis of graphene-based nanosheets via chemical reduction of exfoliated graphite oxide, Carbon N. Y. 45 (2007) 1558–1565, https://doi.org/10.1016/j.carbon.2007.02.034.

[22] T.N. Zhou, X.D. Qi, Q. Fu, The preparation of the poly(vinyl alcohol)/graphene nanocomposites with low percolation threshold and high electrical conductivity by using the large-area reduced graphene oxide sheets, Express Polym. Lett. 7 (2013) 747–755, https://doi.org/10.3144/expresspolymlett.2013.72.

[23] H. Chang, Z. Sun, M. Saito, Q. Yuan, H. Zhang, J. Li, Z. Wang, T. Fujita, F. Ding, Z. Zheng, F. Yan, H. Wu, M. Chen, Y. Ikuhara, Regulating infrared photoresponses in reduced graphene oxide phototransistors by defect and atomic structure control, ACS Nano 7 (2013) 6310–6320, https://doi.org/10.1021/nn4023679.

[24] P. Sehrawat Abid, S.S. Islam, P. Mishra, S. Ahmad, Reduced graphene oxide (rGO) based wideband optical sensor and the role of Temperature, Defect States and Quantum Efficiency, Sci. Rep. 8 (2018), https://doi.org/10.1038/s41598-018-21686-2.

[25] A.G. Olabi, M.A. Abdelkareem, T. Wilberforce, E.T. Sayed, Application of graphene in energy storage device – a review, Renew. Sustain. Energy Rev. 135 (2021) 110026, https://doi.org/10.1016/j.rser.2020.110026.

[26] Z. Zhang, A. Fraser, S. Ye, G. Merle, J. Barralet, Top-down bottom-up graphene synthesis, Nano Futur 3 (2019) 042003, https://doi.org/10.1088/2399-1984/ab4eff.

[27] F. Akbar, M. Kolahdouz, S. Larimian, B. Radfar, H.H. Radamson, Graphene synthesis, characterization and its applications in nanophotonics, nanoelectronics, and nanosensing, J. Mater. Sci. Mater. Electron. 26 (2015) 4347–4379, https://doi.org/10.1007/s10854-015-2725-9.

[28] C. Brodie, XIII. On the atomic weight of graphite, Philos. Trans. R. Soc. London, A 149 (1859) 249–259, https://doi.org/10.1098/rstl.1859.0013.

[29] L. Staudenmaier, Verfahren zur Darstellung der Graphitsäure, Berichte Der Dtsch, Chem. Gesellschaft. 32 (1899) 1394–1399, https://doi.org/10.1002/cber.18990320208.

[30] W.S. Hummers, R.E. Offeman, Preparation of graphitic oxide, J. Am. Chem. Soc. 80 (1958) 1339, https://doi.org/10.1021/ja01539a017, 1339.

[31] Y. Hou, S. Lv, L. Liu, X. Liu, High-quality preparation of graphene oxide via the Hummers' method: understanding the roles of the intercalator, oxidant, and graphite particle size, Ceram. Int. 46 (2020) 2392–2402, https://doi.org/10.1016/j.ceramint.2019.09.231.

[32] A.M. Dimiev, J.M. Tour, Mechanism of graphene oxide formation, ACS Nano 8 (2014) 3060–3068, https://doi.org/10.1021/nn500606a.

[33] A.B. Bourlinos, D. Gournis, D. Petridis, T. Szabó, A. Szeri, I. Dékány, Graphite oxide: chemical reduction to graphite and surface modification with primary aliphatic amines and amino acids, Langmuir 19 (2003) 6050–6055, https://doi.org/10.1021/la026525h.

[34] S. Pei, H.-M. Cheng, The reduction of graphene oxide, Carbon N. Y. 50 (2012) 3210–3228, https://doi.org/10.1016/j.carbon.2011.11.010.

[35] S. Park, J. An, J.R. Potts, A. Velamakanni, S. Murali, R.S. Ruoff, Hydrazine-reduction of graphite- and graphene oxide, Carbon N. Y. 49 (2011) 3019–3023, https://doi.org/10.1016/j.carbon.2011.02.071.

[36] A. Vianelli, A. Candini, E. Treossi, V. Palermo, M. Affronte, Observation of different charge transport regimes and large magnetoresistance in graphene oxide layers, Carbon N. Y. 89 (2015) 188–196, https://doi.org/10.1016/j.carbon.2015.03.019.

[37] Z.-S. Wu, W. Ren, L. Gao, J. Zhao, Z. Chen, B. Liu, D. Tang, B. Yu, C. Jiang, H.-M. Cheng, Synthesis of graphene sheets with high electrical conductivity and good thermal stability by hydrogen arc discharge exfoliation, ACS Nano 3 (2009) 411–417, https://doi.org/10.1021/nn900020u.

[38] M. Ghislandi, E. Tkalya, A. Alekseev, C. Koning, G. de With, Electrical conductive behavior of polymer composites prepared with aqueous graphene dispersions, Appl. Mater. Today 1 (2015) 88–94, https://doi.org/10.1016/j.apmt.2015.11.001.

[39] A.J. Marsden, D.G. Papageorgiou, C. Vallés, A. Liscio, V. Palermo, M.A. Bissett, R. J. Young, I.A. Kinloch, Electrical percolation in graphene–polymer composites, 2D Mater. 5 (2018) 032003, https://doi.org/10.1088/2053-1583/aac055.

[40] Ayesha Khan, Sadia Iqbal, Mehrab Khan, Fauzia Iqbal, Sara Musaddiq, Warda Masoom, Amna Sarwar, A comprehensive review on polymer nanocomposites; classification, properties and potential applications, J. Nanoscope. 4 (2023) 45–74, https://doi.org/10.52700/jn.v4i1.88.

[41] C.W. Nan, Y. Shen, J. Ma, Physical properties of composites near percolation, Annu. Rev. Mater. Res. 40 (2010) 131–151, https://doi.org/10.1146/annurev-matsci-070909-104529.

[42] J.W. Essam, Percolation theory, Rep. Prog. Phys. 43 (1980) 833–912, https://doi.org/10.1088/0034-4885/43/7/001.

[43] I. Mutlay, L.B. Tudoran, Percolation behavior of electrically conductive graphene nanoplatelets/polymer nanocomposites: theory and experiment, Fullerenes Nanotub, Carbon Nanostructures 22 (2014) 413–433, https://doi.org/10.1080/1536383X.2012.684186.

[44] S.C. Mun, M.J. Kim, M. Cobos, L. Gu, C.W. Macosko, Strategies for interfacial localization of graphene/polyethylene-based cocontinuous blends for electrical percolation, AIChE J. 65 (2019), https://doi.org/10.1002/aic.16579.

[45] C. Bessaguet, E. Dantras, G. Michon, M. Chevalier, L. Laffont, C. Lacabanne, Electrical behavior of a graphene/PEKK and carbon black/PEKK nanocomposites in the vicinity of the percolation threshold, J. Non-Cryst. Solids 512 (2019) 1–6, https://doi.org/10.1016/j.jnoncrysol.2019.02.017.

[46] B. Krause, R. Boldt, L. Häußler, P. Pötschke, Ultralow percolation threshold in polyamide 6.6/MWCNT composites, Compos. Sci. Technol. 114 (2015) 119–125, https://doi.org/10.1016/j.compscitech.2015.03.014.

[47] C. Mao, Y. Zhu, W. Jiang, Design of electrical conductive composites: tuning the morphology to improve the electrical properties of graphene filled immiscible polymer blends, ACS Appl. Mater. Interfaces 4 (2012) 5281–5286, https://doi.org/10.1021/am301230q.

[48] R. Dou, Y. Shao, S. Li, B. Yin, M. Yang, Structuring tri-continuous structure multiphase composites with ultralow conductive percolation threshold and excellent electromagnetic shielding effectiveness using simple melt mixing, Polymer (Guildf). 83 (2016) 34–39, https://doi.org/10.1016/j.polymer.2015.12.005.

[49] A. Abbasi, A. Bose, Massive and sustained enhancement of the electrical conductivity of polystyrene using multilayer graphene at Low loadings, and carbon black as a dispersion aid, Colloids Surf. A Physicochem. Eng. Asp. 580 (2019) 123727, https://doi.org/10.1016/j.colsurfa.2019.123727.

[50] A. Mohamed, T. Ardyani, S. Abu Bakar, M. Sagisaka, Y. Umetsu, J.J. Hamon, B. A. Rahim, S.R. Esa, H.P.S. Abdul Khalil, M.H. Mamat, S. King, J. Eastoe, Rational design of aromatic surfactants for graphene/natural rubber latex nanocomposites with enhanced electrical conductivity, J. Colloid Interface Sci. 516 (2018) 34–47, https://doi.org/10.1016/j.jcis.2018.01.041.
[51] S. Maiti, B.B. Khatua, Graphene nanoplate and multiwall carbon nanotube–embedded polycarbonate hybrid composites: high electromagnetic interference shielding with low percolation threshold, Polym. Compos. 37 (2016) 2058–2069, https://doi.org/10.1002/pc.23384.
[52] E. Zhou, J. Xi, Y. Guo, Y. Liu, Z. Xu, L. Peng, W. Gao, J. Ying, Z. Chen, C. Gao, Synergistic effect of graphene and carbon nanotube for high-performance electromagnetic interference shielding films, Carbon N. Y. 133 (2018) 316–322, https://doi.org/10.1016/j.carbon.2018.03.023.
[53] S. Zhang, S. Yin, C. Rong, P. Huo, Z. Jiang, G. Wang, Synergistic effects of functionalized graphene and functionalized multi-walled carbon nanotubes on the electrical and mechanical properties of poly(ether sulfone) composites, Eur. Polym. J. 49 (2013) 3125–3134, https://doi.org/10.1016/j.eurpolymj.2013.07.011.
[54] I. Chakraborty, K.J. Bodurtha, N.J. Heeder, M.P. Godfrin, A. Tripathi, R.H. Hurt, A. Shukla, A. Bose, Massive electrical conductivity enhancement of multilayer graphene/polystyrene composites using a nonconductive filler, ACS Appl. Mater. Interfaces 6 (2014) 16472–16475, https://doi.org/10.1021/am5044592.
[55] F. Wang, H. Wang, J. Mao, Aligned-graphene composites: a review, J. Mater. Sci. 54 (2019) 36–61, https://doi.org/10.1007/s10853-018-2849-4.
[56] M. Monti, M. Natali, L. Torre, J.M. Kenny, The alignment of single walled carbon nanotubes in an epoxy resin by applying a DC electric field, Carbon N. Y. 50 (2012) 2453–2464, https://doi.org/10.1016/j.carbon.2012.01.067.
[57] W. Jiao, M. Shioya, R. Wang, F. Yang, L. Hao, Y. Niu, W. Liu, L. Zheng, F. Yuan, L. Wan, X. He, Improving the gas barrier properties of Fe3O4/graphite nanoplatelet reinforced nanocomposites by a low magnetic field induced alignment, Compos. Sci. Technol. 99 (2014) 124–130, https://doi.org/10.1016/j.compscitech.2014.05.022.
[58] Q. Wang, J. Dai, W. Li, Z. Wei, J. Jiang, The effects of CNT alignment on electrical conductivity and mechanical properties of SWNT/epoxy nanocomposites, Compos. Sci. Technol. 68 (2008) 1644–1648, https://doi.org/10.1016/j.compscitech.2008.02.024.
[59] Z. Wang, X. Shen, N.M. Han, X. Liu, Y. Wu, W. Ye, J.K. Kim, Ultralow electrical percolation in graphene aerogel/epoxy composites, Chem. Mater. 28 (2016) 6731–6741, https://doi.org/10.1021/acs.chemmater.6b03206.
[60] P. Fan, L. Wang, J. Yang, F. Chen, M. Zhong, Graphene/poly(vinylidene fluoride) composites with high dielectric constant and low percolation threshold, Nanotechnology 23 (2012) 365702, https://doi.org/10.1088/0957-4484/23/36/365702.
[61] F. Wang, J. Mao, The self-aligning behaviour of graphene nanosheets in the styrene butadiene rubber by controlling curing temperature, Fullerenes Nanotub, Carbon Nanostructures 26 (2018) 61–68, https://doi.org/10.1080/1536383X.2017.1409730.
[62] S. Wu, R.B. Ladani, J. Zhang, E. Bafekrpour, K. Ghorbani, A.P. Mouritz, A. J. Kinloch, C.H. Wang, Aligning multilayer graphene flakes with an external electric field to improve multifunctional properties of epoxy nanocomposites, Carbon N. Y. 94 (2015) 607–618, https://doi.org/10.1016/j.carbon.2015.07.026.
[63] H. Le Ferrand, S. Bolisetty, A.F. Demirörs, R. Libanori, A.R. Studart, R. Mezzenga, Magnetic assembly of transparent and conducting graphene-based functional composites, Nat. Commun. 7 (2016) 12078, https://doi.org/10.1038/ncomms12078.
[64] Y. Gao, O.T. Picot, E. Bilotti, T. Peijs, Influence of filler size on the properties of poly(lactic acid) (PLA)/graphene nanoplatelet (GNP) nanocomposites, Eur. Polym. J. 86 (2017) 117–131, https://doi.org/10.1016/j.eurpolymj.2016.10.045.
[65] N.M. Han, Z. Wang, X. Shen, Y. Wu, X. Liu, Q. Zheng, J.-K. Kim, Effects of graphene sheet size on electrical conductivity and percolation of graphene aerogel/epoxy composites, in: ICCM Int. Conf. Compos. Mater., 2017.
[66] S. He, J. Zhang, X. Xiao, X. Hong, Y. Lai, Investigation of the conductive network formation of polypropylene/graphene nanoplatelets composites for different platelet sizes, J. Mater. Sci. 52 (2017) 13103–13119, https://doi.org/10.1007/s10853-017-1413-y.
[67] N.M. Han, Z. Wang, X. Shen, Y. Wu, X. Liu, Q. Zheng, T.H. Kim, J. Yang, J.K. Kim, Graphene size-dependent multifunctional properties of unidirectional graphene aerogel/epoxy nanocomposites, ACS Appl. Mater. Interfaces 10 (2018) 6580–6592, https://doi.org/10.1021/acsami.7b19069.
[68] T.S. Sreeprasad, V. Berry, How do the electrical properties of graphene change with its functionalization? Small 9 (2013) 341–350, https://doi.org/10.1002/smll.201202196.
[69] W. Zheng, B. Shen, W. Zhai, Surface functionalization of graphene with polymers for enhanced properties, in: New Prog. Graphene Res., InTech, 2013, https://doi.org/10.5772/50490.
[70] P. Feicht, S. Eigler, Defects in graphene oxide as structural motifs, ChemNanoMat 4 (2018) 244–252, https://doi.org/10.1002/cnma.201700357.
[71] G. Eda, Y.Y. Lin, C. Mattevi, H. Yamaguchi, H.A. Chen, I.S. Chen, C.W. Chen, M. Chhowalla, Blue photoluminescence from chemically derived graphene oxide, Adv. Mater. 22 (2010) 505–509, https://doi.org/10.1002/adma.200901996.
[72] H.J. Salavagione, G. Martínez, G. Ellis, Recent advances in the covalent modification of graphene with polymers, macromol, Rapid Commun. 32 (2011) 1771–1789, https://doi.org/10.1002/marc.201100527.
[73] N. Rubio, H. Au, H.S. Leese, S. Hu, A.J. Clancy, M.S.P. Shaffer, Grafting from versus grafting to approaches for the functionalization of graphene nanoplatelets with poly(methyl methacrylate), Macromolecules 50 (2017) 7070–7079, https://doi.org/10.1021/acs.macromol.7b01047.
[74] R.K. Layek, A.K. Nandi, A review on synthesis and properties of polymer functionalized graphene, Polymer (Guildf). 54 (2013) 5087–5103, https://doi.org/10.1016/j.polymer.2013.06.027.
[75] J. Liu, Y. Ye, Y. Xue, X. Xie, Y.W. Mai, Recent advances in covalent functionalization of carbon nanomaterials with polymers: strategies and perspectives, J. Polym. Sci. Part A Polym. Chem. 55 (2017) 622–631, https://doi.org/10.1002/pola.28426.
[76] S. Park, S. He, J. Wang, A. Stein, C.W. Macosko, Graphene-polyethylene nanocomposites: effect of graphene functionalization, Polymer (Guildf). 104 (2016) 1–9, https://doi.org/10.1016/j.polymer.2016.09.058.
[77] A. Guimont, E. Beyou, P. Cassagnau, G. Martin, P. Sonntag, F. D'Agosto, C. Boisson, Grafting of polyethylene onto graphite oxide sheets: a comparison of two routes, Polym. Chem. 4 (2013) 2828–2836, https://doi.org/10.1039/c3py00160a.
[78] M. Castelaín, G. Martínez, C. Marco, G. Ellis, H.J. Salavagione, Effect of click-chemistry approaches for graphene modification on the electrical, thermal, and mechanical properties of polyethylene/graphene nanocomposites, Macromolecules 46 (2013) 8980–8987, https://doi.org/10.1021/ma401606d.
[79] V.B. Mohan, D. Liu, K. Jayaraman, M. Stamm, D. Bhattacharyya, Improvements in electronic structure and properties of graphene derivatives, Adv. Mater. Lett. 7 (2016) 421–429, https://doi.org/10.5185/amlett.2016.6123.
[80] I. Childres, L.A. Jauregui, W. Park, H. Cao, Y.P. Chen, Raman spectroscopy of graphene and related materials, in: New Dev. Phot. Mater. Res., 2013.
[81] D. Yoon, H. Cheong, Raman spectroscopy for characterization of graphene, in: Raman Spectrosc. Nanomater. Charact., Springer-Verlag Berlin Heidelberg, 2012, pp. 191–214, https://doi.org/10.1007/978-3-642-20620-7_9.
[82] P. Blake, P.D. Brimicombe, R.R. Nair, T.J. Booth, D. Jiang, F. Schedin, L. A. Ponomarenko, S.V. Morozov, H.F. Gleeson, E.W. Hill, A.K. Geim, K. S. Novoselov, Graphene-based liquid crystal device, Nano Lett. 8 (2008) 1704–1708, https://doi.org/10.1021/nl080649i.
[83] H.A. Becerril, J. Mao, Z. Liu, R.M. Stoltenberg, Z. Bao, Y. Chen, Evaluation of solution-processed reduced graphene oxide films as transparent conductors, ACS Nano 2 (2008) 463–470, https://doi.org/10.1021/nn700375n.
[84] D. Vuluga, J.M. Thomassin, I. Molenberg, I. Huynen, B. Gilbert, C. Jérôme, M. Alexandre, C. Detrembleur, Straightforward synthesis of conductive graphene/polymer nanocomposites from graphite oxide, Chem. Commun. 47 (2011) 2544–2546, https://doi.org/10.1039/c0cc04623j.
[85] T. Lalire, B. Otazaghine, A. Taguet, C. Longuet, Correlation between multiple chemical modification strategies on graphene or graphite and physical/electrical properties, FlatChem 33 (2022) 100376, https://doi.org/10.1016/j.flatc.2022.100376.
[86] H. Aguilar-Bolados, M. Yazdani-Pedram, E. Quinteros-Jara, Q. Cuenca-Bracamonte, R. Quijada, J. Carretero-González, F. Avilés, M.A. Lopez-Manchado, R. Verdejo, Synthesis of sustainable, lightweight and electrically conductive polymer brushes grafted multi-layer graphene oxide, Polym. Test. 93 (2021) 106986, https://doi.org/10.1016/j.polymertesting.2020.106986.
[87] A. Arzac, G.P. Leal, J.C. de la Cal, R. Tomovska, Water-borne polymer/graphene nanocomposites, Macromol. Mater. Eng. 302 (2017) 1600315, https://doi.org/10.1002/mame.201600315.
[88] M. Lotya, Y. Hernandez, P.J. King, R.J. Smith, V. Nicolosi, L.S. Karlsson, F. M. Blighe, S. De, Z. Wang, I.T. McGovern, G.S. Duesberg, J.N. Coleman, Liquid phase production of graphene by exfoliation of graphite in surfactant/water solutions, J. Am. Chem. Soc. 131 (2009) 3611–3620, https://doi.org/10.1021/ja807449u.
[89] K.R. Nandanapalli, D. Mudusu, S. Lee, Functionalization of graphene layers and advancements in device applications, Carbon N. Y. 152 (2019) 954–985, https://doi.org/10.1016/j.carbon.2019.06.081.
[90] M. Sumita, K. Sakata, S. Asai, K. Miyasaka, H. Nakagawa, Dispersion of Fillers and the Electrical Conductivity of Polymer Blends Filled with Carbon Black, 1991.
[91] W. Thongruang, R.J. Spontak, C.M. Balik, Bridged double percolation in conductive polymer composites: an electrical conductivity, morphology and mechanical property study, Polymer (Guildf). 43 (2002) 3717–3725, https://doi.org/10.1016/S0032-3861(02)00180-5.
[92] J. Huang, Y. Zhu, L. Xu, J. Chen, W. Jiang, X. Nie, Massive enhancement in the thermal conductivity of polymer composites by trapping graphene at the interface of a polymer blend, Compos. Sci. Technol. 129 (2016) 160–165, https://doi.org/10.1016/j.compscitech.2016.04.029.
[93] Q. Zhang, J. Wang, B.-H. Guo, Z.-X. Guo, J. Yu, Electrical conductivity of carbon nanotube-filled miscible poly(phenylene oxide)/polystyrene blends prepared by melt compounding, Composites, Part B 176 (2019) 107213, https://doi.org/10.1016/j.compositesb.2019.107213.
[94] A.R. Ajitha, S. Thomas, Introduction: polymer blends, thermodynamics, miscibility, phase separation, and compatibilization, in: Compat. Polym. Blends, Elsevier, 2020, pp. 1–29, https://doi.org/10.1016/B978-0-12-816006-0.00001-3.
[95] G.M. Jordhamo, J.A. Manson, L.H. Sperling, Phase continuity and inversion in polymer blends and simultaneous interpenetrating networks, Polym. Eng. Sci. 26 (1986) 517–524, https://doi.org/10.1002/pen.760260802.
[96] C.M. Roland, G.G.A. Böuhm, Shear-induced coalescence in two-phase polymeric systems. I. Determination from small-angle neutron scattering measurements, J. Polym. Sci. Polym. Phys. Ed 22 (1984) 79–93, https://doi.org/10.1002/pol.1984.180220108.
[97] S. Ravati, B.D. Favis, Morphological states for a ternary polymer blend demonstrating complete wetting, Polymer (Guildf). 51 (2010) 4547–4561, https://doi.org/10.1016/j.polymer.2010.07.014.

[98] D.R. Paul, J.W. Barlow, Polymer blends, J. Macromol. Sci. Part C. 18 (1980) 109–168, https://doi.org/10.1080/00222358008080917.
[99] S. Steinmann, W. Gronski, C. Friedrich, Cocontinuous polymer blends: influence of viscosity and elasticity ratios of the constituent polymers on phase inversion, Polymer (Guildf). 42 (2001) 6619–6629, https://doi.org/10.1016/S0032-3861(01)00100-8.
[100] T.S. Omonov, C. Harrats, P. Moldenaers, G. Groeninckx, Phase continuity detection and phase inversion phenomena in immiscible polypropylene/polystyrene blends with different viscosity ratios, Polymer (Guildf). 48 (2007) 5917–5927, https://doi.org/10.1016/j.polymer.2007.08.012.
[101] P.A. Bhadane, M.F. Champagne, M.A. Huneault, F. Tofan, B.D. Favis, Continuity development in polymer blends of very low interfacial tension, Polymer (Guildf). 47 (2006) 2760–2771, https://doi.org/10.1016/j.polymer.2006.01.065.
[102] P. Pötschke, D.R. Paul, Formation of co-continuous structures in melt-mixed immiscible polymer blends, J. Macromol. Sci. Polym. Rev. 43 (2003) 87–141, https://doi.org/10.1081/MC-120018022.
[103] P. Le Corroller, B.D. Favis, Effect of viscosity in ternary polymer blends displaying partial wetting phenomena, Polymer (Guildf). 52 (2011) 3827–3834, https://doi.org/10.1016/j.polymer.2011.06.032.
[104] Y. Shao, R. Dou, S. Li, B. Yin, M. Yang, Morphology evolution and the tri-continuous morphology formation of a PVDF/PS/HDPE ternary blend in melt mixing, RSC Adv. 6 (2016) 38803–38810, https://doi.org/10.1039/C6RA07877J.
[105] R. Tol, G. Groeninckx, I. Vinckier, P. Moldenaers, J. Mewis, Phase morphology and stability of co-continuous (PPE/PS)/PA6 and PS/PA6 blends: effect of rheology and reactive compatibilization, Polymer (Guildf). 45 (2004) 2587–2601, https://doi.org/10.1016/j.polymer.2003.12.072.
[106] A. Taguet, P. Cassagnau, J.-M. Lopez-Cuesta, Structuration, selective dispersion and compatibilizing effect of (nano)fillers in polymer blends, Prog. Polym. Sci. 39 (2014) 1526–1563, https://doi.org/10.1016/j.progpolymsci.2014.04.002.
[107] M. Salzano de Luna, G. Filippone, Effects of nanoparticles on the morphology of immiscible polymer blends – challenges and opportunities, Eur. Polym. J. 79 (2016) 198–218, https://doi.org/10.1016/j.eurpolymj.2016.02.023.
[108] X. Cai, B. Li, Y. Pan, G. Wu, Morphology evolution of immiscible polymer blends as directed by nanoparticle self-agglomeration, Polymer (Guildf). 53 (2012) 259–266, https://doi.org/10.1016/j.polymer.2011.11.032.
[109] J.M. Feng, X.Q. Liu, R.Y. Bao, W. Yang, B.H. Xie, M.B. Yang, Suppressing phase coarsening in immiscible polymer blends using nano-silica particles located at the interface, RSC Adv. 5 (2015) 74295–74303, https://doi.org/10.1039/c5ra13637g.
[110] X.Q. Liu, Q.Y. Wang, R.Y. Bao, W. Yang, B.H. Xie, M.B. Yang, Suppressing phase retraction and coalescence of co-continuous polymer blends: effect of nanoparticles and particle network, RSC Adv. 4 (2014) 49429–49441, https://doi.org/10.1039/c4ra09138h.
[111] H.-B. Zhang, W.-G. Zheng, Q. Yan, Z.-G. Jiang, Z.-Z. Yu, The effect of surface chemistry of graphene on rheological and electrical properties of polymethylmethacrylate composites, Carbon N. Y. 50 (2012) 5117–5125, https://doi.org/10.1016/j.carbon.2012.06.052.
[112] Y. Shen, T.T. Zhang, J.H. Yang, N. Zhang, T. Huang, Y. Wang, Selective localization of reduced graphene oxides at the interface of PLA/EVA blend and its resultant electrical resistivity, Polym. Compos. 38 (2017) 1982–1991, https://doi.org/10.1002/pc.23769.
[113] J. Li, Z. Li, H. Chen, L. Yang, H. Zheng, Y. Shang, D. Yu, J. de Claville Christiansen, S. Jiang, A qualitative analysis of particle-induced viscosity reduction in polymeric composites, J. Mater. Sci. 51 (2016) 3080–3096, https://doi.org/10.1007/s10853-015-9618-4.
[114] M. Wang, R.J. Hill, Anomalous bulk viscosity of polymer-nanocomposite melts, Soft Matter 5 (2009) 3940–3953, https://doi.org/10.1039/b905686f.
[115] M.E. Mackay, T.T. Dao, A. Tuteja, D.L. Ho, B. Van Horn, H.C. Kim, C.J. Hawker, Nanoscale effects leading to non-einstein-like decrease in viscosity, Nat. Mater. 2 (2003) 762–766, https://doi.org/10.1038/nmat999.
[116] R. Eslami, S.R. Ghaffarian, M. Salehi, M. Rafizadeh, Evaluation of non-Einstein rheology behavior of soft nanoparticles/epoxy nano-composites and their multifunctional effects on curing kinetics, Polym. Test. 66 (2018) 350–359, https://doi.org/10.1016/j.polymertesting.2018.02.007.
[117] E. Nilsson, H. Oxfall, W. Wandelt, R. Rychwalski, B. Hagström, Melt spinning of conductive textile fibers with hybridized graphite nanoplatelets and carbon black filler, J. Appl. Polym. Sci. 130 (2013) 2579–2587, https://doi.org/10.1002/app.39480.
[118] T. Chen, H.-Y. Zhao, R. Shi, W.-F. Lin, X.-M. Jia, H.-J. Qian, Z.-Y. Lu, X.-X. Zhang, Y.-K. Li, Z.-Y. Sun, An unexpected N-dependence in the viscosity reduction in all-polymer nanocomposite, Nat. Commun. 10 (2019) 5552, https://doi.org/10.1038/s41467-019-13410-z.
[119] S. Jain, J.G.P. Goossens, G.W.M. Peters, M. Van Duin, P.J. Lemstra, Strong decrease in viscosity of nanoparticle-filled polymer melts through selective adsorption, Soft Matter 4 (2008) 1848–1854, https://doi.org/10.1039/b802905a.
[120] S.P. Pawar, S. Bose, Peculiar morphological transitions induced by nanoparticles in polymeric blends: retarded relaxation or altered interfacial tension? Phys. Chem. Chem. Phys. 17 (2015) 14470–14473, https://doi.org/10.1039/c5cp01644d.
[121] S. Wu, Calculation of interfacial tension in polymer systems, J. Polym. Sci. Part C Polym. Symp. 34 (2007) 19–30, https://doi.org/10.1002/polc.5070340105.
[122] S. Steinmann, W. Gronski, C. Friedrich, Influence of selective filling on rheological properties and phase inversion of two-phase polymer blends, Polymer (Guildf). 43 (2002) 4467–4477, https://doi.org/10.1016/S0032-3861(02)00271-9.
[123] P. Xing, M. Bousmina, D. Rodrigue, M.R. Kamal, Critical experimental comparison between five techniques for the determination of interfacial tension in polymer blends: model system of polystyrene/polyamide-6, Macromolecules 33 (2000) 8020–8034, https://doi.org/10.1021/ma000537x.
[124] L. Elias, F. Fenouillot, J.C. Majeste, P. Cassagnau, Morphology and rheology of immiscible polymer blends filled with silica nanoparticles, Polymer (Guildf). 48 (2007) 6029–6040, https://doi.org/10.1016/j.polymer.2007.07.061.
[125] A. Barber, S. Cohen, H. Wagner, Static and dynamic wetting measurements of single carbon nanotubes, Phys. Rev. Lett. 92 (2004) 186103, https://doi.org/10.1103/PhysRevLett.92.186103.
[126] M. Hadaeghnia, S. Ahmadi, I. Ghasemi, P.M. Wood-Adams, Manipulating the morphology of PA6/POE blends using graphene to achieve balanced electrical and mechanical properties, Compos. Sci. Technol. 200 (2020) 108412, https://doi.org/10.1016/j.compscitech.2020.108412.
[127] L.A. Belyaeva, G.F. Schneider, Wettability of graphene, Surf. Sci. Rep. 75 (2020) 100482, https://doi.org/10.1016/j.surfrep.2020.100482.
[128] S. Wang, Y. Zhang, N. Abidi, L. Cabrales, Wettability and surface free energy of graphene films, Langmuir 25 (2009) 11078–11081, https://doi.org/10.1021/la901402f.
[129] A. Kozbial, Z. Li, C. Conaway, R. McGinley, S. Dhingra, V. Vahdat, F. Zhou, B. Durso, H. Liu, L. Li, Study on the surface energy of graphene by contact angle measurements, Langmuir 30 (2014) 8598–8606, https://doi.org/10.1021/la5018328.
[130] F. Du, J. Huang, H. Duan, C. Xiong, J. Wang, Wetting transparency of supported graphene is regulated by polarities of liquids and substrates, Appl. Surf. Sci. 454 (2018) 249–255, https://doi.org/10.1016/j.apsusc.2018.05.098.
[131] D.K. Owens, R.C. Wendt, Estimation of the surface free energy of polymers, J. Appl. Polym. Sci. 13 (1969) 1741–1747, https://doi.org/10.1002/app.1969.070130815.
[132] F.M. Fowkes, Attractive forces at interfaces, Ind. Eng. Chem. 56 (1964) 40–52, https://doi.org/10.1021/ie50660a008.
[133] D. Li, A.W. Neumann, Equilibrium of capillary systems with an elastic liquid-vapor interface, Langmuir 9 (1993) 50–54, https://doi.org/10.1021/la00025a014.
[134] Z. Li, Y. Wang, A. Kozbial, G. Shenoy, F. Zhou, R. McGinley, P. Ireland, B. Morganstein, A. Kunkel, S.P. Surwade, L. Li, H. Liu, Effect of airborne contaminants on the wettability of supported graphene and graphite, Nat. Mater. 12 (2013) 925–931, https://doi.org/10.1038/nmat3709.
[135] C.D. Van Engers, N.E.A. Cousens, V. Babenko, J. Britton, B. Zappone, N. Grobert, S. Perkin, Direct measurement of the surface energy of graphene, Nano Lett. 17 (2017) 3815–3821, https://doi.org/10.1021/acs.nanolett.7b01181.
[136] L. Bai, R. Sharma, X. Cheng, C.W. Macosko, Kinetic control of graphene localization in Co-continuous polymer blends via melt compounding, Langmuir 34 (2018) 1073–1083, https://doi.org/10.1021/acs.langmuir.7b03085.
[137] L. Bai, S. He, J.W. Fruehwirth, A. Stein, C.W. Macosko, X. Cheng, Localizing graphene at the interface of cocontinuous polymer blends: morphology, rheology, and conductivity of cocontinuous conductive polymer composites, J. Rheol. (N. Y., NY, U. S.) 61 (2017) 575–587, https://doi.org/10.1122/1.4982702.
[138] M. Liebscher, M.O. Blais, P. Pötschke, G. Heinrich, A morphological study on the dispersion and selective localization behavior of graphene nanoplatelets in immiscible polymer blends of PC and SAN, Polymer (Guildf). 54 (2013) 5875–5882, https://doi.org/10.1016/j.polymer.2013.08.009.
[139] A. Göldel, A. Marmur, G.R. Kasaliwal, P. Pötschke, G. Heinrich, Shape-dependent localization of carbon nanotubes and carbon black in an immiscible polymer blend during melt mixing, Macromolecules 44 (2011) 6094–6102, https://doi.org/10.1021/ma200793a.
[140] J. de Aguiar, M. Decol, W.M. Pachekoski, D. Becker, Mixing-sequence controlled selective localization of carbon nanoparticles in PLA/PCL blends, Polym. Eng. Sci. 59 (2019) 323–329, https://doi.org/10.1002/pen.24908.
[141] J. Plattier, L. Benyahia, M. Dorget, F. Niepceron, J.-F. Tassin, Viscosity-induced filler localisation in immiscible polymer blends, Polymer (Guildf). 59 (2015) 260–269, https://doi.org/10.1016/j.polymer.2014.12.044.
[142] C. Tu, K. Nagata, S. Yan, Influence of melt-mixing processing sequence on electrical conductivity of polyethylene/polypropylene blends filled with graphene, Polym. Bull. 74 (2017) 1237–1252, https://doi.org/10.1007/s00289-016-1774-4.
[143] Y. Kou, A.T. Cote, J. Liu, X. Cheng, C.W. Macosko, Robust networks of interfacial localized graphene in cocontinuous polymer blends, J. Rheol. (N. Y., NY, U. S.) 65 (2021) 1139–1153, https://doi.org/10.1122/8.0000294.
[144] L. Elias, F. Fenouillot, J.C. Majesté, G. Martin, P. Cassagnau, Migration of nanosilica particles in polymer blends, J. Polym. Sci., Part B: Polym. Phys. 46 (2008) 1976–1983, https://doi.org/10.1002/polb.21534.
[145] R. Salehiyan, S.S. Ray, Tuning the conductivity of nanocomposites through nanoparticle migration and interface crossing in immiscible polymer blends: a review on fundamental understanding, Macromol. Mater. Eng. 304 (2019) 1800431, https://doi.org/10.1002/mame.201800431.
[146] F. Fenouillot, P. Cassagnau, J.-C. Majesté, Uneven distribution of nanoparticles in immiscible fluids: morphology development in polymer blends, Polymer (Guildf). 50 (2009) 1333–1350, https://doi.org/10.1016/j.polymer.2008.12.029.
[147] J. Feng, C.-M. Chan, J.-X. Li, A method to control the dispersion of carbon black in an immiscible polymer blend, Polym. Eng. Sci. 43 (2003) 1058–1063, https://doi.org/10.1002/pen.10089.
[148] W. Li, X.Z. Tang, H. Bin Zhang, Z.G. Jiang, Z.Z. Yu, X.S. Du, Y.W. Mai, Simultaneous surface functionalization and reduction of graphene oxide with

octadecylamine for electrically conductive polystyrene composites, Carbon N. Y. 49 (2011) 4724–4730, https://doi.org/10.1016/j.carbon.2011.06.077.
[149] C. Vallés, D.G. Papageorgiou, F. Lin, Z. Li, B.F. Spencer, R.J. Young, I.A. Kinloch, PMMA-grafted graphene nanoplatelets to reinforce the mechanical and thermal properties of PMMA composites, Carbon N. Y. 157 (2020) 750–760, https://doi.org/10.1016/j.carbon.2019.10.075.
[150] Y. Tan, L. Fang, J. Xiao, Y. Song, Q. Zheng, Grafting of copolymers onto graphene by miniemulsion polymerization for conductive polymer composites: improved electrical conductivity and compatibility induced by interfacial distribution of graphene, Polym. Chem. 4 (2013) 2939–2944, https://doi.org/10.1039/c3py00164d.
[151] A. Kol, S. Kenig, N. Naveh, Silane-modified graphene oxide as a compatibilizer and reinforcing nanoparticle for immiscible PP/PA blends, Polym. Eng. Sci. 60 (2020) 180–191, https://doi.org/10.1002/pen.25271.
[152] Y. Hao, X. Zhao, J. Dong, Q. Zhang, The compatibilization effects of alkylated-grafted -graphene oxide on polypropylene/polystyrene blends, Int. J. Polym. Sci. 2017 (2017) 1–11, https://doi.org/10.1155/2017/2151205.
[153] J. Shen, Y. Hu, C. Li, C. Qin, M. Ye, Synthesis of amphiphilic graphene nanoplatelets, Small 5 (2009) 82–85, https://doi.org/10.1002/smll.200800988.
[154] S. Pu, Y.-B. Hao, X.-X. Dai, P.-P. Zhang, J.-B. Zeng, M. Wang, Morphological, rheological, crystalline and mechanical properties of ethylene-vinyl acetate copolymer/linear low-density polyethylene/amphiphilic graphene oxide nanocomposites, Polym. Test. 63 (2017) 289–297, https://doi.org/10.1016/j.polymertesting.2017.08.028.
[155] G.P. Kar, S. Biswas, S. Bose, Tailoring the interface of an immiscible polymer blend by a mutually miscible homopolymer grafted onto graphene oxide: outstanding mechanical properties, Phys. Chem. Chem. Phys. 17 (2015) 1811–1821, https://doi.org/10.1039/C4CP04481A.
[156] K.C. Bryson, T.I. Löbling, A.H.E. Müller, T.P. Russell, R.C. Hayward, Using Janus nanoparticles to trap polymer blend morphologies during solvent-evaporation-induced demixing, Macromolecules 48 (2015) 4220–4227, https://doi.org/10.1021/acs.macromol.5b00640.
[157] A. Walther, K. Matussek, A.H.E. Müller, Engineering nanostructured polymer blends with controlled nanoparticle location using Janus particles, ACS Nano 2 (2008) 1167–1178, https://doi.org/10.1021/nn800108y.
[158] H. Alkhodairi, S.T. Russell, J. Pribyl, B.C. Benicewicz, S.K. Kumar, Compatibilizing immiscible polymer blends with sparsely grafted nanoparticles, Macromolecules 53 (2020) 10330–10338, https://doi.org/10.1021/acs.macromol.0c02108.
[159] Z. Fu, H. Wang, X. Zhao, S. Horiuchi, Y. Li, Immiscible polymer blends compatibilized with reactive hybrid nanoparticles: morphologies and properties, Polymer (Guildf) 132 (2017) 353–361, https://doi.org/10.1016/j.polymer.2017.11.004.
[160] H. Wu, W. Yi, Z. Chen, H. Wang, Q. Du, Janus graphene oxide nanosheets prepared via Pickering emulsion template, Carbon N. Y. 93 (2015) 473–483, https://doi.org/10.1016/j.carbon.2015.05.083.
[161] M. Akbari, M. Shariaty-Niassar, T. Matsuura, A.F. Ismail, Janus graphene oxide nanosheet: a promising additive for enhancement of polymeric membranes performance prepared via phase inversion, J. Colloid Interface Sci. 527 (2018) 10–24, https://doi.org/10.1016/j.jcis.2018.05.012.
[162] S.W. Ng, N. Noor, Z. Zheng, Graphene-based two-dimensional Janus materials, NPG Asia Mater. 10 (2018) 217–237, https://doi.org/10.1038/s41427-018-0023-8.
[163] A. Ma, G. Wang, Z. Yang, L. Bai, H. Chen, W. Wang, H. Yang, D. Wei, L. Yang, Fabrication of Janus graphene oxide hybrid nanosheets by Pickering emulsion template for self-healing nanocomposite hydrogels, Chem. Eng. J. 385 (2020) 123962, https://doi.org/10.1016/j.cej.2019.123962.
[164] K. Kultravut, K. Kuboyama, V. Sedlarik, M. Mrlík, J. Osička, P. Dröhsler, T. Ougizawa, Localization of poly(glycidyl methacrylate) grafted on reduced graphene oxide in poly(lactic acid)/Poly(trimethylene terephthalate) blends for composites with enhanced electrical and thermal conductivities, ACS Appl. Nano Mater. 4 (2021) 8511–8519, https://doi.org/10.1021/acsanm.1c01843.
[165] X.R. Sun, T. Gong, J.H. Pu, R.Y. Bao, B.H. Xie, M.B. Yang, W. Yang, Effect of phase coarsening under melt annealing on the electrical performance of polymer composites with a double percolation structure, Phys. Chem. Chem. Phys. 20 (2017) 137–147, https://doi.org/10.1039/c7cp07493j.
[166] R.S. Kurusu, E. Helal, N. Moghimian, E. David, N. Demarquette, The role of selectively located commercial graphene nanoplatelets in the electrical properties, morphology, and stability of EVA/LLDPE blends, Macromol. Mater. Eng. 303 (2018) 1800187, https://doi.org/10.1002/mame.201800187.
[167] Y. Kou, X. Cheng, C.W. Macosko, Polymer/graphene composites via spinodal decomposition of miscible polymer blends, Macromolecules 52 (2019) 7625–7637, https://doi.org/10.1021/acs.macromol.9b01391.
[168] M.M. Rueda, M.-C. Auscher, R. Fulchiron, T. Périé, G. Martin, P. Sonntag, P. Cassagnau, Rheology and applications of highly filled polymers: a review of current understanding, Prog. Polym. Sci. 66 (2017) 22–53, https://doi.org/10.1016/j.progpolymsci.2016.12.007.
[169] E. Helal, R.S. Kurusu, N. Moghimian, G. Gutierrez, E. David, N.R. Demarquette, Correlation between morphology, rheological behavior, and electrical behavior of conductive cocontinuous LLDPE/EVA blends containing commercial graphene nanoplatelets, J. Rheol. (N. Y., NY, U. S.) 63 (2019) 961–976, https://doi.org/10.1122/1.5108919.
[170] L. Zonder, A. Ophir, S. Kenig, S. McCarthy, The effect of carbon nanotubes on the rheology and electrical resistivity of polyamide 12/high density polyethylene blends, Polymer (Guildf). 52 (2011) 5085–5091, https://doi.org/10.1016/j.polymer.2011.08.048.
[171] J. Zhang, S. Ravati, N. Virgilio, B.D. Favis, Ultralow percolation thresholds in ternary cocontinuous polymer blends, Macromolecules 40 (2007) 8817–8820, https://doi.org/10.1021/ma0716480.
[172] H. Kim, Y. Miura, C.W. MacOsko, Graphene/polyurethane nanocomposites for improved gas barrier and electrical conductivity, Chem. Mater. 22 (2010) 3441–3450, https://doi.org/10.1021/cm100477v.
[173] X.S. Du, M. Xiao, Y.Z. Meng, Facile synthesis of highly conductive polyaniline/graphite nanocomposites, Eur. Polym. J. 40 (2004) 1489–1493, https://doi.org/10.1016/j.eurpolymj.2004.02.009.
[174] W.P. Wang, Y. Liu, X.X. Li, Y.Z. You, Synthesis and characteristics of poly(methyl methacrylate)/expanded graphite nanocomposites, J. Appl. Polym. Sci. 100 (2006) 1427–1431, https://doi.org/10.1002/app.23471.
[175] X.H. Li, X. Li, K.N. Liao, P. Min, T. Liu, A. Dasari, Z.Z. Yu, Thermally annealed anisotropic graphene aerogels and their electrically conductive epoxy composites with excellent electromagnetic interference shielding efficiencies, ACS Appl. Mater. Interfaces 8 (2016) 33230–33239, https://doi.org/10.1021/acsami.6b12295.
[176] X. Shen, Z. Wang, Y. Wu, X. Liu, Y.B. He, Q. Zheng, Q.H. Yang, F. Kang, J.K. Kim, A three-dimensional multilayer graphene web for polymer nanocomposites with exceptional transport properties and fracture resistance, Mater. Horiz. 5 (2018) 275–284, https://doi.org/10.1039/c7mh00984d.
[177] Y. Wu, Z. Wang, X. Liu, X. Shen, Q. Zheng, Q. Xue, J.-K. Kim, Ultralight graphene foam/conductive polymer composites for exceptional electromagnetic interference shielding, ACS Appl. Mater. Interfaces 9 (2017) 9059–9069, https://doi.org/10.1021/acsami.7b01017.
[178] K. Kultravut, K. Kuboyama, V. Sedlarik, M. Mrlík, J. Osička, P. Drőhsler, T. Ougizawa, Localization of poly(glycidyl methacrylate) grafted on reduced graphene oxide in poly(lactic acid)/Poly(trimethylene terephthalate) blends for composites with enhanced electrical and thermal conductivities, ACS Appl. Nano Mater. 4 (2021) 8511–8519, https://doi.org/10.1021/acsanm.1c01843.
[179] M. Hadaeghnia, S. Ahmadi, I. Ghasemi, P.M. Wood-Adams, Manipulating the morphology of PA6/POE blends using graphene to achieve balanced electrical and mechanical properties, Compos. Sci. Technol. 200 (2020) 108412, https://doi.org/10.1016/j.compscitech.2020.108412.
[180] Y.X. Pan, Z.Z. Yu, Y.C. Ou, G.H. Hu, New process of fabricating electrically conducting nylon 6/graphite nanocomposites via intercalation polymerization, J. Polym. Sci., Part B: Polym. Phys. 38 (2000) 1626–1633, https://doi.org/10.1002/(SICI)1099-0488(20000615)38:12<1626::AID-POLB80>3.0.CO;2-R.
[181] X.-M. Chen, J.-W. Shen, W.-Y. Huang, Novel electrically conductive polypropylene/graphite nanocomposites, J. Mater. Sci. Lett. 21 (2002) 213–214, https://doi.org/10.1023/A:1014708808230.
[182] G. Chen, C. Wu, W. Weng, D. Wu, W. Yan, Preparation of polystyrene/graphite nanosheet composite, Polymer (Guildf). 44 (2003) 1781–1784, https://doi.org/10.1016/S0032-3861(03)00050-8.
[183] W. Weng, G. Chen, D. Wu, X. Chen, J. Lu, P. Wang, Fabrication and characterization of nylon 6/foliated graphite electrically conducting nanocomposite, J. Polym. Sci., Part B: Polym. Phys. 42 (2004) 2844–2856, https://doi.org/10.1002/polb.20140.
[184] W. Zheng, X. Lu, S. Wong, Electrical and mechanical properties of expanded graphite-reinforced high-density polyethylene, J. Appl. Polym. Sci. 91 (2004) 2781–2788, https://doi.org/10.1002/app.13460.
[185] S. Stankovich, D.A. Dikin, G.H.B. Dommett, K.M. Kohlhaas, E.J. Zimney, E. A. Stach, R.D. Piner, S.B.T. Nguyen, R.S. Ruoff, Graphene-based composite materials, Nature 442 (2006) 282–286, https://doi.org/10.1038/nature04969.
[186] K. Kalaitzidou, H. Fukushima, L.T. Drzal, A new compounding method for exfoliated graphite-polypropylene nanocomposites with enhanced flexural properties and lower percolation threshold, Compos. Sci. Technol. 67 (2007) 2045–2051, https://doi.org/10.1016/j.compscitech.2006.11.014.
[187] C. Yu, B. Li, Morphology and properties of conducting polyvinyl alcohol hydrosulfate/graphite nanosheet composites, J. Compos. Mater. 42 (2008) 1491–1504, https://doi.org/10.1177/0021998308092200.
[188] H. Kim, C.W. Macosko, Morphology and properties of polyester/exfoliated graphite nanocomposites, Macromolecules 41 (2008) 3317–3327, https://doi.org/10.1021/ma702385h.
[189] N. Liu, F. Luo, H. Wu, Y. Liu, C. Zhang, J. Chen, One-step ionic-liquid-assisted electrochemical synthesis of ionic-liquid-functionalized graphene sheets directly from graphite, Adv. Funct. Mater. 18 (2008) 1518–1525, https://doi.org/10.1002/adfm.200700797.
[190] H.J. Salavagione, G. Martínez, M.A. Gómez, Synthesis of poly(vinyl alcohol)/reduced graphite oxide nanocomposites with improved thermal and electrical properties, J. Mater. Chem. 19 (2009) 5027–5032, https://doi.org/10.1039/b904232f.
[191] H. Kim, C.W. Macosko, Processing-property relationships of polycarbonate/graphene composites, Polymer (Guildf). 50 (2009) 3797–3809, https://doi.org/10.1016/j.polymer.2009.05.038.
[192] J. Liang, Y. Wang, Y. Huang, Y. Ma, Z. Liu, J. Cai, C. Zhang, H. Gao, Y. Chen, Electromagnetic interference shielding of graphene/epoxy composites, Carbon N. Y. 47 (2009) 922–925, https://doi.org/10.1016/j.carbon.2008.12.038.
[193] W. Xia, C. Jin, S. Kundu, M. Muhler, A highly efficient gas-phase route for the oxygen functionalization of carbon nanotubes based on nitric acid vapor, Carbon N. Y. 47 (2009) 919–922, https://doi.org/10.1016/j.carbon.2008.12.026.
[194] H. Wang, Q. Hao, X. Yang, L. Lu, X. Wang, Graphene oxide doped polyaniline for supercapacitors, Electrochem. Commun. 11 (2009) 1158–1161, https://doi.org/10.1016/j.elecom.2009.03.036.

[195] P. Steurer, R. Wissert, R. Thomann, R. Mülhaupt, Functionalized graphenes and thermoplastic nanocomposites based upon expanded graphite oxide, Macromol. Rapid Commun. 30 (2009) 316–327, https://doi.org/10.1002/marc.200800754.
[196] S. Ansari, E.P. Giannelis, Functionalized graphene sheet-Poly(vinylidene fluoride) conductive nanocomposites, J. Polym. Sci., Part B: Polym. Phys. 47 (2009) 888–897, https://doi.org/10.1002/polb.21695.
[197] S. Bose, T. Kuila, M.E. Uddin, N.H. Kim, A.K.T. Lau, J.H. Lee, In-situ synthesis and characterization of electrically conductive polypyrrole/graphene nanocomposites, Polymer (Guildf). 51 (2010) 5921–5928, https://doi.org/10.1016/j.polymer.2010.10.014.
[198] N. Du, C. yue Zhao, Q. Chen, G. Wu, R. Lu, Preparation and characterization of nylon 6/graphite composite, Mater. Chem. Phys. 120 (2010) 167–171, https://doi.org/10.1016/j.matchemphys.2009.10.041.
[199] M. Yoonessi, J.R. Gaier, Highly conductive multifunctional graphene polycarbonate nanocomposites, ACS Nano 4 (2010) 7211–7220, https://doi.org/10.1021/nn1019626.
[200] H.-B. Zhang, W.-G. Zheng, Q. Yan, Y. Yang, J.-W. Wang, Z.-H. Lu, G.-Y. Ji, Z.-Z. Yu, Electrically conductive polyethylene terephthalate/graphene nanocomposites prepared by melt compounding, Polymer (Guildf). 51 (2010) 1191–1196, https://doi.org/10.1016/j.polymer.2010.01.027.
[201] R. Feng, G. Guan, W. Zhou, C. Li, D. Zhang, Y. Xiao, In situ synthesis of poly (ethylene terephthalate)/graphene composites using a catalyst supported on graphite oxide, J. Mater. Chem. 21 (2011) 3931–3939, https://doi.org/10.1039/c0jm03600e.
[202] J.R. Potts, D.R. Dreyer, C.W. Bielawski, R.S. Ruoff, Graphene-based polymer nanocomposites, Polymer (Guildf). 52 (2011) 5–25, https://doi.org/10.1016/j.polymer.2010.11.042.
[203] S. Vadukumpully, J. Paul, N. Mahanta, S. Valiyaveettil, Flexible conductive graphene/poly(vinyl chloride) composite thin films with high mechanical strength and thermal stability, Carbon N. Y. 49 (2011) 198–205, https://doi.org/10.1016/j.carbon.2010.09.004.
[204] N.D. Luong, N. Pahimanolis, U. Hippi, J.T. Korhonen, J. Ruokolainen, L. S. Johansson, J. Do Nam, J. Seppälä, Graphene/cellulose nanocomposite paper with high electrical and mechanical performances, J. Mater. Chem. 21 (2011) 13991–13998, https://doi.org/10.1039/c1jm12134k.
[205] S. Vadukumpully, J. Paul, N. Mahanta, S. Valiyaveettil, Flexible conductive graphene/poly(vinyl chloride) composite thin films with high mechanical strength and thermal stability, Carbon N. Y. 49 (2011) 198–205, https://doi.org/10.1016/j.carbon.2010.09.004.
[206] N. Yousefi, M.M. Gudarzi, Q. Zheng, S.H. Aboutalebi, F. Sharif, J.K. Kim, Self-alignment and high electrical conductivity of ultralarge graphene oxide-polyurethane nanocomposites, J. Mater. Chem. 22 (2012) 12709–12717, https://doi.org/10.1039/c2jm30590a.
[207] Z. Tang, H. Kang, Z. Shen, B. Guo, L. Zhang, D. Jia, Grafting of polyester onto graphene for electrically and thermally conductive composites, Macromolecules 45 (2012) 3444–3451, https://doi.org/10.1021/ma300450t.
[208] D. Zheng, G. Tang, H.-B. Zhang, Z.-Z. Yu, F. Yavari, N. Koratkar, S.-H. Lim, M.-W. Lee, In situ thermal reduction of graphene oxide for high electrical conductivity and low percolation threshold in polyamide 6 nanocomposites, Compos. Sci. Technol. 72 (2012) 284–289, https://doi.org/10.1016/j.compscitech.2011.11.014.
[209] D.-X. Yan, P.-G. Ren, H. Pang, Q. Fu, M.-B. Yang, Z.-M. Li, Efficient electromagnetic interference shielding of lightweight graphene/polystyrene composite, J. Mater. Chem. 22 (2012) 18772, https://doi.org/10.1039/c2jm32692b.
[210] Z. Chen, C. Xu, C. Ma, W. Ren, H.-M. Cheng, Lightweight and flexible graphene foam composites for high-performance electromagnetic interference shielding, Adv. Mater. 25 (2013) 1296–1300, https://doi.org/10.1002/adma.201204196.
[211] J. Ling, W. Zhai, W. Feng, B. Shen, J. Zhang, W.G. Zheng, Facile preparation of lightweight microcellular polyetherimide/graphene composite foams for electromagnetic interference shielding, ACS Appl. Mater. Interfaces 5 (2013) 2677–2684, https://doi.org/10.1021/am303289m.
[212] S.T. Hsiao, C.C.M. Ma, H.W. Tien, W.H. Liao, Y.S. Wang, S.M. Li, Y.C. Huang, Using a non-covalent modification to prepare a high electromagnetic interference shielding performance graphene nanosheet/water-borne polyurethane composite, Carbon N. Y. 60 (2013) 57–66, https://doi.org/10.1016/j.carbon.2013.03.056.
[213] C. Wu, X. Huang, G. Wang, L. Lv, G. Chen, G. Li, P. Jiang, Highly conductive nanocomposites with three-dimensional, compactly interconnected graphene networks via a self-assembly process, Adv. Funct. Mater. 23 (2013) 506–513, https://doi.org/10.1002/adfm.201201231.
[214] C. Gao, S. Zhang, F. Wang, B. Wen, C. Han, Y. Ding, M. Yang, Graphene networks with low percolation threshold in abs nanocomposites: selective localization and electrical and rheological properties, ACS Appl. Mater. Interfaces 6 (2014) 12252–12260, https://doi.org/10.1021/am501843s.
[215] A.A. Vasileiou, M. Kontopoulou, A. Docoslis, A noncovalent compatibilization approach to improve the filler dispersion and properties of polyethylene/graphene composites, ACS Appl. Mater. Interfaces 6 (2014) 1916–1925, https://doi.org/10.1021/am404979g.
[216] D. Hofmann, M. Keinath, R. Thomann, R. Mülhaupt, Thermoplastic carbon/polyamide 12 composites containing functionalized graphene, expanded graphite, and carbon nanofillers, Macromol. Mater. Eng. 299 (2014) 1329–1342, https://doi.org/10.1002/mame.201400066.
[217] S.T. Hsiao, C.C.M. Ma, H.W. Tien, W.H. Liao, Y.S. Wang, S.M. Li, C.Y. Yang, S. C. Lin, R. Bin Yang, Effect of covalent modification of graphene nanosheets on the electrical property and electromagnetic interference shielding performance of a water-borne polyurethane composite, ACS Appl. Mater. Interfaces 7 (2015) 2817–2826, https://doi.org/10.1021/am508069v.
[218] S.K. Marka, B. Sindam, K.C. James Raju, V.V.S.S. Srikanth, Flexible few-layered graphene/poly vinyl alcohol composite sheets: synthesis, characterization and EMI shielding in X-band through the absorption mechanism, RSC Adv. 5 (2015) 36498–36506, https://doi.org/10.1039/c5ra04038h.
[219] C. Wan, J. Li, Graphene oxide/cellulose aerogels nanocomposite: preparation, pyrolysis, and application for electromagnetic interference shielding, Carbohydr. Polym. 150 (2016) 172–179, https://doi.org/10.1016/j.carbpol.2016.05.051.
[220] M.Z. Iqbal, A.A. Abdala, V. Mittal, S. Seifert, A.M. Herring, M.W. Liberatore, Processable conductive graphene/polyethylene nanocomposites: effects of graphene dispersion and polyethylene blending with oxidized polyethylene on rheology and microstructure, Polymer (Guildf). 98 (2016) 143–155, https://doi.org/10.1016/j.polymer.2016.06.021.
[221] B. Zhao, C. Zhao, M. Hamidinejad, C. Wang, R. Li, S. Wang, K. Yasamin, C.B. Park, Incorporating a microcellular structure into PVDF/graphene-nanoplatelet composites to tune their electrical conductivity and electromagnetic interference shielding properties, J. Mater. Chem. C 6 (2018) 10292–10300, https://doi.org/10.1039/C8TC03714K.
[222] M.K. Poddar, S. Pradhan, V.S. Moholkar, M. Arjmand, U. Sundararaj, Ultrasound-assisted synthesis and characterization of polymethyl methacrylate/reduced graphene oxide nanocomposites, AIChE J. 64 (2018) 673–687, https://doi.org/10.1002/aic.15936.
[223] F. Xu, R. Chen, Z. Lin, Y. Qin, Y. Yuan, Y. Li, X. Zhao, M. Yang, X. Sun, S. Wang, Q. Peng, Y. Li, X. He, Superflexible interconnected graphene network nanocomposites for high-performance electromagnetic interference shielding, ACS Omega 3 (2018) 3599–3607, https://doi.org/10.1021/acsomega.8b00432.
[224] L. Wei, W. Zhang, J. Ma, S.L. Bai, Y. Ren, C. Liu, D. Simion, J. Qin, Π-Π stacking interface design for improving the strength and electromagnetic interference shielding of ultrathin and flexible water-borne polymer/sulfonated graphene composite, Carbon N. Y. 149 (2019) 679–692, https://doi.org/10.1016/j.carbon.2019.04.058.
[225] W. Gao, N. Zhao, T. Yu, J. Xi, A. Mao, M. Yuan, H. Bai, C. Gao, High-efficiency electromagnetic interference shielding realized in nacre-mimetic graphene/polymer composite with extremely low graphene loading, Carbon N. Y. 157 (2020) 570–577, https://doi.org/10.1016/j.carbon.2019.10.051.
[226] J.L. Beckham, J.T. Li, M.G. Stanford, W. Chen, E.A. McHugh, P.A. Advincula, K. M. Wyss, Y. Chyan, W.L. Boldman, P.D. Rack, J.M. Tour, High-Resolution laser-induced graphene from photoresist, ACS Nano 15 (2021) 8976–8983, https://doi.org/10.1021/acsnano.1c01843.
[227] M.H. Al-Saleh, U. Sundararaj, An innovative method to reduce percolation threshold of carbon black filled immiscible polymer blends, Composer Part A Appl. Sci. Manuf. (2008), https://doi.org/10.1016/j.compositesa.2007.10.010.
[228] L. Shen, F. Wang, W. Jia, H. Yang, Thermodynamically induced self-assembled electrically conductive networks in carbon-black-filled ternary polymer blends, Polym. Int. 61 (2012) 163–168, https://doi.org/10.1002/pi.3163.
[229] J. Parameswaranpillai, M.R. Sanjay, S.A. Varghese, S. Siengchin, S. Jose, N. Salim, N. Hameed, A. Magueresse, Toughened PS/LDPE/SEBS/xGnP ternary composites: morphology, mechanical and viscoelastic properties, Int. J. Light. Mater. Manuf. (2019), https://doi.org/10.1016/j.ijlmm.2018.12.003.
[230] P.J. Brigandi, J.M. Cogen, J.R. Reffner, C.A. Wolf, R.A. Pearson, Influence of carbon black and carbon nanotubes on the conductivity, morphology, and rheology of conductive ternary polymer blends, Polym. Eng. Sci. 57 (2017) 1329–1339, https://doi.org/10.1002/pen.24516.
[231] A.T. Lawal, Graphene-based nano composites and their applications. A review, Biosens. Bioelectron. 141 (2019) 111384, https://doi.org/10.1016/j.bios.2019.111384.
[232] D.N. Trivedi, N.V. Rachchh, Graphene and its application in thermoplastic polymers as nano-filler- A review, Polymer (Guildf). 240 (2022) 124486, https://doi.org/10.1016/j.polymer.2021.124486.
[233] M. Silva, N.M. Alves, M.C. Paiva, Graphene-polymer nanocomposites for biomedical applications, Polym. Adv. Technol. 29 (2018) 687–700, https://doi.org/10.1002/pat.4164.
[234] H. Lu, S. Zhang, L. Guo, W. Li, Applications of graphene-based composite hydrogels: a review, RSC Adv. 7 (2017) 51008–51020, https://doi.org/10.1039/c7ra09634h.
[235] V.B. Mohan, K. tak Lau, D. Hui, D. Bhattacharyya, Graphene-based materials and their composites: a review on production, applications and product limitations, Composites, Part B 142 (2018) 200–220, https://doi.org/10.1016/j.compositesb.2018.01.013.
[236] M. Yusuf, M. Kumar, M.A. Khan, M. Sillanpää, H. Arafat, A review on exfoliation, characterization, environmental and energy applications of graphene and graphene-based composites, Adv. Colloid Interface Sci. 273 (2019) 102036, https://doi.org/10.1016/j.cis.2019.102036.
[237] I. Otero-Navas, M. Arjmand, U. Sundararaj, Carbon nanotube induced double percolation in polymer blends: morphology, rheology and broadband dielectric properties, Polymer (Guildf). 114 (2017) 122–134, https://doi.org/10.1016/j.polymer.2017.02.082.
[238] D. Wang, Y. Bao, J.W. Zha, J. Zhao, Z.M. Dang, G.H. Hu, Improved dielectric properties of nanocomposites based on poly(vinylidene fluoride) and poly(vinyl alcohol)-functionalized graphene, ACS Appl. Mater. Interfaces 4 (2012) 6273–6279, https://doi.org/10.1021/am3018652.
[239] Y.-J. Wan, W.-H. Yang, S.-H. Yu, R. Sun, C.-P. Wong, W.-H. Liao, Covalent polymer functionalization of graphene for improved dielectric properties and thermal stability of epoxy composites, Compos. Sci. Technol. 122 (2016) 27–35, https://doi.org/10.1016/j.compscitech.2015.11.005.

[240] M. Nofar, R. Salehiyan, S.S. Ray, Influence of nanoparticles and their selective localization on the structure and properties of polylactide-based blend nanocomposites, Composites, Part B 215 (2021) 108845, https://doi.org/10.1016/j.compositesb.2021.108845.
[241] D. Arthisree, G.M. Joshi, Graphene oxide derived high dielectric constant of polymer blends, Mater. Res. Express 5 (2018) 075304, https://doi.org/10.1088/2053-1591/aad108.
[242] A. Saboor, A.N. Khan, R. Jan, S. Sharif, M. Khan, Mechanical, dielectric and EMI shielding response of styrene acrylonitrile, styrene acrylonitrile/polyaniline polymer blends, upon incorporation of few layer graphene at low filler loadings, J. Polym. Res. 25 (2018) 248, https://doi.org/10.1007/s10965-018-1648-6.
[243] M. Goodarzi, G. Pircheraghi, H.A. Khonakdar, V. Altstadt, Flexible high dielectric polystyrene/ethylene-α-octene copolymer/graphene nanocomposites: tuning the morphology and dielectric properties by graphene's surface polarity, Polym. Adv. Technol. 33 (2022) 937–951, https://doi.org/10.1002/pat.5569.
[244] M. Sadiq, M.M. Hasan Raza, A.K. Singh, S.K. Chaurasia, M. Zulfequar, A. Arya, J. Ali, Dielectric properties and ac conductivity behavior of rGO incorporated PVP-PVA blended polymer nanocomposites films, Mater. Today Proc. 49 (2022) 3164–3169, https://doi.org/10.1016/j.matpr.2020.11.169.
[245] R. Salehiyan, S. Sinha Ray, Processing of polymer blends, emphasizing: melt compounding; influence of nanoparticles on blend morphology and rheology. Reactive Processing in Ternary Systems; Morphology–Property Relationships; Performance and Application Challenges; and Opportunities, Springer International Publishing, 2018, https://doi.org/10.1007/978-3-319-97792-8_6.
[246] Y. Meng, S. Sharma, J.S. Chung, W. Gan, S.H. Hur, W.M. Choi, Enhanced electromagnetic interference shielding properties of immiscible polyblends with selective localization of reduced graphene oxide networks, Polymers (Basel) 14 (2022) 967, https://doi.org/10.3390/polym14050967.
[247] N. Bagotia, D.K. Sharma, Exfoliated graphene lead to extraordinary electromagnetic interference shielding of polycarbonate/ethylene methyl acrylate blend nanocomposites, J. Polym. Res. 30 (2023) 190, https://doi.org/10.1007/s10965-023-03560-6.
[248] P.A. Eutionnat-Diffo, A. Cayla, Y. Chen, J. Guan, V. Nierstrasz, C. Campagne, Development of flexible and conductive immiscible thermoplastic/elastomer monofilament for smart textiles applications using 3D printing, Polymers (Basel) 12 (2020) 2300, https://doi.org/10.3390/polym12102300.
[249] J. Regnier, A. Cayla, C. Campagne, É. Devaux, Melt spinning of flexible and conductive immiscible thermoplastic/elastomer monofilament for water detection, Nanomaterials 12 (2021) 92, https://doi.org/10.3390/nano12010092.
[250] D. Viana, S.T. Walston, X. Illa, J. del Valle, A. Hayward, A. Dodd, T. Loret, E. Prats-Alfonso, N. de la Oliva, M. Palma, E. del Corro, B. Rodriguez-Meana, M. del P. Bernicola, E. Rodriguez-Lucas, T.A. Gener, J.M. de la Cruz, M. Torres-Miranda, F.T. Duvan, N. Ria, J. Sperling, S. Marti-Sanchez, M.C. Spadaro, C. Hebert, E. Masvidal-Codina, S. Savage, J. Arbiol, A. Guimera-Brunet, M. V. Puig, X. Navarro, B. Yvert, K. Kostarelos, J.A. Garrido, Graphene-based thin film microelectrode technology for in vivo high resolution neural recording and stimulation, bioRxiv 2022 (2022), https://doi.org/10.1101/2022.11.16.515761, 11.16.515761.
[251] S. Kane, E. Van Roijen, C. Ryan, S. Miller, Reducing the environmental impacts of plastics while increasing strength: biochar fillers in biodegradable, recycled, and fossil-fuel derived plastics, Composer Part C Open Access 8 (2022) 100253, https://doi.org/10.1016/j.jcomc.2022.100253.
[252] Q. Zhang, B.-Y. Zhang, Z.-X. Guo, J. Yu, Tunable electrical conductivity of carbon-black-filled ternary polymer blends by constructing a hierarchical structure, Polymers (Basel) 9 (2017) 404, https://doi.org/10.3390/polym9090404.
[253] H. Zhang, J. Chen, X. Cui, Y. Hu, L. Lei, Y. Zhu, W. Jiang, Thermal annealing induced enhancement of electrical properties of a co-continuous polymer blend filled with carbon nanotubes, Compos. Sci. Technol. 167 (2018) 522–528, https://doi.org/10.1016/j.compscitech.2018.08.048.
[254] A. Göldel, G. Kasaliwal, P. Pötschke, Selective localization and migration of multiwalled carbon nanotubes in blends of polycarbonate and poly(styrene-acrylonitrile), Macromol. Rapid Commun. 30 (2009) 423–429, https://doi.org/10.1002/marc.200800549.
[255] J. Chen, X. Cui, K. Sui, Y. Zhu, W. Jiang, Balance the electrical properties and mechanical properties of carbon black filled immiscible polymer blends with a double percolation structure, Compos. Sci. Technol. 140 (2017) 99–105, https://doi.org/10.1016/j.compscitech.2016.12.029.
[256] S.L. Scherzer, E. Pavlova, J.D. Esper, Z. Starý, Phase structure, rheology and electrical conductivity of co-continuous polystyrene/polymethylmethacrylate blends filled with carbon black, Compos. Sci. Technol. 119 (2015) 138–147, https://doi.org/10.1016/j.compscitech.2015.10.003.
[257] I. Karteri, M. Altun, M. Gunes, Electromagnetic interference shielding performance and electromagnetic properties of wood-plastic nanocomposite with graphene nanoplatelets, J. Mater. Sci. Mater. Electron. 28 (2017) 6704–6711, https://doi.org/10.1007/s10854-017-6364-1.
[258] F. Shen, D. Pankratov, Q. Chi, Graphene-conducting polymer nanocomposites for enhancing electrochemical capacitive energy storage, Curr. Opin. Electrochem. 4 (2017) 133–144, https://doi.org/10.1016/j.coelec.2017.10.023.
[259] X. Zhang, P. Samorì, Graphene/polymer nanocomposites for supercapacitors, ChemNanoMat 3 (2017) 362–372, https://doi.org/10.1002/cnma.201700055.
[260] X.Y. Qi, D. Yan, Z. Jiang, Y.K. Cao, Z.Z. Yu, F. Yavari, N. Koratkar, Enhanced electrical conductivity in polystyrene nanocomposites at ultra-low graphene content, ACS Appl. Mater. Interfaces 3 (2011) 3130–3133, https://doi.org/10.1021/am200628c.

List of abbreviations

AGC: Aligned Graphene Composites
AGO: Amphiphilic graphene oxide
ATRP: Atom transfer radical polymerization
BVA: Bovine serum albumin
CB: Carbon black
CNF: Carbon nanofibers
CNT: Carbon nanotube
CrGO: Graphene oxide reduced by chemical treatment
CuAAC: Copper-catalyzed alkyne-azide
CVD: Chemical Vapor Deposition
DLS: Dynamic Light Scattering
EAA: Ethylene acrylic acid
EMI: Electromagnetic interference
EOC: Ethylene- α-octene copolymer
EVA: Ethylene vinyl acetate copolymer
FGO or fGO: Functionalized graphene oxide
FIB-AFM: Focused Ion Beam-Atomic Force Microscope
FTIR: Fourier Transform Infra Red
GN: Graphene nanosheets
GNP: Graphene nanoplatelets
GO: Graphene Oxide
GOAS: Graphene oxide functionalized with aminosilane
HDPE: High density polyethylene
HEMA: Hydroxyethyl methacrylate
HRSEM: High Resolution Scanning Electron Microscopy
JGN: Janus Graphene Nanoparticle
JKR: Johnson, Kendall, and Roberts
JPs: Janus particles
LLDPE: Linear low-density polyethylene
MB: Masterbatch
MPS: Methacryloxypropyl trimethoxysilane
m-rGO: Magnetically responsive reduced graphene oxide
MWCNT: Multi walled carbon nanotube
PA12: Polyamide 12
PA6: Polyamide 6
PAMPS: Poly(2-acrylamido-2-methyl-1-propanesulfonic acid)
PANI: Polyaniline
PC: Polycarbonate
PCL: Poly(caprolactone)
PDMS: Polydimethylsiloxane
PE: Polyethylene
PEDOT:PSS: Poly(3,4-ethylenedioxythiophene):poly(styrenesulfonate)
PEI: Poly(ethylene imine)
PEN: Poly (ethylene-2, 6-naphthalate)
PES: Poly(ether sulfone)
PET: Poly(ethylene terephtalate)
PGMA: Poly(glycidyl methacrylate)
PLA: Polylactic acid
PMMA: Poly(methyl methacrylate)
PMMI: Poly(monomethyl itaconate)
POE: Polyolefin elastomer
POE: Polyolefin elastomer
PP: Polypropylene
PPy: Polypyrrole
PS: Polystyrene
PTT: Poly(trimethylene terephthalate
PTT: Poly(trimethylene terephthalate)
PU: Polyurethane
PVA: Poly(Vinyl alcohol)
PVC: Poly(vinyl chloride)
PVDF: Poly(vinylidene fluoride)
PVP: Polyvinyl pyrrolidone
rGO: Reduced graphene oxide
SAN: Poly(styrene-acrylonitrile)
SAOS: Small Amplitude Oscillatory Shear
SBM: Polystyrene-*block*-polybutadiene-*block*-poly(methyl methacrylate) terpolymer
SBR: Styrene butadiene rubber
SDBS: Sodium dodecylbenzene sulfonate
SEM: Scanning Electron Microscope
SFB: Surface force balance
SPION: Superparamagnetic iron oxide nanoparticles
TGA: Thermal Gravimetric Analysis
TPU: Thermoplastic polyurethane
TRG: Thermally reduced graphene
TrGO: Graphene oxide reduced by thermal treatment
TSE: Twin-screw extrusion
UGA: Unidirectional graphene aerogel
XPS: X-ray photoelectron Spectroscopy
XRD: X-ray diffraction